Columbia University
in the City of New York

DEPARTMENT OF CIVIL ENGINEERING
AND ENGINEERING MECHANICS

INSTITUTE FOR THE STUDY OF FATIGUE AND RELIABILITY

LOW AND HIGH AMPLITUDE INTERNAL FRICTION MEASUREMENTS IN SOLIDS AND THEIR RELATION TO IMPERFECTION MOTIONS

by

W. P. Mason

Sponsoring Agencies
Office of Naval Research
Air Force Materials Laboratory
Advanced Research Projects Agency

Contract No. NONR 266(91)
Project No. NR 064-470

Technical Report No. 46

March 1967

Columbia University
in the City of New York

DEPARTMENT OF CIVIL ENGINEERING
AND ENGINEERING MECHANICS

INSTITUTE FOR THE STUDY OF FATIGUE AND RELIABILITY

LOW AND HIGH AMPLITUDE INTERNAL FRICTION MEASUREMENTS IN SOLIDS AND THEIR RELATION TO IMPERFECTION MOTIONS

by

W. P. Mason

Sponsoring Agencies
Office of Naval Research
Air Force Materials Laboratory
Advanced Research Projects Agency

Contract No. NONR 266(91)
Project No. NR 064-470

Technical Report No. 46

March 1967

ABSTRACT

The mechanical properties of single crystal and polycrystalline metals are determined largely by imperfection motions. Internal friction measurements are very sensitive methods for studying these motions. Low amplitude and high frequency measurements are conventional. A new high amplitude system capable of measuring internal friction and modulus defects is described. This can make measurements of internal friction from 10^{-4} to 0.2 with strain amplitudes up to 10^{-2}.

Typical data are shown for low amplitude, high frequency and high amplitude data. These are interpreted in terms of a modified Granato Lücke model. In the linear range dislocation drag coefficients are shown to be determined by the damping of phonons and electrons. The first non-linear range is associated with the breakaway of dislocations from pinning points. The final range involves the generation of new dislocations and is associated with instabilities and fatigue in the metal.

Publications of the Institute for the Study of Fatigue and Reliability

No.

1) Shinozuka, M. On Upper and Lower Bounds of the Probability of Failure of Simple Structures under Random Excitation. December 1963.

2) Freudenthal, A.M., Weibull, W. and Payne, A.O. First Seminar on Fatigue and Fatigue Design. December 1963.

3) Wood, W.A., Reimann, W.H. and Sargant, K.R. Comparison of Fatigue Mechanisms in Bcc Iron and Fcc Metals. April 1964.

4) Heller, R.A. and Shinozuka, M. Development of Randomized Load Sequences with Transition Probabilities Based on a Markov Process. June 1964.

5) Branger, J. Second Seminar on Fatigue and Fatigue Design. June 1964.

6) Wood, W.A. and Reimann, W.H. Room Temperature Creep in Iron under Tensile Stress and a Superposed Alternating Torsion. June 1964.

7) Ronay, M., Reimann, W.H. and Wood, W. A. Mechanism of Fatigue Deformation at Elevated Temperature. June 1964.

8) Freudenthal, A.M. and Shinozuka, M. Upper and Lower Bounds of Probability of Structural Failure under Earthquake Acceleration. June 1964.

9) Ronay, M. On Strain Incompatibility and Grain Boundary Damage in Fatigue. August 1964.

10) Shinozuka, M. Random Vibration of a Beam Column. October 1964.

11) Wood, W.A. and Reimann, W.H. Some direct Observations of Cumulative Fatigue Damage in Metals. October 1964.

12) Freudenthal, A.M., Garrelts, J.M. and Shinozuka, M. The Analysis of Structural Safety. October 1964.

13) Ronay, M. and Freudenthal, A.M. Second Order Effects in Dissipative Solids. January 1965.

14) Shinozuka, M. and Nishimura, A. On General Representation of a Density Function. February 1965.

15) Wood, W.A. and Nine, H.D. Differences in Fatigue Behavior of Single Copper Crystals and Polycrystalline Copper at Elevated Temperatures. February 1965.

No.

16) Ronay, M. On Second Order Strain Accumulation in Torsion Fatigue. February 1965.

17) Heller, R.A. and Heller, A.S. A Probabilistic Approach to Cumulative Fatigue Damage in Redundant Structures. March 1965.

18) Wood, W.A. and Reimann, W.H. Extension of Copper and Brass under Tension and Cyclic Torsion. April 1965.

19) Grosskreutz, J.C., Reimann, W.H. and Wood, W.A. Correlation of Optical and Electron-Optical Observations in Torsion Fatigue of Brass. April 1965.

20) Freudenthal, A.M. and Shinozuka, M. On Fatigue Failure of a Multiple-Load-Path Redundant Structure. June 1965.

21) Shinozuka, M. and Yao, J.T.P. On the Two-Sided Time-Dependent Barrier Problem. June 1965.

22) Ronay, M. On Second Order Strain Accumulation in Aluminum in Reversed Cyclic Torsion at Elevated Temperatures. June 1965.

23) Freudenthal, A.M. Second Order Effects on Plasticity. August 1965.

24) Wood, W.A. Experimental Approach to Basic Study of Fatigue. August 1965.

25) Ronay, M. Conditions of Interaction of Cyclic Torsion with Axial Loads. August 1965.

26) Heller, R.A., and Donat, R.C. Experiments on the Fatigue Failure of a Redundant Structure. October 1965.

27) Shinozuka, M., Yao, J.T.P. and Nishimura, A. A Note on the Reliability of Redundant Structures. November 1965.

28) Mason, W.P. Internal Friction Measurements and Their Uses in Determining the Interaction of Acoustic Waves With Phonons, Electrons and Dislocations. January 1966.

29) Shinozuka, M., Hakuno, M. and Itagaki, H. Response of a Multi-Story Frame Structure to Random Excitation. February 1966.

No.

30) Wood, W. A., *Suppression of Creep Induced by Cyclic Torsion in Copper under Tension*. April 1966.

31) Shinozuka, M. and Sato, Y., *On the Numerical Simulation of Nonstationary Random Processes*. April 1966.

32) Mason, W. P., *Effect of Electron-Damped Dislocations on the Determination of the Superconducting Energy Gaps of Metals*. May 1966.

33) Murro, R. P., *Creep Behavior of an Aluminum Alloy under Transient Temperatures*. June 1966.

34) Ronay, M., *On the Micro-Mechanism of Second-Order Extension of Aluminum in Reversed Cyclic Torsion*. June 1966.

35) Wood, W. A., *Yield and Second-Order Effects Induced by Cyclic Torsion in Copper under Tension*. June 1966.

36) Nine, H. D., and Wood, W. A., *On Improvement of Fatigue Life by Dispersal of Cyclic Strain*. July 1966.

37) Jacoby, G., *Review of Fractographic Analysis Methods for Fatigue Fracture Surfaces*. July 1966.

38) Donat, R. C. and Heller, R. A., *Experiment on a Fail Safe Structural Model*. September 1966.

39) Freudenthal, A. M., and Gou, P. F., *Accumulation of Second Order Strain in Cyclic Loading of Viscous Bar*. September 1966.

40) Mason, W. P., *Acoustic Waves and Dislocation Motions*. October 1966.

41) Mason, W. P., and Bateman, T. B., *Relation between Third-order Elastic Moduli and the Thermal Attenuation of Ultrasonic Waves in Nonconducting and Metallic Crystals*. October 1966.

42) Wood, W. A., *Re-examination of Mechanical Hysteresis*. February, 1967.

43) Mason, W. P., and Rosenberg, A. *Phonon and Electron Drag Coefficients in Single-crystal Aluminum*. November 1966.

44) Mason, W. P., *Mechanical Instability of Alloy Ti-6Al-4V Under Large Extensional Vibrations*.

45) Wood, W. A., *Instability of Titanium and Ti-6Al-4V Alloy at Room Temperature*.

TABLE OF CONTENTS

FIGURE CAPTIONS

Fig. 1.	Method for measuring modulus change and internal friction at low frequencies.
Fig. 2.	Method for superposing static stresses.
Fig. 3.	Pulse method for measuring high frequency internal friction.
Fig. 4a.	Ceramic transducer, stub transformer and sample.
Fig. 4b.	Ceramic transducer, exponential horn and sample.
Fig. 5a.	Mechanical resistance of transducer plus stub transformer for strains present in the speciman.
Fig. 5b.	Mechanical resistance of transducer plus exponential horn for strains present in the speciman.
Fig. 5c.	Mechanical resistance of system plus 7075 aluminum sample.
Fig. 6.	Characteristic impedances of input and output of stub transformer.
Fig. 7.	Electrode arrangement for eliminating pick-up device.
Fig. 8.	Electrostatic pick-up device.
Fig. 9.	Calibration curves for transducer and stub transformer.
Fig. 10.	Calibration curves for exponential horn system.
Fig. 11.	Internal friction of copper, with various amounts of zinc added, as a function of the strain amplitude.
Fig. 12.	Internal friction as a function of strain and temperature for a 99.995% pure aluminum single crystal.
Fig. 13.	Measured fast and slow shear-wave loss at $300^{\circ}K$ as a function of the frequency. Dashed lines represent a breakdown of the loss into a square law loss and dislocation loss. Assymptotic value indicated by the dashed lines on the right.

I. Introduction

The mechanical properties of single crystal and polycrystalline metals and other types of crystals are largely determined by what types of imperfections can be actuated by the applied mechanical stresses. For metals and some other crystals, the governing imperfection is usually the dislocation. As is well known one type of dislocation, the edge dislocation, results from the absence of a plane of atoms below a plane - known as the glide plane - with respect to the number of planes above the glide plane. The other type of dislocation, the screw dislocation results from a spiral arrangement of the atoms around the dislocation line, which results in the atoms on one side of the dislocation being displaced by the slip distance (the Burgers vector) from those on the other side. Since in the growing crystals, atoms can arrange themselves in a spiral staircase around the dislocation with the expenditure of the least amount of energy, the presence of a few screw dislocations plays a prominent role in crystal growth mechanisms.

These imperfections can move along under the effect of a resolved shearing stress in the glide planes and the interactions of dislocations with impurity atoms, vacancies, other dislocations, thermal waves and electron waves in the solid determine the energy loss and hence the attenuation and velocity dispersion of acoustic waves propagated in the solid.

It is the purpose of this chapter to discuss the various phases of the internal friction and modulus changes that occur at different strain levels. A brief description of the standard measuring methods is given and a long description is given of recently developed high amplitude internal friction and modulus defect measurements since no accounts of these types of measurements have previously been given.

Typical measurements by all types of techniques and over wide stress ranges are next discussed. The internal friction method is a very sensitive one but it requires a model to interpret the results. The model that has received the widest application is the stretched string model due to Granato and Lücke. This suggests three amplitude ranges, a low linear amplitude range where dislocations are mainly damped by interaction with phonons, electrons and impurity atoms, an intermediate range for which internal friction and modulus defects are associated with breakaway of dislocations from pinning points, and a high amplitude range where dislocation effects are increasing due to generation by such mechanisms as Frank-

Read mills and cross-slip. This theory neglects the effects of Peierl's barriers and the motion of pinning points along the dislocation lines which have produced measurable effects.

It is the purpose of this chapter to review the measurements and to compare these with existing theories. It is obvious that considerable experimental and theoretical work remains to be done, particularly in the high amplitude range.

II. Methods For Measuring Internal Friction and Modulus Defects at Small Strain Amplitudes.

A. Low Frequency Measurements

Internal frictions and modulus defects can be measured at low frequencies by exciting some type of a resonance vibration and measuring its response at frequencies slightly different from the resonant frequency, or by observing the decay of the vibration amplitude with time. By using torsional pendulums, flexural vibrations or longitudinal vibrations, frequency ranges from less than a cycle per second (i.e. a Hertz) up to frequencies of several hundred kilohertz have been measured. By exciting the vibration with different amounts of input power, measurements can be carried out over a wide range of strain values. The limits are usually set by the lowest amount of detectible power and by the breaking stress or other limitations of the driving transducer. For quartz crystals which have mostly been used in these measurements, the limitation is from a strain of a few times 10^{-8} to a few times 10^{-4}.

One of the most widely used systems[1] is shown by Fig. 1. It consists of a half wave length quartz crystal - sometimes of the $+5^{\circ}$X cut type in order to produce a longitudinal vibration with a low temperature coefficient of frequency - which is cemented on one end to a half wave length sample of a material to be measured, and on the other to a half wave length quartz crystal with an electrode for use as a monitoring device. The driving crystal is plated on two of its surfaces and is held by two wires attached to the surface by cements or solders. The two wires serve also as electrical connections to the plating. Two small wires are also connected to the pick-up electrodes and these are connected to the terminals of a voltmeter which reads the generated open circuit voltage. To make this device work correctly the resonant frequencies of all three parts have to be adjusted closely - at least within a cycle - in order to measure internal friction and modulus defect values. Frequency changes of one part in 10^6 and internal friction values down to Q^{-1} of 10^{-5} have been claimed for these devices.

Several methods can be used to evaluate the internal friction curves. One method is to observe the width of the resonance curves when the amplitude has decreased by $1/\sqrt{2}$ - i.e. 3 db. The internal friction Q^{-1} is this width Δf divided by the resonant frequency. Another method is to excite the resonance by an applied voltage.

The voltage is then turned off and the rate that the vibration dies down is observed on a timing oscillograph. For this case the internal friction Q^{-1} is equal to $1/\pi ft$, where t is the time required for the oscillation to die down to 1/e of its initial value. Another method is to observe the ratio of the applied to the pick-up voltage as discussed in Section III.

Such measurements are carried out over a range of amplitudes. It is usually found that the internal friction increases and the resonant frequency of the composite structure decreases as a function of the applied strain. The method for deriving the internal friction Q^{-1} and the modulus defect $\Delta S/S$ has been discussed in detail in a chapter by Prof. D. Beshers in Vol. I of this series and the reader is referred to this chapter for a description of the calculations.

It is sometimes desirable to find the effects of a static strain on the vibrational properties of the sample. An apparatus[2] for doing this is shown by Fig. 2. In this system two half wave length steel resonators are placed before and after the sample. These have flanges at the points of minimum motion which can act both as supports for the system and as points for applying static tensions or compressions. Since they are at a node of the motion they do not put much damping on the system.

B. <u>High Frequency Measurements</u>

This type of measurement is limited in frequency to several hundred kilohertz on account of the small lengths of the driving and pick-up crystals. A number of effects require much higher frequencies to study. One of these is the damping of dislocations by phonon and electron damping. Such high frequencies can be obtained by using the arrangement of Fig. 3. Here a thickness vibrating longitudinal (X cut) or shear (Y cut, AT cut) quartz crystals are attached to a speciman and a pulse of acoustic waves is sent into the sample by putting a series of electrical waves onto the crystal. The length of the pulse is usually in the order of 10 or more alternating cycles of the frequency of the wave to be sent into the speciman. This length pulse is necessary in order that the full amplitude will build up in the transducer. For a 10 MHz fundamental this requires a pulse length of about 1 microsecond.

This type transducer produces a pulse of waves which is picked up by another crystal at the other end or more often by the same transducer picking up the reflection from the end of the sample. This requires that the sample has very parallel edges, and this provides a limitation on the top frequency that can be used. By special techniques such as the generation of acoustic waves at the surface of the crystal, frequencies as high as 114 Gigahertz have been employed.[3] Measurements as high as 1 Gigahertz are quite common.

The method of measurement of velocity is to time the received series of pulses. Very good accuracy[4] can be obtained by a pulse superposition method which balances out individual cycles of a series of received pulses. Attenuation measurements are made by determining the rate at which successive pulses decrease in amplitude as a function of the distance. Care must be taken to obtain nearly an exponential decay rate. Factors which prevent this are non-parallelity of the speciman, transducer or cement layer. Another source of difficulty is the loss associated with the diffraction of the beam. Calculations[5] show that this type of loss becomes less at the high frequencies and can usually be neglected above 30 MHz. Some loss also occurs in the cement layer and in the transducer itself. This loss can be evaluated experimentally by putting another crystal on the far end and measuring the increased loss per reflection. For a path length of 4 cms this loss is usually less than 0.06db per cm and is usually much smaller than the attenuation introduced by a metal crystal. For very low loss materials, however, more care is needed in evaluating this loss.

The strain values introduced in the sample is rather small unless a very high voltage is put on the crystal. The strain level introduced in the sample by transducers is discussed in the next section and it is there shown that the strain introduced at the center of the driving crystal is

$$S_{11} \doteq \frac{2dV}{t} \left(\frac{Z_T}{Z_B}\right)$$

where $Z_T = (\rho v)_T$ is the characteristic impedance of the transducer and $Z_B \doteq (\rho v)_S$ is the characteristic impedance of the speciman. Since the velocity is continuous into the speciman from the transducer, the strain in the speciman is (v_T/v_S) times that in the transducer, or the strain in the speciman is

$$S_{11} = \frac{2dV}{t} \left(\frac{c_{11_T}}{c_{11_S}}\right)$$

where c_{11_T} and c_{11_S} are the elastic stiffnesses of the two materials. For example for an applied voltage of 2800 volts, $d_{11} = 2.25 \times 10^{-12}$ coulombs per Newton for quartz, a 20 MHz X cut crystal with a thickness of 0.000145 meters and with the elastic moduli assumed equal, the strain induced in the speciman is 8.7×10^{-5}. This is a high enough strain to introduce non-linearity in lead and very soft crystals but not in aluminum. If the crystal is used at a high harmonic, the strain introduced is the inverse of the harmonic number. By going to a ceramic transducer with a much larger value of d, the strain can be made much larger for a given voltage.

III. Method For Generating and Measuring the Properties of Materials at High Strain Amplitudes

A. Introduction

The methods for measuring the internal friction and modulus change discussed in the previous section are limited in the amount of strain amplitudes that can be generated. The low frequency method is limited by the breaking strain in the quartz crystal which is a few times 10^{-4}

in longitudinal strain. The high frequency method is limited by the voltage breakdown characteristic of the crystal as well as by the limiting strain that the crystal and cements will stand.

Some time ago a method was derived by the writer[6] for producing higher strains in a metal sample and for measuring the internal friction and modulus change in a sample under high strain. This method has been considerably improved recently, and it is possible to measure internal frictions and modulus defects from less than 10^{-4} to values of 0.2 for strain ranges from 10^{-7} up to 10^{-2}. The upper limit may be pushed even higher by using different types of alloys in the transformers and horns of different shapes. It is the purpose of this section to describe the properties of these measuring systems.

B. Description of Systems

The systems used, as shown by Figs. 4a and 4b consist of ceramic transducers - in this case Clevite PZT 4 - cemented to mechanical transformers by thin layers of epoxy resins. Fig. 4a shows a half wave transformer consisting of two quarter wave stubs of different areas. On the end of the transformer is a new type sample held in place by a screw and friction joint which is sufficient since the joint comes at a point of small strain. As shown in Section IIIC the stub transformer increases the sample impedance by a factor $(D_1/D_2)^4$ where D_1 is the diameter of the large end and D_2 the diameter of the small end. As shown also in Section IIIC, the strain in the speciman section is increased by a factor of 5 over that in the horn and is very uniform throughout the small part. For the aluminum transformer employed, the amplitude transformation ratio is 25 since D_1 = 2.5 inches and D_2 = 0.5 inches, and the motion on the end is 25 times as large as the motion on the end of the ceramic transducer. This larger strain is enhanced by a new type of sample for which the strain in the small section is quite uniform and equal to 5 times the strain generated by the transformer. With the two large sections of the sample on the end, each equal to half the length of the small section, the length of the sample is much reduced over that for a half wave length section necessary to produce resonance at the resonant frequency of the driver. The sample is stiff enough flexurally to not cause trouble and reproducible results have been obtained up to strains of 3×10^{-3} in samples of 7075 aluminum.

The quarter wave stub transformer of Fig. 4a is very advantageous for measuring internal friction since with the large impedance transformation ratio of 625 most of the damping on the transducer is due to the sample impedance. The damping of the transducer itself and the stub transformer can be separately measured and subtracted from the total as discussed in the measurement Section IIIE. However, the strain that can be generated and measured in the sample is limited by the linearity of the stub transformer. Fig. 5 curve A shows a measurement of the mechanical resistance of the transducer plus stub transformer as a function of the r.m.s. longitudinal strain. Since the strain is measured by a pick-up voltage from the transducer or from an electrostatic pickup, it is more convenient to express the strain in terms of the r.m.s. voltage which is $2/\pi$ times the maximum voltage. In the same way the maximum strain is $\pi/2$ (56 percent) higher than the r.m.s. strain. Fig. 5 shows that a strain of about 6×10^{-4} (r.m.s.) can be used before much nonlinearity is encountered. Furthermore the change in frequency of the transducer horn system is less than 1 cycle in 15,000 over this amplitude range. Also if much higher strains are used, the resistance of the measuring system does not repeat since some dislocation production occurs and it is necessary to anneal the horn before it comes back to normal.

The reason for this relatively small strain in the measuring system is that to get a high motion on the end, the strain in the center of the stub transformer is determined from the equation

$$\delta x = \left(\frac{2}{\pi} \ell x S_{11}\right) \qquad (1)$$

where δx is the displacement on the end, ℓ the length of the quarter wave stub and S_{11} the strain at the connecting point of the stub. The velocity on the end is the angular frequency ω times the displacement δx. Furthermore the length of the stub is determined by the quarter wave condition

$$\frac{\omega \ell}{v} = \frac{\pi}{2} \qquad (2)$$

where v is sound velocity (determined by Young's modulus Y_o divided by the density ρ). Hence the particle velocity

$$\dot{u} = \omega\delta x = vS_{11} \tag{3}$$

Different types of vibrators satisfy the equation

$$\dot{u} = \varphi vS_{11} \tag{4}$$

where φ has been defined by Eisner[7] as a figure of merit which depends only on the shape of the vibrator. For a bar, Equation (3) shows that $\varphi = 1$. For the stepped transformer, the discontinuity acts as a stress raiser, and Eisner suggest that the figure of merit is about 0.8.

For the exponential horn shown by Fig. 4b, the point of maximum strain comes at a point where the area of the horn is larger than at the end. In Section IIID, it is shown that the figure of merit is ϵ or 2.73. Other shapes such as the Gaussian horn[7] may have a figure of merit as high as 5. However, such horns have not come into general use and the present section is limited to a discussion of exponential horns.

Using the horn of Fig. 4b, an amplitude step up of 12 to 1 is obtained and an impedance transformation ratio of 144 to 1. If the strain in the sample is limited by the range of the linear strain in the measuring system, this can be 3.4 times as large as that for the stub transformer or about 2×10^{-3}. The sample shape gives another factor of 5 so that if the sample can take it, strains as high as 10^{-2} are possible. Usually a large increase in internal friction or fatigue in the sample occurs before this strain is reached.

The exponential horn is also advantageous if the damping gets very high since the damping on the transducer due to the speciman is only multiplied by 144 rather than 625. Hence both types of systems are of use.

C. Equations for Stub Transformers and Speciman Shapes

Since the properties of the measuring system depend on the transformation ratios that can be obtained in the transformer sections it appears worthwhile to derive the equations of motion for such sections. Account can also be taken of the effect of dissipation in the structures. All of these structures are designed on the assumption that plain longitudinal waves will exist in all the elements and that the forces and velocities are continuous across the interfaces. At first sight this might seem somewhat questionable but experimentally it is found that the equations derived on these assumptions appear to be in good agreement with the experiments. Slight corrections to the lengths of the individual parts sometimes have to be made to match resonant frequencies.

The equations of motion of extensional waves in a rod have been derived in a number of references.[8] Starting with the equations of motion

$$\rho \frac{\partial^2 u}{\partial t^2} = Y_o \frac{\partial^2 u}{\partial x^2} \tag{5}$$

it is readily shown[8] that the force and particle velocity on the end of a rod is given in terms of the force and particle displacement at the beginning of the rod by the equations

$$F_2 = F_1 \cos \frac{\omega x}{v} - j\dot{u}_1 Z_o \sin \frac{\omega x}{v} \; ; \; \dot{u}_2 = \dot{u}_1 \cos \frac{\omega x}{v} - j \frac{F_1}{Z_o} \sin \frac{\omega x}{v} \tag{6}$$

where Z_o the characteristic impedance of the infinite rod is equal to

$$Z_o = \rho v s \tag{7}$$

where s is the cross-sectional area of the rod. This equation holds for a more general case[9] if the velocity $v = Y_o/\rho$ is replaced by

$$v = \sqrt{\frac{Y_o}{\rho}} \left[1 - \left(\frac{\pi\sigma a}{\lambda}\right)^2\right] \tag{8}$$

where σ is Poisson's ratio, a is the radius of the rod and λ the wave length. For the largest rod of aluminum used, a is 3.22 cms, $\sigma = 0.355$ and λ is 32.3 cms at the operating frequency of 15,500 cycles. Hence the correction to the velocity is just over 1 percent.

Since dissipation is to be measured by the system, the equation of motion is generalized to take account of some form of dissipation. The one most easily accounted for is a viscous type of dissipation which occurs in a metal due to conversion of acoustic energy to thermal phonons or electrical charges. For the present purpose this is sufficiently general. The equation of motion then becomes

$$\rho \frac{\partial^2 u}{\partial t^2} = Y_o \frac{\partial^2 u}{\partial x^2} + \eta \frac{\partial^3 u}{\partial t \partial x^2} = (Y_o + j\omega\eta) \frac{\partial^2 u}{\partial x^2} \tag{9}$$

where η is the coefficient of viscosity. A solution for this equation is

$$u = [A\epsilon^{\Gamma x} + B\epsilon^{-\Gamma x}]\epsilon^{-j\omega t} \tag{10}$$

Substituting this equation in (9) it is found to be a solution if

$$\Gamma^2 = \frac{-\omega^2 \rho}{Y_o + j\omega\eta} \tag{11}$$

Γ is then complex and we designate the two parts as

$$\Gamma = \alpha + j\beta \tag{12}$$

where α is an attenuation usually expressed in nepers per cm. and β is a phase shift expressed in radians per cm. The expression in (11) can be simplified somewhat if $\omega\eta << Y_o$ which is always the case with a metal. Under these circumstances it is readily shown that

$$\beta = \omega\sqrt{\frac{\rho}{Y_o}} = \frac{\omega}{v}\ ; \quad 2\alpha\beta = \beta^2 \left(\frac{\eta\omega}{Y_o}\right) \tag{13}$$

Hence

$$\frac{\alpha}{\beta} = \frac{\eta\omega}{2Y_o} \quad \text{or} \quad \alpha = \frac{\eta\omega^2}{2Y_o \times \sqrt{Y_o/\rho}} = \frac{\eta\omega^2}{2\rho v^3} \tag{14}$$

It will presently be shown that the ratio of the resistance at resonance to the effective mass of a vibrating rod at resonance - which is defined as the internal friction Q^{-1} of the sample - is equal to

$$\frac{2\alpha}{\beta} = Q^{-1} \ ; \text{ Hence } \alpha = \frac{Q^{-1}\beta}{2} \tag{15}$$

Hence the internal friction of a sample can be determined in terms of the attenuation and phase shift of the sample.

Returning to the solution of Equation (10) the particle velocity and the force on the sample are given by

$$\dot{u} = \frac{\partial}{\partial t} u = -j\omega[Ae^{\Gamma x} + Be^{-\Gamma x}]e^{-j\omega t} \tag{16}$$

$$F = s(Y_o+j\omega\eta)\frac{\partial u}{\partial x} = s(Y_o+j\omega\eta)\Gamma(Ae^{\Gamma x} - Be^{-\Gamma x})e^{-j\omega t}$$

The constants A and B can be evaluated in terms of F_1 and $\dot{u}_1$, the force and velocity at the input of the rod. The values are

$$A = \frac{j\dot{u}_1/\omega + F_1/s(Y_o+j\omega\eta)\Gamma}{2} \ ; \ B = \frac{j\dot{u}_1/\omega - F_1/s(Y_o+j\omega\eta)\Gamma}{2} \tag{17}$$

Introducing these values of A and B into Equation (16) and collecting terms, the two equations of (16) can be written

$$\dot{u} = \dot{u}_1\cosh(\alpha+j\beta)x - \frac{F_1}{Z_o}\sinh(\alpha+j\beta)x \tag{18}$$

$$F = F_1\cosh(\alpha+j\beta)x - \dot{u}_1 Z_o\sinh(\alpha+j\beta)x$$

where

$$Z_o = \frac{s(Y_o+j\omega\eta)\Gamma}{j\omega} = s\sqrt{(Y_o+j\omega\eta)\rho} = s\sqrt{Y_o\rho}\,\left(1 + \frac{j\omega\eta}{2Y_o}\right)$$

Since $\omega\eta << Y_o$, the characteristic impedance becomes

$$Z_o \doteq s\sqrt{Y_o\rho} \tag{19}$$

which is the same as that for the non-dissipative material.

1. <u>Equations for a Simple Rod</u>

Equations (18) are useful in determining the dissipative properties of a rod or combination of rods. For a single rod driven by a transducer on one end and with the other end free, we can set F_2 equal to zero in the last of Equation (18) and solve for the ratio of $F_1/\dot{u}_1$. The result is

$$\frac{F_1}{\dot{u}_1} = Z_o \tanh(\alpha+j\beta)\ell = Z_o\left[\frac{\tanh\alpha\ell + j\tan\beta\ell}{1+j\tanh\alpha\ell\tan\beta\ell}\right] \tag{20}$$

At the resonant frequency of the bar $\beta\ell = \pi$ and $\tan\beta\ell = 0$ so that the impedance is a resistance equal to

$$R_M = Z_o \tanh \alpha\ell \doteq Z_o(\alpha\ell) \quad . \tag{21}$$

Near the resonant frequency

$$\tan\beta\ell = \tan\frac{(\omega_R+\Delta\omega)\ell}{v} = \tan\pi(1+\frac{\Delta\omega}{\omega_R}) \tag{22}$$

where ω_R is the angular resonant frequency. Using the multiple angle formulae, we have

$$\tan\pi(1+\frac{\Delta\omega}{\omega_R}) = \frac{\tan\pi + \tan\frac{\pi\Delta\omega}{\omega_R}}{1+\tan\pi\tan\frac{\pi\Delta\omega}{\omega_R}} = \tan\frac{\pi\Delta\omega}{\omega_R} \doteq \frac{\pi\Delta\omega}{\omega_R}\ , \tag{23}$$

since $\tan\pi = 0$ and $\Delta\omega/\omega_R$ is assumed to be a small quantity. Hence near the resonant frequency the mechanical impedance of the speciman is

$$Z_M = Z_o\left[\alpha\ell + j\,\frac{\pi\Delta\omega}{\omega_R}\right] \tag{24}$$

This combination can be represented by a mass M, a stiffness S and a resistance R_M which resonate at the same frequency as the bar resonates. Then

$$Z_M = j\omega M - \frac{jS}{\omega} + R_M = -\frac{jS}{\omega}\left[1 - \frac{\omega^2 M}{S}\right] + R_M \tag{25}$$

Since the ratio S/M is set equal to the angular mechanical resonance ω_R, the equation reduces to

$$\frac{j2S}{\omega_R}\frac{\Delta\omega}{\omega_R} = jZ_o\frac{\pi\Delta\omega}{\omega_R} \tag{26}$$

Hence

$$S = \frac{\pi}{2} Z_o\omega_R = \frac{\pi^2}{2}\frac{s\sqrt{Y_o\rho} \times \sqrt{Y_o/\rho}}{\ell} = \frac{\pi^2}{2}\frac{sY_o}{\ell} \tag{27}$$

when we make use of the fact that $\omega_R\ell/v = \pi$ and $v = \sqrt{Y_o/\rho}$. The mass M is determined by the fact that the stiffness and mass have to resonate at ω_R. Hence

$$M = \frac{1}{2} s\ell\rho \tag{28}$$

or half the static mass of the bar.

The quality factor Q of a resonant circuit is defined as the ratio of the reactance of one of the elements to the resistance of the circuit or

$$Q = \frac{\omega_R M}{R_M} = \frac{\omega_R s\ell\rho}{2xs\sqrt{Y_o\rho}\, x\ell\alpha} = \frac{\omega_R}{2\alpha V} = \frac{\beta}{2\alpha} \tag{29}$$

Hence as indicated in Equation (15) the internal friction, which is defined as the inverse of Q is given by

$$Q^{-1} = \frac{2\alpha}{\beta} \quad \text{and} \quad Z_M = Z_o\left[\frac{\pi}{2} Q^{-1} + j \frac{\pi\Delta\omega}{\omega_R}\right] \tag{30}$$

This equation indicates one way of measuring the internal friction Q^{-1}. If the frequency is changed until Z_M has increased by the square root of 2 - i.e. 3db - then

$$Z_M = \sqrt{2}\,\frac{\pi}{2} Q^{-1} Z_o = Z_o \sqrt{\left(\frac{\pi}{2} Q^{-1}\right)^2 + \left(\frac{\pi\Delta\omega}{\omega_R}\right)^2}$$

Hence

$$Q^{-1} = \frac{2\Delta\omega}{\omega_R} = \frac{\Delta f}{f_R} \tag{31}$$

Since $2\Delta\omega$ is 2π times the whole frequency difference Δf between the two three db frequencies, the internal friction Q^{-1} is this frequency difference divided by the resonant frequency f_R.

2. Equations for a Stub Transformer

The two quarter wave sections of rod shown by Fig. 4a, result in a mechanical transformer which increases the particle velocity on the small end by the ratio $(D_1/D_2)^2$ and increases the impedance of the terminating sample by the ratio $(D_1/D_2)^4$ on the driving transducer. To show this we first consider the case of two dissipationless rods, each a quarter wave length long, joined together at the mid point. The diameter of the large section is D_1 and that of the small section is D_2. From Equations (6), the equations for the two rods are

$$F_2 = F_1 \cos\frac{\omega \ell_1}{V} - jZ_{o_1}\dot{u}_1 \sin\frac{\omega \ell_1}{V}; \quad F_4 = F_3 \cos\frac{\omega \ell_1}{V} - jZ_{o_2}\dot{u}_3 \sin\frac{\omega \ell_1}{V}$$

$$\dot{u}_2 = \dot{u}_1 \cos\frac{\omega \ell_1}{V} - j\frac{F_1}{Z_{o_1}} \sin\frac{\omega \ell_1}{V}\ ; \ \dot{u}_4 = \dot{u}_3 \cos\frac{\omega \ell_1}{V} - j\frac{F_3}{Z_{o_2}} \sin\frac{\omega \ell_1}{V} \tag{26}$$

At the joint between the two rods, it is assumed that the total force F_2 exerted by the first rod is equal to the force F_3 exerted on the beginning of the second rod and similarly the velocities are considered continuous between the rods. Hence

$$F_2 = F_3; \quad \dot{u}_2 = \dot{u}_3 \tag{27}$$

Inserting these values, we can eliminate the interior variables and express the output variables F_4 and $\dot{u}_4$ in terms of the input variables F_1, $\dot{u}_1$. The result is

$$F_4 = F_1\left[\cos^2\frac{\omega \ell_1}{v} - \frac{Z_{o_2}}{Z_{o_1}} \sin^2\frac{\omega \ell_1}{v}\right] - j\dot{u}_1\left[\frac{Z_{o_1} + Z_{o_2}}{2}\right] \sin^2\frac{\omega \ell_1}{v}$$

$$\dot{u}_4 = \dot{u}_1\left[\cos^2\frac{\omega \ell_1}{v} - \frac{Z_{o_1}}{Z_{o_2}} \sin^2\frac{\omega \ell_1}{v}\right] - F_1\left[\frac{Z_{o_1} + Z_{c_2}}{2Z_{o_1} Z_{o_2}}\right] \sin^2\frac{\omega \ell_1}{v} \tag{28}$$

These are the equations of a transforming band pass filter such as have been discussed in Reference (10). It is there shown that if these equations are written in the form

$$F_4 = F_1 A - \dot{u}_1 B; \quad \dot{u}_4 = \dot{u}_1 C - F_1 D \tag{29}$$

that the structure is equivalent to a transforming band pass filter which has the image impedance Z_{I_1} on the input side and Z_{I_2} on the output side, as shown by Fig. 6, and a propagation constant θ.

These quantities are given by the equations

$$Z_{I_1} = \sqrt{\frac{BC}{AD}} \; ; \; Z_{I_2} = \sqrt{\frac{AB}{CD}} \; ; \quad \tanh\theta = \sqrt{\frac{BD}{AC}} \tag{30}$$

If we replace ℓ_1 the half length of the transformer by $\ell/2$, where ℓ is the total length, these equations become

$$Z_{I_1} = \sqrt{Z_{o_1} Z_{o_2}} \sqrt{\frac{\cos^2 \frac{\omega\ell}{2v} - \frac{Z_{o_1}}{Z_{o_2}} \sin^2 \frac{\omega\ell}{2v}}{\cos^2 \frac{\omega\ell}{2v} - \frac{Z_{o_2}}{Z_{o_1}} \sin^2 \frac{\omega\ell}{2v}}}$$

$$Z_{I_2} = \sqrt{Z_{o_1} Z_{o_2}} \sqrt{\frac{\cos^2 \frac{\omega\ell}{2v} - \frac{Z_{o_2}}{Z_{o_1}} \sin^2 \frac{\omega\ell}{2v}}{\cos^2 \frac{\omega\ell}{2v} - \frac{Z_{o_1}}{Z_{o_2}} \sin^2 \frac{\omega\ell}{2v}}} \tag{31}$$

$$\tanh\theta = -j \frac{\frac{Z_{o_1}+Z_{o_2}}{2\sqrt{Z_{o_1} Z_{o_2}}} \sin \frac{\omega\ell}{v}}{\sqrt{1 - \sin^2 \frac{\omega\ell}{v} \left[\frac{(Z_{o_1}+Z_{o_2})^2}{4Z_{o_1} Z_{o_2}}\right]}}$$

Plots of Z_{I_1} and Z_{I_2} are shown on Fig. 6. The resulting structure is a low and band pass filter with a mid band when

$$\frac{\omega\ell}{v} = \pi \text{ or } f = \frac{v}{2\ell} \tag{32}$$

or at a half-wave resonance of the complete bar. The pass band is determined by the condition

$$\sin^2 \frac{\omega\ell}{v} = \frac{4Z_{o_1} Z_{o_2}}{(Z_{o_1}+Z_{o_2})^2} = \frac{4\,\dfrac{Z_{o_2}}{Z_{o_1}}}{\left(1+\dfrac{Z_{o_2}}{Z_{o_1}}\right)^2} \tag{33}$$

For example for diameter of 2.5 inches and 0.5 inches, Z_{o_2}/Z_{o_1} is equal to $(.5/2.5)^2 = 0.04$ and $\omega\ell/v = 157.2^\circ$ and 202.8°. Hence the band width of the transformer is

$$\frac{f_2-f_1}{f_M} = \frac{202.8 - 157.2}{180} = 0.254 \tag{34}$$

Within this frequency range the device will act as a transformer.

The impedance ratio of the transformer at mid-band is determined by setting $\omega\ell/2v = \pi/2$. Hence

$$\frac{Z_{I_1}}{Z_{I_2}} = \frac{\sqrt{Z_{o_1}Z_{o_2}} \times \dfrac{Z_{o_1}}{Z_{o_2}}}{\sqrt{Z_{o_1}Z_{o_2}} \times \dfrac{Z_{o_2}}{Z_{o_1}}} = \frac{Z_{o_1}^2}{Z_{o_2}^2} = \left(\frac{D_1}{D_2}\right)^4 \tag{35}$$

In using such a transformer, it is necessary to adjust the half wave length frequency to the resonant frequency of the transducer driving the system. At the resonant frequency $F_4 = 0$ and

$$Z_T = \frac{F_1}{\dot{u}_1} = j\,\frac{\left(\dfrac{Z_{o_1}+Z_{o_2}}{2}\right)\sin\dfrac{\omega\ell}{v}}{\cos^2\dfrac{\omega\ell}{2v} - \dfrac{Z_{o_2}}{Z_{o_1}}\sin^2\dfrac{\omega\ell}{2v}} = 0 \text{ at } \frac{\omega_R\ell}{v} = \pi \tag{36}$$

Near the resonant frequency, the transformer can be represented by an equivalent mass, stiffness and resistance as can a single rod. The mass and stiffness can be calculated by taking a frequency difference $\Delta\omega$ from the resonant angular frequency ω_R. By using the multiple angle formulae it is readily shown that

$$\sin\frac{\omega \ell}{v} = \sin\pi\left(1 + \frac{\Delta f}{f_R}\right) = -\frac{\pi\Delta f}{f_R}$$

$$\cos^2\frac{\omega \ell}{2v} = \left[\cos\frac{\pi}{2}\left(1 + \frac{\Delta f}{f_R}\right)\right]^2 = \frac{\pi^2}{4}\left(\frac{\Delta f}{f_R}\right)^2 \tag{37}$$

$$\sin^2\frac{\omega \ell}{2v} = \left[\sin\frac{\pi}{2}\left(1 + \frac{\Delta f}{f_R}\right)\right]^2 = 1 - \frac{\pi^2}{4}\left(\frac{\Delta f}{f_R}\right)^2$$

Neglecting squares and higher powers of $(\Delta f/f_R)$ we have

$$Z_s = j\left(\frac{Z_{o_1}+Z_{o_2}}{2}\right)\frac{Z_{o_1}}{Z_{o_2}}\left(\frac{\pi\Delta f}{f_R}\right) \tag{38}$$

This impedance is to be compared with the impedance of a mass and stiffness given by Equation (25) and (26). Equating the two expressions we have

$$S = \frac{\pi^2}{4}Y_o\left[\frac{s_1}{\ell}\right]\left[1 + \frac{D_1^2}{D_2^2}\right] ; \quad M = \frac{s_1 \ell \rho}{4}\left[1 + \frac{D_1^2}{D_2^2}\right] \tag{39}$$

The total mass is equal to half the mass of the large section plus half the mass of the small section transformed in the ratio $(D_1/D_2)^4$. Similarly if account is taken of the resistance of the sample, the resistance at resonance is the resistance of the large section R_{M_1} plus $(D_1/D_2)^4$ times the resistance R_{M_2} of the small section. Since the small section is strained more highly its resistance will be higher and when transformed in the ratio $(D_1/D_2)^4$, provides practically all of the damping. The total stiffness S is $\pi^2/8$ times the stiffness of the large section plus $\pi^2/8$ times the stiffness of the small section transformed in the ratio $(D_1/D_2)^4$.

When a speciman resonating at the frequency ω_R is attached to the end of the transformer it is of interest tc find out what impedance is obtained on the large end of the transformer, since this impedance will damp the transducer. To determine this we set, in Equation (28)

$$\frac{F_4}{\dot{u}_4} = -\frac{jS_B}{\omega}\left[1 - \frac{\omega^2}{\omega_R^2}\right] + R_B = \frac{2j\Delta f}{f_R} \times \frac{S_B}{\omega_R} + R_B = Z_B \qquad (40)$$

Inserting this value in Equation (29), and solving for $F_1/\dot{u}_1$ we find

$$\frac{F_1}{\dot{u}_1} = \frac{jB + CZ_B}{A + jDZ_B} = \frac{\left(\frac{Z_{o_1}+Z_{o_2}}{2}\right)\sin\frac{\omega\ell}{v} + \left[\cos^2\frac{\omega\ell}{2v} - \frac{Z_{o_1}}{Z_{o_2}}\sin^2\frac{\omega\ell}{2v}\right] Z_B}{\left[\cos^2\frac{\omega\ell}{2v} - \frac{Z_{o_2}}{Z_{o_1}}\sin^2\frac{\omega\ell}{2v}\right] + j\left[\frac{Z_{o_1}+Z_{o_2}}{2Z_{o_1}Z_{o_2}}\right]\sin\frac{\omega\ell}{v} \times Z_B} \qquad (41)$$

If we develop this expression around the condition $\omega_R\ell/v = \pi$; the expression becomes

$$\frac{F_1}{\dot{u}_1} = \frac{j\left(\frac{Z_{o_1}+Z_{o_2}}{2}\right)\left(-\frac{\pi\Delta f}{f_R}\right) - \frac{Z_{o_1}}{Z_{o_2}}\left[\frac{2j\Delta f}{f_R} \times \frac{S_B}{\omega_R} + R_B\right]}{-\frac{Z_{o_2}}{Z_{o_1}} + j\left(\frac{Z_{o_1}+Z_{o_2}}{2Z_{o_1}Z_{o_2}}\right)\left(-\frac{\pi\Delta f}{f_R}\right)\left[\frac{2j\Delta f}{f_R}\ \frac{S_B}{\omega_R} + R_B\right]} \tag{42}$$

The denominator can be set equal to $-Z_{o_2}/Z_{o_1}$ since this is large compared to the square of the term $\Delta f/f_R$ and hence

$$\frac{F_1}{\dot{u}_1} = \frac{j(Z_{o_1}+Z_{o_2})}{2}\left(\frac{Z_{o_1}}{Z_{o_2}}\right)\left(\frac{\pi\Delta f}{f_R}\right) + \left(\frac{Z_{o_1}}{Z_{o_2}}\right)^2 \left[\frac{2j\Delta f}{f_R}\ \frac{S_B}{\omega_R} + R_B\right] \tag{43}$$

Hence the resistance and reactance components of the load are multiplied in the ratio

$$\left(\frac{Z_{o_1}}{Z_{o_2}}\right)^2 = \left(\frac{s_1}{s_2}\right)^2 = \left(\frac{D_1}{D_2}\right)^4 \tag{44}$$

and this impedance adds to the resistance and reactance components of the transformer. Hence to obtain the properties of the speciman alone, it is only necessary to evaluate the properties of the transducer and transformer alone and subtract these values from a measurement of the whole system.

3. Speciman Shapes of Use For Measurements

The success of this system depends on obtaining a high strain in the speciman to be measured while still maintaining the strain in the linear low amplitude range for the transducer and the transformer. At the same time it is desirable to produce a nearly constant strain over the highly strained region. Both requirements are met by the sample shape shown on Fig. 4a or 4b which terminate the stub transformer or the exponential horn.

This speciman takes the place of two stub transformers back to back, but the length is much shorter than two half wave lengths. In deriving the equations for this speciman shape, account is taken of the dissipation of the center section, but this is neglected for the large sections at the beginning and end. Hence the three sets of equations are those shown by Eq. (45). These are joined together at the interfaces by assuming that the forces and velocities are continuous. The equations become

$$F_2 = F_1 \cos\frac{\omega \ell}{4v} - j\dot{u}_1 Z_{o_1} \sin\frac{\omega \ell}{4v}\ ; \quad \dot{u}_2 = \dot{u}_1 \cos\frac{\omega \ell}{4v} - \frac{jF_1}{Z_{o_1}} \sin\frac{\omega \ell}{4v}$$

$$F_3 = F_2 \cosh\frac{(\alpha+j\beta)\ell}{2} - \dot{u}_2 Z_{o_2} \sinh\frac{(\alpha+j\beta)\ell}{2}; \quad \dot{u}_3 = \dot{u}_2 \cosh\frac{(\alpha+j\beta)\ell}{2} - \frac{F_2}{Z_{o_2}} \sinh(\alpha+j\beta)\frac{\ell}{2}$$

$$F_4 = F_3 \cos\frac{\omega \ell}{4v} - j\dot{u}_3 Z_{o_1} \sin\frac{\omega \ell}{4v}\ ; \quad \dot{u}_4 = \dot{u}_3 \cos\frac{\omega \ell}{4v} - \frac{jF_3}{Z_{o_1}} \sin\frac{\omega \ell}{4v} \qquad (45)$$

Here ℓ is the total length of the sample, v the velocity of propagation, F the force and $\dot{u}$ the particle velocity, α is the attenuation in nepers/meter, β the phase shift in radians per meter - i.e. ω/v - Z_o the characteristic impedance of each section i.e. ρv times area. These units would be in the MKS system. For the cgs system which has largely been used in the mechanical properties of materials the attenuation and phase shift are 100 times as large while the characteristic impedance Z_o is 1000 times as large. The units used here are the cgs units.

If we combine these equations, we have the two

$$F_4 = F_1\left[\cosh(\alpha+j\beta)\frac{\ell}{2}\cos\frac{\omega\ell}{2v} + \frac{j\left(\frac{Z_{o_2}}{Z_{o_1}} + \frac{Z_{o_1}}{Z_{o_2}}\right)}{2}\sinh(\alpha+j\beta)\frac{\ell}{2}\sin\frac{\omega\ell}{2v}\right]$$

$$- j\dot{u}_1\left[Z_{o_1}\sin\frac{\omega\ell}{2v}\cosh\frac{(\alpha+j\beta)\ell}{2} - jZ_{o_2}\left[\cos^2\frac{\omega\ell}{4v} - \frac{Z_{o_1}^2}{Z_{c_2}^2}\sin^2\frac{\omega\ell}{4v}\right]\sinh(\alpha+j\beta)\frac{\ell}{2}\right]$$

$$\dot{u}_4 = \dot{u}_1\left[\cosh(\alpha+j\beta)\frac{\ell}{2}\cos\frac{\omega\ell}{2v} + \frac{j\left(\frac{Z_{o_2}}{Z_{o_1}} + \frac{Z_{o_1}}{Z_{o_2}}\right)}{2}\sinh(\alpha+j\beta)\frac{\ell}{2}\sin\frac{\omega\ell}{2v}\right] \quad (46)$$

$$- jF_1\left[\frac{\sin\frac{\omega\ell}{2v}\cosh\frac{(\alpha+j\beta)\ell}{2}}{Z_{o_1}} - \frac{j}{Z_{o_2}}\left[\cos^2\frac{\omega\ell}{4v} - \frac{Z_{o_2}^2}{Z_{o_1}^2}\sin^2\frac{\omega\ell}{4v}\right]\sinh\frac{(\alpha+j\beta)\ell}{2}\right]$$

Since $\alpha\ell$ is much smaller than $\beta\ell$, we can set

$$\cosh(\alpha+j\beta)\frac{\ell}{2} = \cosh\frac{\alpha\ell}{2}\cos\frac{\beta\ell}{2} - j\sinh\frac{\alpha\ell}{2}\sin\frac{\beta\ell}{2} = \cos\frac{\omega\ell}{2v} - j\frac{\alpha\ell}{2}\sin\frac{\omega\ell}{2v}$$

$$\sinh(\alpha+j\beta)\frac{\ell}{2} = \sinh\frac{\alpha\ell}{2}\cos\frac{\beta\ell}{2} + j\cosh\frac{\alpha\ell}{2}\sin\frac{\beta\ell}{2} = \frac{\alpha\ell}{2}\cos\frac{\omega\ell}{2v} + j\sin\frac{\omega\ell}{2v}$$

(47)

Since the force F_4 on the end of the sample is zero, we can solve for the ratio of $F_1/\dot{u}_1$ from the first of (46) and obtain the impedance of the sample. Introducing the values of (47) in (46) and separating out the real and imaginary parts, we have

$$Z_B = \frac{F_1}{\dot{u}_1} = \frac{j(Z_{o_1}+Z_{o_2})\sin\frac{\omega\ell}{2v}\left(\cos^2\frac{\omega\ell}{4v} - \frac{Z_{o_1}}{Z_{o_2}}\sin^2\frac{\omega\ell}{4v}\right) + \frac{A\ell}{2}\left[Z_{o_1}\sin^2\frac{\omega\ell}{2v} + Z_{o_2}\cos\frac{\omega\ell}{4v}\left(\cos^2\frac{\omega\ell}{4v} - \frac{Z_{o_1}^2}{Z_{o_2}^2}\sin^2\frac{\omega\ell}{4v}\right)\right]}{\left[\cos^2\frac{\omega\ell}{2v} - \frac{(Z_{o_1}^2+Z_{o_2}^2)}{2Z_{o_1}Z_{o_2}}\sin^2\frac{\omega\ell}{2v}\right] + j\frac{A\ell}{2}\left[\sin\frac{\omega\ell}{2v}\cos\frac{\omega\ell}{2v}\left(1 - \frac{(Z_{o_1}^2+Z_{o_2}^2)}{2Z_{o_1}Z_{o_2}}\right)\right]} \tag{48}$$

At the resonant frequency the imaginary part of the numerator is zero, which occurs when

$$\tan^2\frac{\omega\ell}{4v} = \frac{Z_{o_2}}{Z_{o_1}} = \left(\frac{D_2}{D_1}\right)^2 ; \quad \tan\frac{\omega\ell}{4v} = \frac{D_2}{D_1} \tag{49}$$

For this condition

$$\sin\frac{\omega\ell}{2v} = \frac{2\sqrt{Z_{o_1}Z_{o_2}}}{(Z_{o_1}+Z_{o_2})}; \quad \cos\frac{\omega\ell}{2v} = \frac{Z_{o_1}-Z_{o_2}}{Z_{o_1}+Z_{o_2}}; \quad \sin^2\frac{\omega\ell}{4v} = \frac{Z_{o_2}}{Z_{o_1}+Z_{o_2}}; \quad \cos^2\frac{\omega\ell}{4v} = \left(\frac{Z_{o_1}}{Z_{o_1}+Z_{o_2}}\right)$$

Introducing these values into (48), the impedance Z_B at resonance is

$$\frac{F_1}{\dot{u}_1} = \frac{Z_{o_1}\left(\frac{\alpha\ell}{2}\right)\left[\frac{4Z_{o_1}Z_{o_2} - (Z_{o_1}-Z_{o_2})^2}{(Z_{o_1}+Z_{o_2})^2}\right]}{-1 - j\,\frac{A\ell}{2}\left(\frac{Z_{o_1}-Z_{o_2}}{\sqrt{Z_{o_1}Z_{o_2}}}\right)} \tag{50}$$

The last term in the denominator is small compared to unity and can be neglected. Hence the resistance at resonance is

$$R_B = \frac{Z_{o_1}\alpha\ell}{2}\left[\frac{(Z_{o_1}-Z_{o_2})^2 - 4Z_{o_1}Z_{o_2}}{(Z_{o_1}+Z_{o_2})^2}\right] \tag{51}$$

If we expand (48) in powers of $\Delta\omega/\omega$ it is readily shown that

$$Z_B = R_B + j\, Z_{o_1} \left(\frac{\Delta\omega}{\omega}\right)\left(\frac{\omega_R \ell}{v}\right) \tag{52}$$

Comparing this with the reactance and resistance of a mass stiffness and resistance, we find

$$M = \frac{Z_{o_1} \ell}{2v} = \frac{\rho v s_1 \ell}{2v} = \frac{\rho s_1 \ell}{2} \tag{53}$$

This is half the mass of a sample of length ℓ, density ρ and area equal to the large part of the speciman. The stiffness S is determined from the resonant frequency f_R according to the equation

$$S = \omega_R^2 M = \omega_R^2 \left(\frac{\rho s_1 \ell}{2}\right) \tag{54}$$

The internal friction of the strained part of the sample which has a nearly uniform strain is given by

$$Q^{-1} = \frac{\alpha\ell}{\beta\ell} \text{ ; Hence } R_B = \frac{Z_o Q^{-1} \beta\ell}{2} \left[\frac{(Z_{o_1} - Z_{o_2})^2 - 4Z_{o_1} Z_{o_2}}{(Z_{o_1} + Z_{o_2})^2}\right] \tag{55}$$

Since $Z_o = s_1 \rho v$, $\beta = \omega_R / v$, this becomes

$$Q^{-1} = \frac{2R_B}{(s_1 \ell \rho)\omega_R} \left[\frac{(Z_{o_1} + Z_{o_2})^2}{(Z_{o_1} - Z_{o_2})^2 - 4Z_{o_1} Z_{o_2}}\right] = \frac{R_B}{\omega_R M} \left[\frac{(Z_{o_1} + Z_{o_2})^2}{(Z_{o_1} - Z_{o_2})^2 - 4Z_{o_1} Z_{o_2}}\right] \tag{56}$$

For the transformer of Fig. 4a, the correction factor is 1.4 times the ratio of resistance to reactance of the speciman.

The question arises as to how much the strain in the small part of the sample is increased and how uniform the strain is through the small section. A derivation is given here for the dissipationless case. However, the results should be quite accurate for even the highly stressed samples since the attenuation is small compared to the phase shift. To obtain the strain in the sample, we have to know the particle velocity at any point along the sample. From Equations (45) - neglecting dissipation - and replacing $\ell/2$ by x the distance from the junction in the second set of equations, we find that

$$\dot{u}_3 = u_1\left[\cos\frac{\omega\ell}{4v}\cos\frac{\omega x}{v} - \frac{Z_{o_1}}{Z_{o_2}}\sin\frac{\omega\ell}{4v}\sin\frac{\omega x}{v}\right] - jF_1\left[\frac{\sin\frac{\omega\ell}{4v}\cos\frac{\omega x}{v}}{Z_{o_1}} + \frac{\cos\frac{\omega\ell}{4v}\sin\frac{\omega x}{v}}{Z_{o_2}}\right] \tag{57}$$

At the resonant frequency $F_1 = 0$. Differentiating $\dot{u}_3$ by x, we find

$$\frac{\partial\dot{u}_3}{\partial x} = j\omega\frac{\partial u_3}{\partial x} = j\omega S_{11} = -\dot{u}_1\frac{\omega}{v}\left[\cos\frac{\omega\ell}{4v}\sin\frac{\omega x}{v} + \frac{Z_{o_1}}{Z_{o_2}}\sin\frac{\omega\ell}{4v}\cos\frac{\omega x}{v}\right] \tag{58}$$

At the edge of the sample x = 0 and

$$S_{11} = \frac{\dot{u}_1}{v}\left[\frac{Z_{o_1}}{Z_{o_2}} \times \sin\frac{\omega\ell}{4v}\right] \tag{59}$$

For the 5 to 1 sample of Fig. 4a, this gives

$$S_{11} = \frac{\dot{u}_1}{v}\left[\frac{Z_{o_1}}{Z_{o_2}}\sqrt{\frac{Z_{o_2}}{Z_{o_1}+Z_{o_2}}}\right] = \frac{\dot{u}_1}{v}\left[25\sqrt{\frac{1}{26}}\right] = 4.9\,\frac{\dot{u}_1}{v} \tag{60}$$

At the center of the sample the strain is

$$\frac{\dot{u}_1}{v}\left[\left(\frac{Z_{o_1}}{Z_{o_2}}+1\right)\frac{\sin\frac{\omega\ell}{2v}}{2}\right]=\frac{\dot{u}_1}{v}\left[\left(\frac{Z_{o_1}+Z_{o_2}}{Z_{o_2}}\right)\frac{\sqrt{Z_{o_1}Z_{o_2}}}{Z_{o_1}+Z_{o_2}}\right]=\frac{\dot{u}_1}{v}\sqrt{\frac{Z_{o_1}}{Z_{o_2}}}=5\,\frac{\dot{u}_1}{v} \quad (61)$$

Hence the strain is very uniform through the small part of the sample. With this small length sample no trouble has been experienced with the generation of flexure modes. Since the strain in the transformer is from Equations (3), equal to $\dot{u}_1/v$, the sample has increased the strain in the small section by a factor of 5.

D. Exponential Horns

The other type of a mechanical transformer used in these measurements is the exponential horn shown by Fig. 4b. This has the advantage of being able to produce a larger strain in the speciman, but since its transformation ratio is less for a given ratio of input to output radii it does not concentrate the damping in the speciman as well as the stub transformer does. If the damping is very large, this is an advantage.

The equations for an exponential horn have been previously discussed[11] and will be outlined only here. Since the largest diameter used is less than a quarter-wave length, the elastic modulus can be taken without much error to be the Young's modulus Y_o. Normal horn theory gives a good representation of the measured results. The equation for a horn, first given by A. G. Webster,[12] is

$$\frac{d^2\dot{u}}{dx^2}+\frac{1}{s}\frac{ds}{dx}\frac{d\dot{u}}{dx}+\frac{\omega^2}{v^2}\dot{u}=0 \quad (62)$$

where s is the cross-sectional area of the horn. For an exponentially varying area, we can write

$$s = s_o e^{-\gamma x} \quad \text{or} \quad \gamma = \frac{1}{\ell} \frac{s_o}{s_1} \tag{63}$$

where s_o is the initial area and s_1 the final area at a distance ℓ from the beginning. For the exponential taper, Equation (62) becomes

$$\frac{d^2\dot{u}}{dx^2} - \gamma \frac{d\dot{u}}{dx} + \frac{\omega^2}{v^2}\dot{u} = 0 \tag{64}$$

A solution of this equation is

$$\dot{u} = e^{\gamma x/2}\left[A\cos\frac{\omega x}{v'} + B\sin\frac{\omega x}{v'}\right] \text{ where } v' = \frac{v}{\sqrt{1 - \frac{\gamma^2 v^2}{4\omega^2}}} \tag{65}$$

A and B are constants and v' is the wave velocity in the tapered rod. In order to make v' real, we must have

$$\omega = 2\pi f \geq \frac{\gamma v}{2} \quad \text{or} \quad f_o = \gamma v/4\pi \tag{66}$$

Below f_o, the velocity v is imaginary. This corresponds to an attenuation without phase shift. Above f_c, real propagation takes place and the horn acts as a transformer. On account of the term $e^{\gamma x/2}$, the particle velocity increases as the square root of the ratio s_o/s_1 and therefore the ratio of the starting diameter D_o to the final diameter D_1.

The tapered rods are ordinarily used as half wave length devices for which the stresses are low at the two ends. The stress at any point x is given in terms of the particle displacement u and the particle velocity $\dot{u}$ by

$$T = -\frac{Y_o \partial u}{2x} = -\frac{Y_o}{j\omega}\frac{\partial \dot{u}}{\partial x} = \frac{jY_o}{\omega}\left\{\epsilon^{\gamma x/2}\left[\left(\frac{A\gamma}{2}+\frac{\omega B}{v'}\right)\cos\frac{\omega x}{v'}+\left(\frac{B\gamma}{2}-\frac{A\omega}{v'}\right)\sin\frac{\omega x}{v'}\right]\right\} \quad (67)$$

If we terminate the horn in the impedance of the speciman which is adjusted to resonate at the half-wave frequency of the horn, we can set

$$\frac{F}{\dot{u}} = Z_B = R_B + jZ_{o_1}\left(\frac{\Delta f}{f_R}\right)\frac{\omega_R \ell}{V} = \frac{Ts_1}{\dot{u}_1} = \frac{jY_o s_o}{\omega}\;\frac{\left[\epsilon^{-\gamma\ell/2}\;\left(\frac{A\gamma}{2}+\frac{\omega B}{v'}\right)\cos\frac{\omega\ell}{v'}+\left(\frac{B\gamma}{2}-\frac{A\omega}{v'}\right)\sin\frac{\omega\ell}{v'}\right]}{\epsilon^{\gamma\ell/2}\left[A\cos\frac{\omega\ell}{v'}+B\sin\frac{\omega\ell}{v'}\right]}$$

(68)

since $s_1 = s_o\epsilon^{-\gamma\ell}$. Since $\cos\frac{\omega\ell}{v'} = -1$ and $\sin\frac{\omega\ell}{v'} = 0$, this equation determines a relation between A and B

$$B = \frac{Av'}{\omega}\left[\frac{-\gamma}{2}+\frac{Z_B\omega\epsilon^{\gamma\ell}}{jY_o s_o}\right] \quad (69)$$

The impedance "looking" into the horn at x = 0, is

$$\frac{F_o}{\dot{u}_o} = \frac{Ts_o}{\dot{u}_o} = \frac{jY_o s_o}{\omega}\;\frac{\left[A\;\frac{\gamma}{2}+\left(\frac{\omega}{v'}\right)\left(\frac{v'}{\omega}\right)\left(-\frac{\gamma}{2}+\frac{Z_B\omega\epsilon^{\gamma\ell}}{jY_o s_o}\right)\right]}{A} = Z_B\epsilon^{\gamma\ell} = \frac{Z_B s_o}{s_1} \quad (70)$$

Therefore the horn working at its half wave frequency steps up the terminating impedance in the ratio s_o/s_1, the area ratio.

We are also interested in the maximum strain in the horn required to produce a given particle velocity $\dot{u}_1$, at the small end of the horn. The strain is given by

$$S_{11} = \frac{\partial u}{\partial x} = \frac{1}{j\omega}\left(\frac{\partial \dot{u}}{\partial x}\right) = \frac{j}{\omega} \epsilon^{\gamma x/2}\left\{ \left(\frac{A\gamma}{2} + \frac{\omega}{v'} B\right) \cos\frac{\omega x}{v'} + \left(\frac{B\gamma}{2} - \frac{A\omega}{v'}\right) \sin\frac{\omega x}{v'} \right\} \tag{71}$$

When the terminating impedance Z_B is zero we have from (69)

$$B = \frac{-Av'}{2\omega} \gamma \tag{72}$$

Hence the strain as a function of the distance x is

$$S_{11} = \frac{-jA\epsilon^{\gamma x/2} \sin\frac{\omega x}{v'}}{\sqrt{1 - \frac{\gamma^2 v^2}{4\omega^2}}} \tag{73}$$

The strain is zero on the two ends and reaches a maximum at a distance of 71 percent from the large diameter. Since the velocity on the end is

$$\dot{u} = A\epsilon^{\gamma \ell/2} \tag{74}$$

we have the relation

$$\dot{u} = \frac{vS_{11}\sqrt{1 - \frac{\gamma^2 v^2}{4\omega^2}}}{\epsilon^{\gamma(x-\ell)/2} \sin\frac{\omega x}{v'}} = \phi v S_{11} \tag{75}$$

If we insert the value of x corresponding to the point of maximum strain it has been shown[7] that the factor $\phi \doteq 2.72$. Hence the exponential horn will produce a larger particle velocity $\dot{u}$ for a given maximum strain than will a stub transformer.

When the measuring frequency is slightly off resonance it is readily shown by expanding $(\omega_R+\Delta\omega)\ell/v' = \omega_R\ell/v' \; (1 + \Delta\omega/\omega_R)$ that the effective mass at the input of the horn, the effective stiffness and the resistance values are

$$M = \frac{1}{2}\,\rho\ell s_o; \quad S = \frac{\pi^2}{2}\,\frac{Y_o s_o}{\ell\left(1 - \frac{\gamma^2 v^2}{4\omega^2}\right)}; \quad R = Z_o\,\frac{\pi}{2}\,Q^{-1} \tag{76}$$

where $Z_o = \sqrt{\rho Y_o/(1 - \gamma^2 v^2/4\omega^2)}\;s_o$. The resistance of the horn and transducer are separately determined and subtracted from the measured value of the sample, transducer and horn. Fig. 5 curve C shows a measurement of the mechanical resistance of exponential aluminum horn and transducer.

To determine the internal resistance of the sample the resistance of the horn and sample are subtracted. From Equation (56) the internal friction Q^{-1} of the small, highly strained part of the sample is equal to the resistance measured at the transducer divided by the effective mass of the sample multiplied by the transformation ratio of the horn and by the ratios of the characteristic impedances of the large and small portions of the speciman.

E. Transducer Equations and Methods For Evaluating the Internal Friction, the Modulus Defect and the Longitudinal Strain

All the measurements required to determine the internal friction, modulus defect or longitudinal strain involve measuring the applied voltage, a pick-up voltage obtained from an electrode on the transducer or the voltage generated by an electrostatic pick-up device. The latter device is used as a calibration device after which all quantities can be determined from the applied and pick-up voltages. Hence it is necessary to derive the transducer equations in order to evaluate these measurements.

The transducer system, as shown by Fig. 4a consists of a ceramic transducer - in this case Clevite PZT4 - constructed in the form of a concentric cylinder of outside radius r_2, inside radius r_1 and length ℓ. The inside surface is completely silvered while the outside surface has one large electrode and two small electrodes near the driving end. The electrode nearest the transformer acts as a pick-up electrode, the next electrode is a grounded electrode to prevent any electrostatic pick-up between the large driving electrode and the pick-up electrode. For the transducer used on the stub transformer the total length is 9.85 centimeters and the distance from the free end of the transducer to the center of the pick-up electrode is 9.48 cms. The pick-up electrode is 0.635 cms wide and its edge is 0.053 cms from the driving end of the transducer. An insulated space of 1/8 inch (0.318 cms) separates the shielding electrode (0.635 cms) from the driving and pick-up electrodes. Hence the total length of the driving electrode is 7.89 cms.

The transducer is strongly cemented to the transformer by an epoxy resin. Before cementing the transducer its resonant frequency was measured to be 15,490 cycles. This determines the compliance modulus and the velocity of propagation to be

$$s_{11}^E = 1.46\times10^{-11}\ M^2/\text{Newton or } 1.46\times10^{-12}\ \text{cms}^2/\text{dyne},$$
$$v = 3.03\times10^5 \text{cms/sec} \tag{77}$$

since the density is 7.5 grams/cm^3 or 7.5×10^3 kilograms/M^3.

The equations of motion of a transducer without dissipation are well known to be[13]

$$(F+\varphi V_A) = (F_1+\varphi V_A)\cos\frac{\omega x}{v} - j\dot{u}_1 Z_T \sin\frac{\omega x}{v}$$
$$\dot{u} = \dot{u}_1 \cos\frac{\omega x}{v} - \frac{j(F_1+\varphi V_A)}{Z_T}\sin\frac{\omega x}{v} \tag{78}$$
$$i = V_A(j\omega C_o) - \varphi(\dot{u}_2 - \dot{u}_1)$$

where F is the force applied to the transducer at a distance x, from the free end, F_1 is the force on the free end, $\dot{u}$ the particle velocity at the free end, i the current into the transducer, V_A the applied voltage, φ the electro-mechanical transformation ratio and Z_T the characteristic impedance of the transducer which is equal to $\pi(r_2^{\,2}-r_1^{\,2})\rho v$ where ρ is the density and v the sound velocity in the transducer. With the dimensions of the transducer $r_2 = 2.86$ cms, $r_1 = 2.22$ cms this impedance becomes 2.33×10^7 cgs mechanical ohms or 2.33×10^4 MKS mechanical ohms. The value of φ, the force voltage ratio is

$$\varphi = \frac{d_{31}(\text{area})}{s_{22}^E(\text{thickness})} = \frac{d_{31}\pi(r_2^{\,2}-r_1^{\,2})}{s_{22}^E(r_2-r_1)} = \frac{d_{31}\pi(r_2+r_1)}{s_{22}^E} \tag{79}$$

where d_{31} is the piezo-electric constant which for PZT4 is given[14] as 123×10^{-12} coulombs per Newton. Since the value may be slightly different for the transducer with partial plating, the value is determined from the measurements of the electrostatic pick-up device. The value of 121×10^{-12} calibrated is close to the quoted value.

When account is taken of the dissipation in the transducer, Equation (78) becomes

$$
\begin{aligned}
(F+\varphi V_A) &= (F_1+\varphi V_A)\cosh(\alpha+j\beta)x - \dot{u}_1 Z_T \sinh(\alpha+j\beta)x \\
\dot{u} &= \dot{u}_1 \cosh(\alpha+j\beta)x - \left(\frac{F_1+\varphi V_A}{Z_T}\right)\sinh(\alpha+j\beta)x
\end{aligned}
\qquad (80)
$$

where α is the attenuation per unit length and $\beta = \omega/v$ is the phase shift in radians per unit length. Since the voltage in the pick-up plating is proportional to the strain in the pick-up, we wish to know the strain as a function of the distance along the transducer. From the second of Equations (80)

$$
S_{11} = \frac{\partial u}{\partial x} = \frac{\partial \dot{u}}{\partial x} \times \frac{1}{j\omega} = \frac{\alpha+j\beta}{j\omega}\left[\dot{u}_1 \sinh(\alpha+j\beta)x - \left(\frac{F_1+\varphi V_A}{Z_T}\right)\cosh(\alpha+j\beta)x\right] \qquad (81)
$$

Since the end of the transducer is free, $F_1 = 0$. At the end of the transducer $x = \ell$, the ratio of $F_2/\dot{u}_2 = Z_B$, where Z_B is the mechanical impedance looking into the transformer and speciman. Replacing x by ℓ the equations to solve are

$$
\begin{aligned}
\dot{u}_2 &= \left[\varphi V_A(\cosh(\alpha+j\beta)\ell - 1) - \dot{u}_1 Z_T \sinh(\alpha+j\beta)\ell\right] / Z_B \\
\dot{u}_2 &= \dot{u}_1 \cosh(\alpha+j\beta)\ell - \frac{\varphi V_A}{Z_T} \sinh(\alpha+j\beta)\ell
\end{aligned}
\qquad (82)
$$

Solving for $\dot{u}_1$ we find

$$\dot{u}_1 = \frac{\varphi V_A}{Z_T}\left[\frac{\cosh(\alpha+j\beta)\ell - 1 + \frac{Z_B}{Z_T}\sinh(\alpha+j\beta)\ell}{\frac{Z_B}{Z_T}\cosh(\alpha+j\beta)\ell + \sinh(\alpha+j\beta)\ell}\right] \qquad (83)$$

As long as $(Z_B/Z_T) = [R_B + j2K(\Delta f/f_R)](D_1/D_2)^4 \Big/ Z_T$ -where $K = S_B/\omega_R$ - is smaller than unity we can replace

$$\sinh(\alpha+j\beta)\ell = \alpha\ell\cos\frac{\omega\ell}{v} + j\sin\frac{\omega\ell}{v} = \alpha\ell\left(\cos\frac{\omega_R}{v}\cos\frac{\Delta\omega\ell}{v} - \sin\frac{\omega_R\ell}{v}\sin\frac{\Delta\omega\ell}{v}\right) +$$

$$+ j\left(\sin\frac{\omega_R\ell}{v}\cos\frac{\Delta\omega\ell}{v} + \cos\frac{\omega_R\ell}{v}\sin\frac{\Delta\omega\ell}{v}\right) = -\alpha\ell - j\frac{\Delta\omega\ell}{v} = -\left(\alpha\ell + j\frac{\pi\Delta f}{f_R}\right)$$

$$\cosh(\alpha+j\beta)\ell = -1 + j\pi\alpha\ell(\Delta f/f_R)$$

If we insert these values in the denominator of (83) and determine the minimum value, this results when $\Delta f = 0$ or the transducer resonates at the unloaded resonant frequency as long as Z_B resonates at this frequency. Hence the expressions for $\dot{u}_1$ and $\dot{u}_2$ become

$$\dot{u}_1 = \varphi V_A\left[\frac{-2-\alpha\ell R_B/Z_T}{-[R_B+Z_T\alpha\ell]}\right]; \qquad \dot{u}_2 = -\varphi V_A\left[\frac{2-(\alpha\ell)^2}{R_B+Z_T\alpha\ell}\right] \qquad (84)$$

Inserting this value of $\dot{u}_1$ in Equation (81) we find

$$S_{11} = \frac{(\alpha+j\beta)\ell}{j\omega\ell Z_T}\left[\frac{[2+\frac{\pi}{2}Q^{-1}\frac{R_B}{Z_T}]}{\left(\frac{R_B}{Z_T}+\frac{\pi}{2}Q^{-1}\right)}\left[\frac{\pi Q^{-1}}{2}\left(\frac{\omega_R x}{v}\right)\cos\frac{\omega_R x}{v} + j\sin\frac{\omega_R x}{v}\right] - \left[\cos\frac{\omega_R x}{v} + j\frac{\pi}{2}Q^{-1}\sin\frac{\omega_R x}{v}\right]\right] \qquad (85)$$

As long as the value of Q^{-1} of the transducer is small and R_B/Z_T is smaller than unity, this expression reduces to

$$S_{11} = \frac{\varphi V_A}{vZ_T}\left[\frac{2j \sin \frac{\omega x}{v}}{\frac{R_B}{Z_T} + \frac{\pi}{2} Q^{-1}}\right] \tag{86}$$

Up to values of $(R_B/Z_T + (\pi/2) Q^{-1})$ of 0.25 the corrections terms are small and Equation (86) gives reasonable results. For higher damping values it is more desirable to use the exponential horn since this gives only 23 percent of the damping that the stub transformer does.

The distance from the center of the pick-up electrode is 9.48 cm, $v = 3.03\text{x}10^5$ cms/sec. If ω is the resonant frequency 2πx15, 490 then

$$\sin \frac{\omega_R \text{x} 9.48}{3.03\text{x}10^5} = \sin 174^\circ = 0.1045; \quad \cos 174^\circ = -0.9945 \tag{87}$$

The device will also work over a frequency range from 15200 to 15700, which involves a range of values of the sine term.

Since the impedance of the pick-up electrode is in the order of 4000 ohms at the resonant frequency, any voltmeter will measure the open circuit voltage. This is determined by the average strain in the pick-up electrode. For a zero current drawn from the ceramic, the relation between the strain and the open circuit voltage is from the last of Equations (78)

$$V_{pu}(j\omega C_o) = \varphi(\dot{u}_2 - \dot{u}_1) = j\omega\varphi(u_2 - u_1) \quad \text{or } V_{pu} = \frac{\varphi(u_2-u_1)}{C_o} \tag{88}$$

Since the strain is $(u_2-u_1)/\ell_E$ and $C_o = \pi(r_1+r_2)\ell_E\epsilon^T/r_2-r_1$, the open circuit voltage is

$$V_{pu} = + \frac{\varphi S_{11}(r_2-r_1)}{\pi(r_1+r_2)\epsilon^T} \quad ; \quad \epsilon^T = \text{free dielectric constant} \tag{89}$$

Inserting the value of S_{11} from (88), the ratio of the pick-up voltage to the applied voltage is

$$\frac{V_{pu}}{V_A} = \frac{\varphi^2(r_2-r_1)}{(r_2+r_1)\pi v\epsilon^T Z_T} \left[\frac{2j \sin \omega x/v}{Z_B/Z_T + \pi/2\ Q^{-1}}\right] \tag{90}$$

when we use the relation $\omega\ell/v = \pi$. Inserting the value of φ^2 from (79) and $v = 1/\sqrt{\rho s_{22}}$, we have

$$\frac{V_{pu}}{V_A} = \frac{d_{31}^2}{s_{22}^E\epsilon^T} \left[\frac{\pi(r_2^2-r_1^2)\sqrt{\rho/s_{22}^E}}{Z_T}\right]\left[\frac{2j \sin \frac{\omega x}{v}}{Z_B/Z_T + \pi/2\ Q^{-1}}\right] \tag{91}$$

Since $\pi(r_2^2-r_1^2)\sqrt{\rho/s_{22}^E}$ is the characteristic impedance of the transducer and $d_{31}^2/s_{22}^E\epsilon^T$ is the square of the electromechanical coupling factor, this reduces to

$$\frac{V_{pu}}{V_A} = k^2 \left[\frac{2j \sin \frac{\omega x}{v}}{Z_B/Z_T + \pi/2\ Q^{-1}}\right] \tag{92}$$

Hence by determining the coupling coefficient, the ratio of the pick-up voltage to the applied voltage will determine the resistance R_B applied to the transducer in terms of the transducer characteristic impedance Z_T. As long as Z_B/Z_T is small the first term predominates and the second can be neglected. It will be noted that the second term places a limit on the ratio of Z_B/Z_T that can be measured. Since the phase angle of the ratio V_{pu}/V_A is not measured we deal with the absolute values. This results in

$$\frac{Z_B}{Z_T} + \frac{\pi}{2} Q^{-1} = 2k^2 \frac{V_A}{V_{pu}} \sin \frac{\omega x}{v} \tag{93}$$

We are also interested in the strain in the transformer and the strain in the sample as measured by the applied and pick-up voltages. These values can be calculated from the displacement velocity $\dot{u}_2$ given by Equation (84). Since the velocity is continuous across the interface, the velocity on the end of the transformer will be $\dot{u}_2$ multiplied by the transformation ratio $(D_1/D_2)^2=25$ for the transformer shown by Fig. 4a. From Equation (3), the strain at the center of the transformer is

$$S_{11} = \frac{\dot{u}}{v} = \frac{25\text{x}2\varphi(V_A)}{(Z_B+Z_T\alpha\ell)v} = \frac{50V_A d_{31}}{(r_2-r_1)(\frac{Z_B}{Z_T} + \frac{\pi}{2} Q^{-1})} \tag{94}$$

when we insert the value of φ and $Z_T = \pi(r_2^2-r_1^2)\sqrt{\rho/s_{22}^E}$. The strain generated depends on the degree of damping of the horn and speciman. If we insert the value of the damping from (93) the strain is equal to

$$S_{11} = \frac{25V_{pu}s_{22}^E \epsilon^T}{d_{31}\sin\frac{\omega x}{v}(r_2-r_1)} \tag{95}$$

Hence the maximum strain in the transformer is directly proportional to the pick-up voltage.

Since the velocity is continuous between the transformer output and speciman input, then since the strain in the sample is from Equation (61) equal to

$$S_{11} = \frac{5\dot{u}_1}{v_5} \tag{96}$$

the strain in the sample is 5 times that in the horn, if the velocity of the sample is the same as that in the horn; otherwise the value is

$$S_{11_S} = \frac{5v_H}{v_S} \times S_{11_H} \tag{97}$$

It will be noted that the correction terms disappear if the pick-up electrode is located at the center of the transducer. Furthermore the ratio of the pick-up voltage to the applied voltage increases for a given value of $Z_B/Z_T + (\pi/2)Q^{-1}$. Hence a higher damping value can be measured with this form of plating arrangement. It is also obvious that a slight variation of frequency from the resonant frequency will not cause a change in sensitivity since the value of $\sin(\omega x/v)$ changes very little.

This type of arrangement was tried on the transducer mounted on the exponential horn. The electrode arrangement is shown by Fig. 7. To preserve symmetry two small pick-up electrodes are used mounted diametrically opposite. These are surrounded by narrow grounded electrodes to prevent pick-up from the driving electrodes. The area of each of the pick-up electrodes is 1 square centimeter which gives an impedance of 12,200 ohms at the resonant frequency of 17,500 cycles. With this type of electrode the ratio of $(Z_B/Z_T + \pi/2\, Q^{-1})$ and the strain in the speciman are equal to

$$\frac{Z_B}{Z_T} + \frac{\pi}{2} Q^{-1} = 2k^2 x \left(\frac{V_A}{V_{pu}}\right); \quad S_{11} = \frac{5x(T.R)xV_{pu} x s_{22}^{T}}{d_{31} x (\gamma_2 - \gamma_1)} = 1.1x10^{-6} (T.R.) x V_{pu} \tag{98}$$

where TR is the transformation ratio. In order to measure a high internal friction in the sample, at a high strain, a lower transformation ratio (TR) is desirable. The internal friction Q^{-1} in the sample was shown to be (Eq. 56).

$$Q^{-1} = \frac{R_B x 1.4}{\omega_R M (TR)^2} = \frac{2.22x10^{-6} R_B}{(TR)^2} \tag{99}$$

where M, the mass of the sample is a half the total weight or 6.5 grams. This is multiplied by $(TR)^2$ to give the reactance at the same spot that R_B is measured.

Hence we find that

$$\frac{R_B}{Z_T} = \frac{(TR)^2 Q^{-1}}{(51.6)}; \quad V_{pu} = \left(\frac{2k^2}{R_B/Z_T}\right) V_A = \frac{174x51.6 V_A}{(TR)^2 Q^{-1}}, \quad S_{11} = \frac{10^{-5} V_A}{(TR) Q^{-1}} \tag{100}$$

With 250 volts available and a transformation ratio of 12 for the exponential horn, a Q^{-1} of 0.20 can be measured for an rms strain of 10^{-3}. For larger strains or higher values of internal friction, a larger amplifier is desirable. With a strain of 10^{-3} in the sample the maximum strain in the horn is $1.36x10^{-4}$ and the strain in the transducer is 2.75×10^{-5}. Hence all the components are in the linear range except for the speciman.

F. Calibration of Properties of the System By Means of an Electrostatic Pickup

Since it is desirable to prove experimentally the equations derived above and also to obtain exact values for the constants entering the equations it is necessary to measure the displacements on the ends of the horn or sample by means of a displacement measuring device. The simplest such device, and the easiest one to calibrate is an electrostatic pick-up device, which for this system is shown in Fig. 8. For this case a micrometer, calibrated in mil inches, is mounted on an insulated panel and backed off a known distance from the position that electrical contact is made with the horn. The horn is grounded and is connected to a 45 volt battery on one end and to the grounded terminal of a 10 megohm voltmeter. The battery is connected to a megohm resistor, the end of which is connected to the active side of the voltmeter and to the micrometer. The wire to the micrometer is run in a shielded cable in order to prevent pick up from outside sources. The shield of the cable is grounded and hence a static capacitance is put across the input to the voltmeter. In order to find out how much this capacitance was, a 100 picofarad condenser was put across the input and the voltage ratio was measured for a given setting of the micrometer. The ratio indicated a capacitance of 117 picofarads across the input.

Since there is no assurance that the micrometer and end surface of the horn are exactly parallel, the voltage pick up was measured when the setting was 2 mil inches and 4 mil inches spacing from the point where electrical contact was maintained with the horn. From the theory of the electrostatic pick up,[15] the alternating voltage generated is

$$V = \frac{V_o \frac{\delta x}{x} C_T}{C_T + C_o} = \frac{45 \times \frac{\delta x}{d\mathrm{x}10^{-3}} \left(\frac{8.85\mathrm{x}10^{-14}\mathrm{x}s}{d\mathrm{x}10^{-3}\mathrm{x}2.54}\right)}{117\mathrm{x}10^{-12} + \left(\frac{8.85\mathrm{x}10^{-14} s}{d\mathrm{x}10^{-3}\mathrm{x}2.54}\right)} \tag{101}$$

where d is the spacing in mil inches. The diameter of the micrometer was 0.3 inches so that s the area is 0.455 sq. cms. The displacement δx from Equation (1) is inserted in (101) and the complete equation reduces to

$$V = \frac{8.72 \times 10^3 S_{11}}{d} \Big/ (1 + 7.41d) \tag{102}$$

since the length of the small diameter of the horn is 3.06 inches. When the spacing d was 2 mil inches beyond contact, the voltage pick up was 0.079 volts while when d was increased to 4 mil inches, the voltage was 0.025 volts. To determine the actual displacement taking account of non-parallelism, the equation to solve is

$$\frac{0.079}{0.025} = 3.6 = \frac{(d+2)\,(1+7.41\,(d+2)\,)}{d\,(1+7.41d)} \tag{103}$$

This is a quadratic equation which has the solution d = 2.5 mils. Hence the strain is from Equation (102) since d = 4.5 mils,

$$0.025 = \frac{1.94\text{x}10^{-4} S_{11}}{1 + 33.2} = 568\ S_{11} \qquad (104)$$

Hence the indicated strain - which will be the r.m.s. strain, i.e. $(2/\pi)$ times the maximum strain, since the voltage measured is r.m.s.- is

$$S_{11} = 4.4\text{x}10^{-5} \qquad (105)$$

The applied and pick-up voltages V_A and V_{pu} for this case were

$$V_A = 1.5;\ V_{pu} = 0.95;\ f_R = 15470 \qquad (106)$$

Hence from Equation (86) - neglecting the square root term - the strain indicated by the measurement is

$$S_{11} = \frac{25\text{x}0.95\text{x}1.46\text{x}10^{-11}\text{x}1300\text{x}8.85\text{x}10^{-12}}{d_{31}\text{x}0.118\text{x}0.635\text{x}10^{-2}} = \frac{5.31\text{x}10^{-15}}{d_{31}} \qquad (107)$$

Setting $S_{11} = 4.4\text{x}10^{-5}$, gives a value of d_{31} equal to $121\text{x}10^{-12}$, which is in good agreement with the listed value.[14] With this value the coupling coefficient squared is

$$k^2 = \frac{d_{31}^{\ 2}}{s_{22}^{\ E}\epsilon^T} = \frac{(1.21\text{x}10^{-10})^2}{1.46\text{x}10^{-11}\text{x}1300\text{x}8.85\text{x}10^{-12}} = 0.087 \qquad (108)$$

Using these values, a set of curves can be drawn for the stub transformer system for various frequencies of operation as shown by Fig. 9. This is given for ratios of applied to pick-up voltages from 0.1 to 20 since larger ratios do not give good measurements. These determine the ratio of $(Z_B/Z_T + (\pi/2) Q^{-1})$ as a function of V_A/V_{pu}. From (95) the strain is determined by $(Z_B/Z_T + (\pi/2) Q^{-1})$ and the applied voltage V_A. A single curve on Fig. 9 shows the relation between $(Z_B/Z_T + (\pi/2) Q^{-1})$ and the strain in the stub transformer. This has to be multiplied by $5V_A$ to give the strain in the speciman. A single curve suffices for the transducer with pick-up electrode at the center. This relation is shown in Fig. 10, for the exponential horn of Fig. 4b.

The ratio of the electrostatic pick-up voltage has been compared with the transducer pick-up voltage over a wide range of inputs and the two are found to be proportional. The electrostatic voltage at the end of the sample has been found to be the same as that at the end of the transformer for the same transducer pick-up voltage. Hence the input and output velocities are the same as is expected from Equation (46) with the dissipation neglected. This verifies that the strain in the speciman is in agreement with theory.

IV. Experimental Results

A large number of internal friction and modulus defect measurements have been made over wide frequency and amplitude ranges by the techniques discussed in Sections II and III. It is the purpose of this section to show some typical measurements which illustrate the mechanisms discussed in Section 5.

Typical of low frequency measurements are the results of Figs. 11 and 12. Fig. 11 shows measurements[16] of the internal friction of 99.999 percent pure copper as a function of strain amplitude for a flexure bar at 2000 cycles. The strains shown are the maximum values for the vibration. The effect of adding certain percentages of zinc is to lower the internal friction in the linear region and to raise the strain for which the internal friction starts to increase. Somewhat similar results[17] are shown in Fig. 12 for a 99.995 percent pure aluminum crystal measured as a function of strain amplitude and temperature.

The data of Fig. 11 shows the effects of impurity atoms introduced in the pure material in pinning dislocations. This results in a lower internal friction in the linear range and an increase in the strain range for which the internal friction is independent of the amplitude. This relation between internal friction and modulus defect and the number of pinning points on a dislocation has been used[18] to study radiation damage and the diffusion of point defects. The data of Fig. 12, shows that for a given impurity content the dislocations in aluminum are more closely pinned than in copper. The cause of the different pinning distances in different metals is not clearly understood. For titanium for which data are given in Fig.16 , it appears that the pinning is much closer still and dislocation effects do not occur up to strains of 10^{-3} or higher. The data of Fig. 12 show also that temperature has a large effect on the number of pinning points. At high temperatures the pins seem to be boiled off the dislocations and the internal friction increases and the non-linear effect occurs at smaller stresses.

High frequency ultrasonic measurements have been used to study the damping mechanisms of dislocations. This follows from the fact that dislocations are overdamped and the internal friction that they produce above the peak value falls off inversely proportional to the frequency. Fig. 19 shows the calculation of Oen, Holmes and Robinson[19] for the internal friction due to dislocations for two different types of loop length distributions. The internal friction is plotted against a normalized angular frequency ω_o equal to

$$\omega_o = \frac{\mu b^2}{B\ell_o^2} \qquad (109)$$

where ℓ_o is the loop length for a delta function distribution or the exponent in the distribution function

$$N(\ell) = \frac{\bar{N}}{\ell_o^2} \epsilon^{-\ell/\ell_o} \qquad (110)$$

where $N(\ell)$ is the number of loops having a length ℓ and $\bar{N}$ the total number of dislocations per square cm. At frequencies above the peak value the internal friction approaches the value

$$Q^{-1}f = \frac{\mu b^2 \bar{N} R}{2\pi B} \tag{111}$$

Hence if the product $Q^{-1}f$ can be approximated and $\bar{N}$ determined by etch pit counts or by X-ray scattering the value of B can be determined. $\bar{N}$ usually cannot be determined better than a factor of 3 to 5 so that B is not accurately determined. However the variation with temperature can be determined and compared with different models for the damping mechanisms. The internal friction is related to the attenuation by the equation

$$\alpha = \frac{\omega Q^{-1}}{2v} \tag{112}$$

where α is in nepers per cm and v the velocity of propagation. Since one neper is 8.68db, this can be expressed in terms of

$$\alpha_{(db/cm)} = \frac{8.68\omega Q^{-1}}{2v} \tag{113}$$

Fig. 20 shows the normalized attenuation plotted against the normalized frequency. This is the type of curve which has to be compared with the attenuation due to dislocations in order to obtain the drag coefficient B. Since the sound velocity of Equation (113) usually runs from $(0.1 \text{ to } 1.0)\times 10^6$, Equation (113) can be expressed in terms of the attenuation in db per microsecond by the equation

$$\frac{\alpha}{(\frac{1}{v})} = \frac{\text{db}}{(\text{delay for 1 cm})} = \frac{\text{db}(0.1 \text{ to } 1.0)}{\text{microsecond}} = 4.34\ \omega Q^{-1} \tag{114}$$

and this expression is often used.

In order to obtain the damping coefficient B it is necessary to separate out the dislocation component from other sources of attenuation. This has been done by a variety of techniques. For copper the attenuation of well annealed single crystals have been measured over a wide frequency range,[20] after which the crystals have been neutron irradiated. The difference of the attenuation measured before and after irradiation is taken as the dislocation component. Using this technique Granato and Sterns[20] and Alers and Thompson have concluded that the drag coefficient B is around 6.5×10^{-4} dyne-sec/cm^2 at room temperature. For lithium fluoride the pinning points appear to pin the dislocations at room temperature and to produce any dislocation attenuation it is necessary to introduce fresh dislocations by deforming the crystal. A dislocation component has been derived by O.M.M. Mitchell[21] which gradually disappears at room temperature and within an hour at 100°C. Using this component she finds $B \doteq 3.5 \times 10^{-4}$. Other experimenters[22] find values from 7 to 13×10^{-4} dyne-sec/cm^2. The writer has recently measured the attenuation of lead[23] and aluminum[24] over a wide frequency and temperature range and found that it was possible to separate the measured attenuation into a dislocation component and a square law component which could be separately evaluated. Fig. 13 shows a measurement for one of the shear waves in aluminum. This process has recently been applied to copper crystals and Fig. 14 shows a measurement of one of the shear waves for copper. Using this technique the damping coefficient has been evaluated over a wide temperature range with results which will be discussed in the next section.

The final set of data were obtained by using the high amplitude measuring device discussed in detail in Section III. Fig. 15 shows the modulus defect and the internal friction Q^{-1} for two different types of aluminum. One is the standard 7075T6 aluminum which has the composition Aℓ 91%, Mg 2.8%, Zn 6% with traces of other materials. This has a static yield stress of 78,000 lbs/sq. inch (5.35×10^9 dynes/cm^2). The other material is a very pure aluminum having in the order of 100 part per million impurities. This is a very soft material which is easily bent. Both materials show dislocation effects occuring at different strain levels. The 7075T6 has three ranges while the very soft aluminum may have four ranges. These are discussed in the next section.

The final data curves (Fig. 16) are for commercial titanium and the alloy Ti-6% Aℓ-4%V. Both these materials show a much different behavior than the aluminum. The internal friction and modulus defects are practically independent of the strain amplitude up to strains in the order of 2×10^{-3}. At these values the materials become unstable and exhibit large increases in internal friction and modulus defects. Fatigue has been observed in some sample for strains of this order.

V. Theoretical Interpretations

A. Introduction

The internal friction technique is a very sensitive one but it requires a model to interpret the results. The model that has received the widest application in interpreting the results is the Granato-Lücke[25] model of Fig. 17. In this model a dislocation is assumed to cross the Peierl's barriers in a more or less straight line as indicated by Fig. 18. If however, the dislocation lies at only a small angle from the direction of the Peierl's minimums- which are directions for which the dislocation has its minimum energy- it was calculated[26] that the lowest energy state will be obtained if the dislocation lies partly in the Peierl's trough and partly across the Peierl's barrier in a "kink" or width w. The width of the kink depends on the height of the Peierl's barrier; the higher the barrier the smaller the width. In the Granato-Lücke model it is assumed that most dislocations are not kinked but are held straight by the line tension T which has been evaluated to be about $\mu b^2/2$.

Recently modifications of the Granato Lücke theory have been proposed. In the low amplitude range, it is proposed that most dislocations follow the kink model of Fig. 18. In the high temperature range the model produces results[27] which are very similar to the string model but at very low temperatures the barriers to kink motion are large enough so that the modulus defect $\Delta c/c_o$ approaches zero at absolute zero. For face centered metals about one-third of the modulus defect has disappeared[28] at 0.1^oK. For body centered metals, a considerably smaller part is left[29] at 1.5^oK. For materials with very high Peierl's barriers, such as the crystals silicon and germanium which crystallize in the diamond structure, the motion of kinks - which are probably in the form of a very narrow kinks - i.e. regions for which the extra planes of atoms extend one atomic spacing lower on one side of the region that they do on the other - requires the breaking of a primary bond between adjacent atoms. According to the measurements of Southgate[30] this requires an energy of 1.61 e.v. For all temperatures up to about 600^oC[31] the stress-strain curves are linear and fracture occurs by brittle fracture at imperfections on the surface. Above this temperature, dislocations become free, due to thermal agitation, and plastic dislocation effects occur.[31]

In the first non-linear range, ascribed by Granato and Lücke to the breakaway of dislocations from pinning points, non-linear effects can occur[32] in the kink model before breakaway occurs. Another effect not envisaged by the Granato-Lücke theory is the motion of pinning points along the dislocation in the presence of a moderate ultrasonic vibration. This effect may cause a time dependence of the internal friction in the breakaway region and may be the origin of acoustic "softening" of metals which allows forming of brittle materials. These effects are discussed in detail in Section VC.

For the linear range it appears that for all temperatures above $20^{\circ}K$, the Granato Lücke mechanism for the linear range is in good agreement with experiment.

B. <u>Linear Range For Dislocation Damping, Introduction</u>

The linear phase of the theory occurs when the dislocations are bowed out under the action of the applied stress as shown by Fig. 17b and c. In this region, the dislocation bows out under the application of a shearing stress in the glide plane. It is damped by the drag coefficient B, and may be resonant due to the mass term M. However, for all drag coefficients measured, the dislocation is overdamped and no resonance effects have been measured. By neglecting the mass term M, Oen, Holmes, and Robinson[19] have obtained a solution in closed form both for the single loop case and the exponential distribution of loop lengths given by Equation (115)

$$N(\ell)d\ell = \frac{\bar{N}}{\ell_o^{\,2}} \ \ell^{\,-\ell/\ell_o} \ d\ell \qquad (115)$$

where ℓ_o is the average spacing between impurity atoms. $\bar{N}$ is the total dislocation length per c.c. and $N(\ell)$ is the number of loops of length ℓ in a cubic centimeter of material. This type of distribution[18] results when the positions of the pinning points are random.

There are two normalized curves presented on Fig. 19, one for a single loop length and one for the exponential distribution. The ordinate is the ratio of the internal friction Q^{-1} to the product

$\bar{N}R\ell_o^2$ where R is an orientation factor which relates the strain in the acoustic wave to the average strain in the glide planes. The abscissa is the normalized angular frequency which is the ratio of the angular frequency ω to ω_o where $\omega_o = \mu b^2/B\ell_o^2$. Here μ is the shearing modulus in the glide plane, b is the Burger's distance, B the drag coefficient and ℓ_o the average loop length of Equation (115). In terms of the elastic moduli c_{11}, c_{12} and c_{44} of a cubic face centered crystal

$$\mu = (c_{11} - c_{12} + c_{44})/3 \qquad (116)$$

It is obvious that independent of the distribution, the internal friction Q^{-1} becomes inversely proportional to the frequency at very high frequencies. Introducing the normalized coordinates we find

$$Q_L^{-1} = \frac{\bar{N}R\mu b^2}{\omega B} \quad \text{or} \quad B = \frac{\bar{N}R\mu b^2}{(\omega Q^{-1})_L} \qquad (117)$$

Hence if the product of the limiting slope Q_L^{-1} by the angular frequency is determined, the drag coefficient B can be measured in terms of the number of dislocations $\bar{N}$, the orientation factor R, the shear modulus μ and the Burger's distance b. The last three quantities are known when the orientation of the crystal is determined and $\bar{N}$ can be approximated from etch pit patterns or from X-ray scattering results. This value is the least accurately determined quantity and is probably not known to better than a factor of 4. Hence absolute values are not too accurate but relative values over a temperature range can be obtained.

In all the measurements made it is the attenuation and not the internal friction that is measured. The two are related through the equation

$$\frac{2Av}{\omega} = Q^{-1} \tag{118}$$

where A is the attenuation in neper/cm - 1 neper = 8.68db- and v is the sound velocity. The normalized attenuation curve is then shown by Fig. 20. Here the ordinate is $2AvB/\bar{N}R\mu b^2$. When a match to the shape of the dislocation attenuation is obtained, the limiting attenuation A_L in nepers per cm can be determined. From this value the drag coefficient B- which is defined as the force per unit length on the dislocation occurring when it is moving with a velocity of 1 cm/sec- can be determined from the equation

$$B = \frac{NR\mu b^2}{2A_L v} \tag{119}$$

The success of this method for determining the drag coefficient for the dislocation depends on being able to separate the part of the attenuation due to dislocations from the remainder due to other causes. One method that has been widely employed is to measure the attenuation of an annealed crystal as a function of frequency and temperature and then to remeasure it after it has been neutron irradiated. Neutrons produce[18] impurity atoms and vacancies which diffuse to the dislocation, pinning them and removing the dislocation loss. The difference between the first and second measurement represents the dislocation attenuation. This method has been used[20,25] to evaluate the drag coefficient in copper. In lithium fluoride[34] new dislocations were produced in the crystal by plastic deformation. These produced an added attenuation which could be removed by annealing the crystal at 100°C for an hour. The difference in the attenuation between the deformed and annealed crystal was taken to be the dislocation contribution. In all these cases, the shape of the dislocation contribution agreed with that given in Figs. 19 and 20 and it was possible to obtain asymptotic values which allowed the drag coefficient to be obtained.

In two recent papers[35,36] a separation of the dislocation component has been made by observing that for pure annealed crystals the attenuation consists of a dislocation component of the type shown by Fig. 20 plus an attenuation which varies as the square of the frequency. This latter term is due to direct conversion of acoustic energy into heat through the thermoelastic effect and the phonon viscosity term plus the conversion of acoustic energy to electron motion through electron viscosity. The success of such a division depends on there being two standard curves, a square law curve and an attenuation of the form of Fig. 20.

The success of this process is shown by the measured attenuation shown by Fig. 21 for the two shear modes and the longitudinal mode propagated along the <110> direction. The longitudinal mode shows a definite square law attenuation plus a dislocation component which follows the standard high frequency form of Fig. 20. The square law terms for the shear modes are small and cannot be determined accurately. For the slow shear mode the square term is probably less than 1.5db/cm at 102 MHz.

Plotting the internal friction (for dislocations) as a function of the frequency, the curve labelled L<110> of Fig. 22 results. From the shape of the curve one finds that the maximum value occurs at a frequency 4.1 MHz/sec., the value of Q_M^{-1} is 1.02×10^{-3} and the asymptotic value is shown by the dashed line. This form is confirmed by the two shear attenuation curves which are labelled S(1$\bar{1}$0) and S(100). All three curves are parallel but differ in value on account of the different orientation factors R for the three modes. The orientation factors for waves along the <110> direction have been calculated by Alers and Thompson[20] with the results

$$R_L = \frac{1}{3}\left[\frac{c_{44}^{\,2} + \left(\frac{c_{11}-c_{12}}{2}\right)^2}{\left(\frac{c_{11}+c_{12}+2c_{44}}{2}\right)\left(c_{11}-c_{12}+c_{44}\right)}\right] = 0.057$$

$$R_{c_{44}} = \frac{1}{3}\left[\frac{c_{44}}{c_{11}-c_{12}+c_{44}}\right] = 0.216 \tag{120}$$

$$R_{\left(\frac{c_{11}-c_{12}}{2}\right)} = \frac{1}{2}\left[\frac{c_{11}-c_{12}}{c_{11}-c_{12}+c_{44}}\right] = 0.173$$

The numerical values are the results obtained for lead by substituting the elastic moduli of Equation (121).

$$c_{11} = 4.85 \times 10^{11};\ c_{12} = 4.09 \times 10^{11};\ c_{44} = 1.44 \times 10^{11} \text{ dynes/cm}^2 \quad (121)$$

The ratios between the Q^{-1} curves are in rough agreement with the ratios between the orientation factors R.

The dislocation drag coefficient B can be determined from the asymptotic values of $Q^{-1}f$ which are shown by the dashed lines of Fig. 22. The drag coefficient is given by

$$B = \frac{\bar{N}R\mu b^2}{(\omega Q^{-1})_L}$$

Taking the shear wave with polarization along <100> as being the most accurate and taking the number of dislocations for a freshly produced crystal as the reasonable value of $\bar{N} = 10^7$ per cc, one finds the drag coefficient B to be

$$B = \frac{10^7 x .216 x 7.33 x 10^{10} x 12.25 x 10^{-16}}{5.3 \times 10^5} = 3.7 \times 10^{-4} \quad (122)$$

which is close to the theoretical value as will be discussed in Section VC. Some information on the average loop length ℓ_o of Equation (115) can also be obtained from the frequency of the maximum Q_M^{-1} and the value of Q_M^{-1}. By fitting the measured values to the standard curve, it is found that

$$\omega_M = 2\pi \times 4.1 \times 10^6 = 2.55 \times 10^7;\ Q_M^{-1} = 3 \times 10^{-3} \quad (123)$$

From the form of the standard curve it is seen that

$$\omega_M = \frac{0.38 \times \mu b^2}{B\ell_o^2}\ ;\quad Q_M^{-1} = 0.35 \times \bar{N}R\ell_o^2 \quad (124)$$

From one equation $\ell_o = 6\times10^{-5}$ cm while the other gives 6.3×10^{-5} cms, a reasonable check. This value is similar to that found[37] at low temperatures for copper of a comparable purity i.e. 99.999%. Table I shows that the loop length does not change with temperature for lead.

C. <u>Evaluation of Square Law Attentuation and Dislocation Drag Terms for Single Crystal Lead, Aluminum and Copper</u>

This process has been carried out over a temperature range for the longitudinal mode for single crystal lead, the longitudinal and two shear modes for copper crystals and for the two shear waves in aluminum single crystals. Since the measurements have been given in previous papers[35,36] only the values of the square law attentuation at 150 MHz and the drag coefficients are given here. However measurements have been made to lower temperatures in aluminum which alter the values given previously to a small extent. The measurements for copper are new.

The longitudinal mode for lead along the <110> direction has been measured for lead from 66°K to 300°K. The square law attenuation measured at 150 MHz is shown by the circles of Fig. 23. Two theoretical mechanism, which are discussed in Section VD, are shown and their sum, as shown by the solid line is compared with the measured points. The corresponding drag coefficients are shown by the circles of Fig. 24 and they are compared with the sum of three drag mechanisms which are discussed in Section VE. By evaluating the values of ω_M and Q_M^{-1}, as discussed in Section VB, the loop length has been evaluated over a temperature range and as shown by Table I, it is approximately constant over a temperature range and substantially equal to the value found at low temperatures for a copper of comparable purity,[37] i.e. 99.999%.

Similar measurements have been made in copper single crystals to a low enough temperature to evaluate the electronic component of the square law and dislocation drag effect. Fig. 25 shows the square law values obtained for the slow shear mode (direction <110>, polarization <1$\bar{1}$0>) for a <110> type crystal. On account of its low velocity - 1.63×10^5 cms/sec - this mode has a high enough square law loss to be evaluated in the presence of a larger dislocation component. This allows an evaluation of the non-linear coefficient for the interaction between acoustic waves and phonons. A second crystal was obtained[38] for which the resistance ratio from 300°K to 4.2°K was known to be 600. This had its length along the <100> direction. Measurements were made for the longitudinal mode and the shear mode which is controlled by the c_{44} elastic constant and has a velocity of 2.9×10^5 cm/sec. With this high a velocity, the square law component was too small to be evaluated. However it could be evaluated for the longitudinal mode and this is shown plotted on Fig. 26 These measurements were carried down to 20°K and hence give a good evaluation of the electronic viscosity damping coefficient. Measurements were also made for the dislocation damping coefficient for all three modes and these are shown plotted on Fig. 27. The method for determining these values is discussed in Section VE.

Finally more complete measurements have been made for the two shear modes along the <110> direction for an aluminum single crystal. These also have been carried down to $20^{\circ}K$ and provide a better determination of the electronic damping coefficient. Fig. 28 shows the square law attenuation at 150 MHz for the slow shear mode (polarization $<1\bar{1}0>$, velocity 3.11×10^5 cm/sec) along <110> direction, while Fig. 29 shows a similar curve for the fast shear mode (polarization <100>, velocity 3.41×10^5 cms/sec). Fig. 30 shows the drag coefficient measured for the slow shear mode. The values for the fast shear mode are similar but are not as accurate on account of the smaller resolved shear stress factor R.

D. Sources of Square Law Attenuation

1. Thermoelastic Effect

The thermoelastic loss of a solid is one of the principal sources of conversion of acoustic energy to thermal energy. It results from the flow of heat from the compressed part of the wave to the cool expanded part of the wave. The thermoelastic loss for a cubic crystal is given by the formula[39,40]

$$A_{(\text{nepers/cm})} = \frac{\omega^2 \Delta c \tau}{2\rho V_{\ell}^3} \qquad (125)$$

where Δc is the difference between the adiabatic and isothermal elastic moduli and τ is the relaxation time for the interchange of heat between the hot and cold regions in the crystal. The quantities have the values for cubic crystals

$$\Delta c = \frac{\alpha^2 (c_{11}+2c_{12})^2 T}{\rho C_v} \; ; \quad \tau = \left(\frac{K}{\rho C_v v_\ell^2} \right) \qquad (126)$$

where $c_{11}+2c_{12}$ is the sum of elastic moduli for cubic crystals, K is the total thermal conductivity due to electrons and phonons, ρC_v is the specific heat per unit volume, v_ℓ is the velocity of the longitudinal elastic wave and T the absolute temperaaure. The values of α, the temperature expansion coefficient, K the thermal conductivity and ρC_v the specific heat per unit volume (for lead) are shown plotted as a function of the temperature for lead by Fig. 31. From these values the calculated attenuation in db per cm - 1 neper is 8.68 db - is shown plotted by the dashed line of Fig. 23. This accounts for about half the measured frequency square law attenuation at room temperature but only about one-third of that measured at 60°K. Similar values are shown for copper on Fig. 26.

For non-conducting crystals, for which all the thermal conductivity is by phonons, this source of loss accounts for only about 4 percent of the measured value. Furthermore it does not account for any shear loss in either a metal or a non-conducting crystal.

2. Phonon Viscosity

Akheiser[41] first pointed out another source of conversion of acoustic waves to thermal waves which is similar in principal to a viscosity concept. In this effect a suddenly applied strain causes a separation of the temperatures of the different phonon modes by amounts which depend on the type of strain applied and on the direction and type of the phonon modes. The amount of the separation is determined by the values of the non-linear elastic moduli - i.e. the third order elastic moduli - as discussed in a number of references.[42] This sudden change in the phonon temperatures results in an energy storage equal to

$$\frac{1}{2} \Delta c S_j^{\,2} \tag{127}$$

where Δc is an increase in the elastic modulus associated with the strain component S_j. By summing all the contributions to the thermal energy, it was shown[42] that the modulus increase is equal to

$$\Delta c = 3 \sum_i E_i (\gamma_i^{\,j})^2 \tag{128}$$

where E_i is the thermal energy of mode i and $\gamma_i^{\,j}$ is the Grüneisen number associated with the particular mode and strain. For a longitudinal mode of vibration, the difference between the isothermal and adiabatic moduli has to be subtracted since, for equilibrium conditions, the temperatures do not relax down to the unstrained value but rather to the adiabatic value associated with the average temperature rise ΔT. Hence for longitudinal waves, the modulus change associated with the non-equilibrium temperature distribution due to a suddenly applied strain is

$$\Delta c = 3 \sum_i E_i (\gamma_i^{\,j})^2 - \gamma^2 \rho C_v T_o \tag{129}$$

where γ is the ordinary Grüneisen constant associated with a volume expansion.

This energy storage is relaxed down to a thermal equilibrium temperature with a relaxation time τ. For an acoustic shear wave, which can communicate its energy directly with the thermal phonons, the relaxation time is equal to the thermal relaxation time

$$\tau = \frac{3K}{\rho C_v \bar{V}^2} \tag{130}$$

where K is the lattice thermal conductivity, ρC_v is the specific heat per unit volume and $\bar{V}$ the Debye average velocity,[43] which for lead is 9.53×10^4 cms/sec. Longitudinal acoustic waves do not couple directly to the thermal phonons but interact only with shear and longitudinal waves in the same frequency range. Hence the mean free path, and therefore the relaxation time τ, is larger for longitudinal waves. Experimentally the factor appears to be in the order of 2.

The rate for which the wave energy is transformed into thermal energy is determined by the product

$$\eta_p = \Delta c\tau \tag{131}$$

where, in analogy with the expression for the viscosity of an ordinary gas or liquid, the product $\Delta c\tau$ is equal to a viscosity.[44] To simplify the expression for Δc we note that in the high temperature approximation, the thermal energy of each mode E_i is proportional to the total thermal energy E_o. So far the 39 pure modes existing for a cubic crystal have been used to evaluate the expression for Δc. Hence for this case a non-linearity constant D is defined equal to

$$D = 3\left[\frac{3\Sigma_i (\gamma_i^j)^2}{n} - \frac{\gamma^2 \rho C_v T}{E_o}\right] \qquad (132)$$

In terms of this constant the "phonon viscosity" term is

$$\eta_\ell = 2D\left(\frac{E_o K}{\rho C_v V^2}\right)_{(long)} \quad ; \quad \eta_s = D\left(\frac{E_o K}{\rho C_v V^2}\right)_{shear} \qquad (133)$$

For a shear term $\gamma = 0$ and the last term drops out of (132).

The constant D has been evaluated[45] for six non-conducting crystals from the measured third order moduli with good quantitative agreement. The D values for shear waves vary from 0.29 (ytrium iron garnet) to 2.0 ($NaC\ell$ and MgO). The longitudinal values range from 4.5 (silicon) to 40 ($NaC\ell$). For a metal it is necessary to separate the lattice thermal conductivity from the electronic since it is only the former that determines the relaxation time. The lattice thermal conductivity of a metal can be determined from thermal conductivity measurements made on the metal with varying impurities content and for copper has been shown to fit the equation[46]

$$K = 32.5/T \qquad (134)$$

from temperatures above 30^oK. Using this value in Equation (133) and a value of D = 42 calculated from the recently measured[47] third order moduli for copper, it is found that the phonon viscosity loss, determined by the equation

$$A_{(\text{neps/cm})} = \frac{\omega^2 \tau_p}{2\rho V_\ell^3} \tag{135}$$

agrees well with the difference between the measured values and the thermoelastic loss and electron viscosity losses shown by Fig. 26.

For lead no measurements exist for the lattice thermal conductivity but this can be estimated from a calculation due to Leibfried[48] and Schlömann. Using a simple model for a cubic crystal they derive the formula

$$K_{L(\text{watts/cm})} = 3.6aA\theta^3/\gamma^2 T \tag{136}$$

where a is the lattice spacing, A a constant equal to 92.9, θ is the Debye temperature and γ the Grüneisen constant. With $\theta = 105^\circ K$,[43] $a = 4.9496 \times 10^{-8}$ cms and $\gamma = 2.65$ from the data of Fig. 31 one finds

$$K_{L(\text{watts/cm}^2)} = 2.75/T \tag{137}$$

This formula tends to overestimate[46] the value so that it is assumed that the lattice thermal conductivity is

$$K_{L(\text{watts/cm}^2)} = 2/T \tag{138}$$

Using this value and determining the ratio of E_o to ρC_v from tables of Debye functions,[49] the quantities necessary to calculate $E_o K/\rho C_v \bar{V}^2$ are given in Table II. $\bar{V} = 9.53 \times 10^4$ cms^2/sec.[43]

If we insert the value of $2D(E_o K/\rho C_v \bar{V}^2) = \eta_\ell$ into Equation 21 with $\omega = 2\pi x 1.5 x 10^8$, $\rho = 11.34$ and $\bar{V}_\ell = 2.285 x 10^5$ cms/sec - the velocity of a longitudinal wave along the <110> direction - the value of D to agree with the phonon viscosity attenuation of Fig. 23 is 35.2. This value is consistent with that found for copper and other crystals. Over a temperature range the sum of the thermoelastic attenuation plus the phonon viscosity attenuation is in good agreement with the measurements. The shear attenuation indicated for the slow shear mode - i.e. 1.5 db at 150 MHz - indicates a non-linear constant D in the order of unity.

For copper the data of Fig. 25 indicates a non-linearity factor of D=3.0 for the slow shear mode. On account of the large velocity for the fast shear mode, the constant cannot be measured. In calculating the drag coefficient of Fig. 27, it is assumed to be equal to that for the other mode.

Finally the shear curves for aluminum, as shown by Figs. 28 and 29, indicate non-linearity constants of D = 8.6 and D = 7.25 for the slow wave and fast wave respectively. Since these constants are important for dislocation drag terms, the non-linearity constant for the glide plane is given by

$$D_G = \frac{2x8.6+7.25}{3} = 8.15 \qquad (139)$$

since the elastic constant $(c_{11}-c_{12}+c_{44})/3$ is twice the elastic constant for the slow shear wave plus that for the fast shear wave. With these evaluations of D, the measured square law attenuation is in good agreement with the electron viscosity component, discussed in the next section, plus the phonon viscosity loss. For shear waves there is no thermoelastic loss.

3. Electron Viscosity

It is well known that acoustic waves are damped principally at low temperatures by the presence of free electrons in a metal. The action is equivalent to a viscosity as was first pointed out by the writer.[50] For a free electron model the viscosity was shown to be

$$\eta_e = \frac{9\times10^{11}\hbar^2(3\pi^2 N)^{2/3}}{5e^2\rho} \tag{140}$$

where $\hbar$ is Planck's constant h divided by 2π, N is the number of free electrons per cc, e is the charge 4.8×10^{-10} e.s.u and ρ is the electrical resistivity in ohm-cms. This value gives a good agreement with experiment for those materials for which the Fermi surface approximates a sphere, notably copper, gold, silver, sodium and potassium. If, however, the Fermi surface differs substantially from a spherical surface, the amount of damping becomes anisotropic and may differ from the free electron value.

For aluminum, for which data are given by Figs. 28 and 29 the measured values agree with (140) provided that we assume 1.43 electrons per atom. This is somewhat different from the measurements of Lax[51] and Filson[52] which would indicate a larger attenuation. The measured attenuation is consistent with an electron viscosity determined by the equation

$$\eta_e = \frac{9 \times 10^{11} \hbar^2 (4.3\pi^2 N)^{2/3}}{5e^2 \rho} = \frac{1.64 \times 10^{-8}}{\rho} \text{ (aluminum)} \quad (141)$$

since $N = 6.11 \times 10^{22}$ atoms per cc for aluminum.

The solid lines of Figs. 28 and 29 marked electron viscosity represent the calculated attenuation at 150 MHz for a shear wave along the <110> direction with partical motions along <1$\bar{1}$0> and <100> respectively which have the velocities 3.11×10^5 and 3.41×10^5 cms/sec. The electronic viscosity is calculated from Equation (141) by using the measured resistivities of Fig. 32.

The difference between the measured points- shown by the circles- and that due to the electron viscosity has been used to evaluate the non-linearity constants for the two waves as discussed in the preceeding section. The lattice thermal conductively over this range was taken as 107/T watts/cm^2 as discussed in the previous paper. The Debye temperature θ is taken as 425°K. Table III shows a calculation of the product $(E_o K/\rho C_v \bar{V}^2)$ needed to determine the shape and constant D for the phonon viscosity term. The agreements with the sum of the electron and phonon viscosity attenuation, with the measured values, is quite good.

For copper $N = 8.5 \times 10^{22}$ atoms per c.c. and the number of electrons is taken equal to the number of atoms. Hence the factor 1.61×10^{-8} takes the place of 1.64×10^{-8} for aluminum. The resistivity of copper is also shown by Fig. 31. The agreement with the experimental values of Figs. (25) and (26) is good.

E. Mechanisms For The Damping of Dislocations

When a dislocation moves through a perfect crystal, the only interaction possible is with the phonon and electron waves present in the crystal. The latter interaction occurs only in electrical conductors and is important only at low temperatures.

The first interaction mechanism proposed was the conversion of the energy of the dislocation into heat by means of the thermoelastic effect.[53] This interaction is smaller than the other two mechanisms and furthermore does not account for any drag on screw dislocations since a screw is surrounded only by a shear strain field. Hence it will not be discussed here.

A larger source of dislocation damping by phonons is the scattering of thermal phonons by a moving dislocation first derived by Leibfried.[54] This source of dislocation damping takes the form

$$B = \frac{aE_o}{10v_s} \tag{142}$$

where a is the lattice constant, v_s, the shear velocity in the glide plane and E_o is the thermal energy density. This expression has been rederived on a kink basis by Eshelby[55] with a very similar result. On account of the low shear velocity - 8.09×10^4 cms/sec - this source of dissipation is particularly large for lead. It is shown plotted on Fig. 24. The values for copper are considerably less as shown by the curves Figs. 27. For aluminum the value is less and has been neglected in comparison to the other two sources which are much larger.

This other source of phonon dislocation damping, proposed by the writer,[56a,b] is damping due to phonon viscosity. This follows since the dislocation is surrounded by a strain field which varies as the dislocation moves through the crystal. The energy loss w which is equal to the square of the rate of change of the shear strain multiplied by the viscosity and integrated over the region surrounding the dislocation, is for a screw dislocation[56a]

$$w = b^2 \eta_s u^2 / 8\pi a_o^2 \tag{143}$$

where u is the velocity of the dislocation and a_o a cut off radius below which the concept of phonons is not valid. This energy loss is equated to that caused by the drag coefficient B, equal to

$$w = Bu^2 = \frac{b^2 \eta_s u^2}{8\pi a_o^2}, \quad \text{Hence} \quad B = \frac{b^2 \eta_s}{8\pi a_o^2} \tag{144}$$

This drag coefficient depends critically on the radius a_o, on which there are two limitations. The first of these has to do with the size of the region around the dislocation which can exchange energy with the surrounding phonon field. It has been suggested that material inside a radius equal to the mean free phonon path should be excluded from the calculation. It was first shown by Suzuki, Ikushima and Aoki[22] that this suggestion only holds when the dislocation is moving with the speed of sound. For slower speeds there is more time to interchange energy between a suddenly stressed region and the phonons, and Suzuki et. al. suggest that the radius should be

$$r = \bar{l}u/\bar{v} \tag{145}$$

where $\bar{l}$ is the mean free phonon path, u the velocity of the dislocation and $\bar{v}$ the Debye average sound velocity. Hence it is only if u is equal to the sound velocity, that $\bar{l}$ determines the excluded radius.

This result can be seen from the fact that in the neighborhood of the dislocation, the strain changes discontinuously when the extra plane moves over by the Burger's vector b. To determine whether the material at the edge of the dislocation should be included in the calculation, the criterion is whether the phonon modes can be equilibrated in a time less than the time between jumps. If they cannot, then energy is not lost to the phonons but is returned to the dislocation. This criterion results in the inequality

$$\tau/t = u\tau/b \leq 1 \tag{146}$$

where t is the time the strain remains constant. If all the material is to be included up to the dislocation edge

$$u\tau = u\bar{l}/\bar{v} \leq b \tag{147}$$

For all the measurements reported here, this criterion is satisfied. A similar criterion holds for the damping by electron viscosity with τ replaced by electron-phonon relaxation time. This time is equal to

$$\tau = \frac{9x10^{11} m}{Ne^2 \rho} = \frac{3.55x10^3}{N\rho} \tag{148}$$

where m is the mass of an electron. For all cases considered here Equation (146) is more than satisfied and the radius is determined by the second limitation.

The other limitation is that the concept of the phonon as an acoustic wave transmitted through the medium may breakdown sufficiently close to the dislocation on account of the non-linear terms in the elastic energy. An estimate of the relative amounts of energy stored in the various terms can be obtained from the expression

$$w = \frac{1}{2!} c_{ijk\ell} S_{ij} S_{k\ell} + \frac{1}{3!} C_{ijk\ell mn} S_{ij} S_{k\ell} S_{mn} + \ldots \qquad (149)$$

For measured values of third order moduli of metals,[47] the second order terms have energies about 50 percent of the first order terms for strains of about 20 percent. This corresponds to a value of $a_o \doteq (3/4\ b)$ for a screw dislocation. Using this value of a_o, the drag coefficient is

$$B = 0.0706\ \eta_s \qquad (150)$$

Similar calculations for an edge dislocation[56a] show that the drag coefficient for this case is given by

$$B = \frac{3}{4} \left(\frac{b^2 \eta_s}{8\pi (1-\sigma)^2 a_o^2} \right) + \frac{1}{72\pi} \left(\frac{b^2 \mu^2 \chi}{\kappa^2 (1-\sigma)^2 a_o^2} \right) \qquad (151)$$

where μ is the shear modulus $(c_{11}-c_{12}+c_{44})/3$, κ is the bulk modulus $(c_{11}+2c_{12})/3$, σ is Poisson's ratio, and χ is a compressional viscosity given by

$$\eta_\ell - \frac{2}{3} \eta_s = \chi \qquad (152)$$

Although η_ℓ is much larger than η_s for lead, the multiplying constants reduce the effect so that the indicated drag coefficient for edge dislocations is in the order of twice that for screw dislocations. If half the number of dislocations are screw and half edge the resulting internal friction is

$$Q^{-1} = \frac{1}{2}\frac{\bar{N}R\mu b^2}{\omega}\left[\frac{1}{B_s} + \frac{1}{B_\ell}\right] = \frac{1}{2}(1.5)\frac{\bar{N}R\mu b^2}{\omega B_s} = \frac{3}{4}\frac{\bar{N}R\mu b^2}{\omega B_s} \qquad (153)$$

This results in a combined drag modulus which is about (4/3)rds of the screw drag constant. From the measured square law attenuation for the slow shear mode - 1.5 db/cm at 150 MHz, - we find

$$\eta_s \le 1.9\text{x}10^{-3}\text{poise. Hence } B_s = 0.0706\eta_s \le 1.3\text{x}10^{-4}\ \frac{\text{dyne x sec}}{\text{cm}^2} \qquad (154)$$

Fig. 24 shows a plot of B assuming a value of $1.5\text{x}10^{-4}$ at 300^{o}K and a temperature variation similar to $(E_oK/\rho C_v\bar{V}^2)$ of Table II. For aluminum the average non-linear value of D = 8.15 (from Equation 139) is used with the values of $(E_oK/\rho C_v\bar{V}^2)$ listed in Table III. The resulting dislocation drag term is shown on Fig. 30 by the top dashed curve. The compressional viscosity term χ is assumed small enough to neglect. For copper the curve shown by Fig. 27 results from the values of $E_oK/\rho C_v\bar{V}^2$ shown by Table IV and the non-linearity constant D = 3.0.

The final source considered is the damping of dislocations by electron viscosity. This source is entirely similar to damping by phonon viscosity and in fact the same formulas hold with the exception that χ is zero for electron damping. The non-linearity radius, however, is different since it depends on the where m is the mass of an electron. For all cases considered here Equation (146) is more than satisfied and the radius is determined by the second limitation.

The other limitation is that the concept of the phonon as an acoustic wave transmitted through the medium may breakdown sufficiently close to the dislocation on account of the non-linear terms in the elastic energy. An estimate of the relative amounts of energy stored in the various terms can be obtained from the expression

$$w = \frac{1}{2!} c_{ijk\ell}S_{ij}S_{k\ell} + \frac{1}{3!} C_{ijk\ell mn}S_{ij}S_{k\ell}S_{mn} + \ldots \tag{149}$$

For measured values of third order moduli of metals,[47] the second order terms have energies about 50 percent of the first order terms for strains of about 20 percent. This corresponds to a value of $a_o \doteq (3/4\ b)$ for a screw dislocation. Using this value of a_o, the drag coefficient is

$$B = 0.0706\ \eta_s \tag{150}$$

Similar calculations for an edge dislocation[56a] show that the drag coefficient for this case is given by

$$B = \frac{3}{4}\left(\frac{b^2\eta_s}{8\pi(1-\sigma)^2 a_o^2}\right) + \frac{1}{72\pi}\left(\frac{b^2\mu^2\chi}{\kappa^2(1-\sigma)^2 a_o^2}\right) \tag{151}$$

where μ is the shear modulus $(c_{11}-c_{12}+c_{44})/3$, κ is the bulk modulus $(c_{11}+2c_{12})/3$, σ is Poisson's ratio, and χ is a compressional viscosity given by

$$\eta_\ell - \frac{2}{3}\eta_s = \chi \tag{152}$$

Although η_ℓ is much larger than η_s for lead, the multiplying constants reduce the effect so that the indicated drag coefficient for edge dislocations is in the order of twice that for screw dislocations. If half the number of dislocations are screw and half edge the resulting internal friction is

$$Q^{-1} = \frac{1}{2}\,\frac{\bar{N}R\mu b^2}{\omega}\left[\frac{1}{B_s} + \frac{1}{B_\ell}\right] = \frac{1}{2}(1.5)\,\frac{\bar{N}R\mu b^2}{\omega B_s} = \frac{3}{4}\,\frac{\bar{N}R\mu b^2}{\omega B_s} \qquad (153)$$

This results in a combined drag modulus which is about (4/3)rds of the screw drag constant. From the measured square law attenuation for the slow shear mode - 1.5 db/cm at 150 MHz, - we find

$$\eta_s \le 1.9\times10^{-3}\,\text{poise. Hence } B_s = 0.0706\,\eta_s \le 1.3\times10^{-4}\ \frac{\text{dyne x sec}}{\text{cm}^2} \qquad (154)$$

Fig. 24 shows a plot of B assuming a value of 1.5×10^{-4} at 300°K and a temperature variation similar to $(E_oK/\rho C_v\bar{V}^2)$ of Table II. For aluminum the average non-linear value of D = 8.15 (from Equation 139) is used with the values of $(E_oK/\rho C_v\bar{V}^2)$ listed in Table III. The resulting dislocation drag term is shown on Fig. 30 by the top dashed curve. The compressional viscosity term χ is assumed small enough to neglect. For copper the curve shown by Fig. 27 results from the values of $E_oK/\rho C_v\bar{V}^2$ shown by Table IV and the non-linearity constant D = 3.0.

The final source considered is the damping of dislocations by electron viscosity. This source is entirely similar to damping by phonon viscosity and in fact the same formulas hold with the exception that χ is zero for electron damping. The non-linearity radius, however, is different since it depends on the non-linearity of the Fermi surface rather than for the elastic constants. This damping is discussed in two former papers[57] and arguments are given for assuming that a_o is in the order of 10^{-7} cm. With this value the electron drag coefficient will be equal to

$$B_e = \frac{b^2 \eta_e}{8\pi a_o^2} = 3.96 \times 10^{12} b^2 \eta_e \tag{155}$$

Actual determinations for the ratio of the non-linearity radii for phonons and electrons can be obtained for copper and aluminum by comparing the values of η_p to η_e at the temperature for which they are equal. For this case

$$\frac{a_{oe}}{a_{op}} = \sqrt{\frac{\eta_e}{\eta_p}} \tag{156}$$

For copper this ratio appears to be about 3.5 while for aluminum it is 3.4. An average value 5.0 is close to the ratio of (3/4 b) to 10^{-7} cm. The dashed curves of Figs. 27 and 30 are plotted on the assumption that $a_{op} = (3/4)b$ while a_{oe} is determined by the above ratios. The agreement with experiment is within experimental error. Electron damping is shown for lead by Fig. 24, but the measurements are not carried out to a low enough temperature to make this a factor.

F. <u>High Amplitude Region</u>

As the strain becomes higher, a value is reached above which the internal friction and the modulus change increase as a function of the applied strain. The strain to produce the non-linear effect depends on the purity of the sample, as shown in Fig. 11, and for a given purity content it also depends markedly on the temperature, Fig. 12. For strains about 30 to 50 times that required to initiate the second region, a third region occurs for which both the internal friction and the modulus defect increase very rapidly with strain. This region is associated with fatigue in metals which can occur throughout this region for a sufficiently large number of cycles.

According to the original mechanisms shown by Fig. 17, the second region is associated with the breakaway of dislocations from their pinning points whereas the third region is associated with the generation of new dislocation loops by the Frank-Read sources shown by Fig. 17F and G. The only theoretical derivation is the one given for the second source, Fig. 17D and E, which is ascribed to the breakaway of dislocations from their pinning points and the subsequent repinning later in the cycle. This cyclic variation generates a hysteresis loop which produces a loss proportional to the frequency. For a single loop length, this causes a sudden increase in loss followed by a decrease in the internal friction at higher strains. This follows since the width of the hysteresis loop is constant so that the energy loss is proportional to the applied stress whereas the energy stored is proportional to the square of the applied stress. When account is taken of an exponential distribution of loop lengths, the product of the internal friction times the shearing strain is given by

$$Q_H^{-1} S_{13} = C_1 C_2 \, e^{-C_2/S_{13}} \tag{157}$$

where

$$C_1 = R \left(\frac{2}{\pi}\right)^4 \bar{N}\ell_N/\pi\ell_A; \qquad C_2 = \frac{\mu\epsilon_o b}{4Y_o R\ell_A} = S_{13}^{\,o}$$

the average shear strain required to produce breakaway. Y_o is the value of Young's modulus, ϵ_o is Cottrell's misfit parameter $(r_1-r)/r$ where r_1 is the diameter of the pinning atom and r the diameter of solvent atom. Since 4R is usually in the order of unity, μ/Y_o is in the order of one-third and ϵ_o in the order of 0.1 to 0.2, the shearing stress to cause breakaway is in the order of 1/30 to 1/15 of b/ℓ_A. Since the strain to produce an actuation of the Frank-Read sources is in the order of $b/R\ell_A$, then the third region of internal friction occurs for strains in the order of 30 to 50 times that for the breakaway region.

Equation (157) has been compared with experiment in several review papers[58,59] with fair agreement. The tests consist in plotting log $Q_H^{-1} S_{13}$ against $1/S_{13}$ since a straight line should result. If the strain is limited to a 10 to 1 region, straight lines are usually obtained with increasing slopes for increasing concentrations of impurities. As the temperature increases, the slope decreases. A simplified treatment for the effect of temperature has been given by Friedel[60] who finds that the activation energy for breakaway from impurity atoms in the presence of a finite temperature is given by

$$(W_M) \cong (T_{13}-T_{13_o})bd\lambda + kT\,\ell n\,\frac{\nu b}{20\nu_o\lambda Q^{-1}} \tag{158}$$

where $d \cong b$ is the width of the dislocation, T_{13} is the applied shearing stress, T_{13_o} a possible Peierl's stress, ν is the atomic frequency, ν_o is the frequency of the applied stress λ the average length between pinning points and Q^{-1} the internal friction. Binding energies of a few tenths of an electron volt are obtained in this way for various metals.

Two other effects not considered in the original theory have recently been discussed. One involves the kink model for which calculations indicate[32] that non-linearities can appear at lower strain values than are required to produce breakaway. This might lower the stress level for non-linearity effects to appear. The other and more important effect is the diffusion of pinning points along the dislocation under the action of an ultrasonic vibration. The origin of this effect[61] is that the vibration of long dislocation loops produce a force on the pinning point, directed away from the loop, which is larger than the force exerted in the opposite direction by a smaller loop. The result is that pinning points tend to diffuse along the dislocation in a direction to make large loops larger and small loops smaller. A criterion for this effect to be of importance is that

$$E = \frac{S_{13}^{2}\mu \ell^{3}}{8} \geq kT \tag{159}$$

For example for loop lengths of $4x10^{-5}$ cms found for alloyed copper, strains in the order of $3x10^{-6}$ could produce some change. For strains in the first non-linear region, a large effect should be produced. At the same time the vibration can lower the diffusion constant for the motion of pinning points along the dislocation by several orders of magnitude.[61] This effect may well be the origin of a time dependent increase in internal friction observed in the breakaway region and may contribute to acoustic softening of refractive material observed by Langenecker[62] and associates. Further experimental studies are desirable for this region.

The final phase has been studied to some extent by B. J. Lazan[63] and the writer.[64] This phase starts when dislocation loops can be generated by sources such as Frank-Read dislocation mills or by cross slips. The approximate strain level is given by

$$S = \frac{b}{R\ell_N} \tag{160}$$

where R is an orientation factor and ℓ_N an average network length. Examples for two purities of aluminum are shown by Fig. 15. With orientation factors of 0.25 and with $b=2.86\times10^{-8}$ cms, the loop length L_N become 3×10^{-2}, and 1.0×10^{-4} cms for the three materials. These represent the longest loops present in the materials.

During the final phase the internal friction and modulus defect change with time and definate values are not possible. Due to the large amount of plastic strain produced the network lengths L_N become shorter on account of the entanglement of many loops and the material becomes harder. Many vacancies can be generated by cross dislocation cutting in the body of the material and in slip bands. These can be the origin of fatigue cracks which can occur throughout this high amplitude region.

The titanium and titanium alloy data of Fig. 16, show that the dislocations are very closely pinned and do not exhibit the first two dislocation phases of the aluminum. At strains in the order of 1 to 3×10^{-3}, breakaway occurs from the pinning points and the dislocations are free to move. According to W. A. Wood, who discovered this effect,[65] creep occurs indefinitely for stresses of this order.

REFERENCES

1. Marx, J. W., Rev. Sci. Instruments, 22, 503, 1951; Marx, J.W. and Sivertsen, J. M., J. Appl. Phys., 24, 81, 1953.

2. Baker, G. S., J. Appl. Phys., 28, 734, 1957.

3. Ilakor, J. J. and Jacobsen, E. H., paper E5, 1966 Ultrasonic Symposium of IEEE.

4. McSkimin, H. J., Chap. IV, IA, Physical Acoustics , edited by W. P. Mason, Academic Press, 1965.

5. Williams, Jr. A.O., J. Acous. Soc. Amer. 23, 1, 1951; Seki, H., Granato, A. and Truell, R., J. Acous. Soc. Amer., 28, 230, 1950; Papadakis, E., J. Acous. Soc. Amer., 40. 863, 1966.

6. Mason, W. P., Physical Acoustics and the Properties of Solids , D. Van Nostrand Co. 172-178, 1958.

7. Eisner, E., Chap. 14, IB, Physical Acoustics , edited by W. P. Mason, Academic Press, 1965.

8. See for example reference (6), 32-34.

9. See reference (6), 42.

10. Mason, W. P., Electromechanical Transducers and Wave Filters , D. Van Nostrand Co., 2nd Edition, 1948, 20-27.

11. See reference (6), 156-162.

12. Webster, A. G., Proc. Nat. Acad. Sciences, 5, 275, 1919.

13. See reference (10), 204.

14. Berlincourt, D. A., Curran, D. R. and Jaffe, H., Chap. 3, Vol. IA, Physical Acoustics , Academic Press, 202, 1965.

15. See reference (10), 193-195.

16. Tokahashi, S., J. Phys. Soc. Japan 1, No. 12, 1253-1261, Dec. 1956.

17. Baker, G. S., J. Appl. Phys., 28, 734-737, June 1957.

18. Thompson, D. O. and Paré, V. K., Chap. 7, IIIA, Physical Acoustics , edited by W. P. Mason, Academic Press, 1966.

19. Oen, O. S., Holmes, D. K. and Robinson, M. T., U.S. Atomic Energy Comm. Report ORNL-3017, 1960.

20. Alers, G. A. and Thompson, D.O., J. Appl. Phys., 32, 283, 1961; Granato, A. V. and Sterns, R. M., J. Appl. Phys. 33, 2880, 1962.

21. Mitchell, O.M.M., J. Appl. Phys., 36, 2083, 1965.

22. Suzuki, T., Ikushima, A. and Aoki, M., Acta Met. 12, 1231, 1964.

23. Mason, W. P. and Rosenburg, A., "Damping of Dislocations in Lead Single Crystals, scheduled for March 1967, J. Appl. Phys.

24. Mason, W. P. and Rosenburg, A., Phys. Rev., 151, 434, 1966.

25. Granato, A. and Lücke, K., J. Appl. Phys. 27, 789, 1956; 27, 583, 1956.

26. Cottrell, A. H., Dislocations and Plastic Flow in Crystals, p. 65, Oxford Press, 1963.

27. Seeger, A. and Schiller, P., Act. Met., 10, 348, 1962; Seeger, A. and Schiller, P., Chap VIII, IIIA, Physical Acoustics , edited by W. P. Mason, Academic Press, 1965; Suzuki, T. and Elbaum, C., J. Appl. Phys., 35, 1539, 1964; Alefeld, G., J. Appl. Phys., 36, 2642, 1965.

28. Alers, G. and Zimmerman, J. E., Phys. Rev., 139, A414, 1963; see also Chap. 7, IVA, Physical Acoustics, Academic Press, edited by W. P. Mason, Fig. 10.

29. Schultz, J. and Chambers, R., Bull. Am. Phys. Soc. 9, 214, 1964.

30. Southgate, P. D. and Attard, A. E., J. Appl. Phys., 34, 855, 1963.

31. Pearson, G. L., Read, W. T. and Feldman, W. L., Acta Met., 5, 181, 1957.

32. Alefeld, Georg, J. Appl. Phys., 36, 2642, 1965.

33. Suzuki, T., Ikushima, A., and Aoki, M., Acta Met., 12, 1231, 1964.

34. Mitchell, O.M. Mracek, J. Appl. Phys., 36, 2083, 1965.

35. Mason, W. P. and Rosenburg, A., "Damping of Dislocations in Lead Single Crystals", J. Appl. Phys., 1967.

36. Mason, W. P. and Roserburg, A., "Phonon and Electron Drag Coefficients in Single Crystal Aluminum", Phy. Rev., 151, 434, 1966.

37. Mason, W. P., Fifth National Congress of Applied Mechanics Proceedings, 361-383, 1966.

38. Thanks are due to Dr. O.M.M. Mitchell for this crystal.

39. Lücke, K., J. Appl. Phys., 27, 1433, 1956.

40. Mason, W. P., Piezoelectric Crystals and Their Application to Ultrasonics, Sec. A7.2, 479-481, D. Van Nostrand Co. Inc., 1950.

41. Akheiser, A., J. Phys. U.S.S.R. 1, 277, 1939.

42. Mason, W. P., Temperature Dependence of Elastic and Anelastic Properties of Solids, High Temperature Structures and Materials, edited by A. M. Freudenthal, B. A. Boley and H. Liebowitz, Pergamon Press, 1964. Chapt. VI, IIIB, Physical Acoustics, Academic Press, 1965; Mason, W. P. and Bateman, T. B., J. Acous. Soc. Amer. 36, 644, 1964.

43. See Chap. II by Anderson, O.L., Vol. IIIB of Physical Acoustics, edited by W. P. Mason, Academic Press, 1965, for a discussion and evaluation of Debye Velocities.

44. See Maxwell, J. C., Phil. Trans. Roy. Soc., London 157, 49, 1867; Phil. Mag. Ser. 4, 35, 129, 1868 for deviation of this formula for a gas.

45. Mason, W. P. and Bateman, T. B., J. Acous. Soc. Amer., 40, 852, 1966.

46. White, G. K., and Woods, S. B., Phil. Mag., 45, 1343, 1954.

47. Hiki, Y. and Granato, A.V., Phys. Rev., 144, 411, 1966.

48. Leibfried, G. and Schlömann, E., Nachr. Akad. Wiss. Gott. 11a, 71, 1954.

49. American Institute of Physics Handbook, p. 457-58, for Tables, McGraw-Hill Company, 1963.

50. Mason, W. P., Phys. Rev., 97, No. 2, 557, Jan. 15, 1955.

51. Lax, E., Phys. Rev., 115, 1591, 1959.

52. Filson, D. H., Phys. Rev., 115, 1516, 1959.

53. Eshelby, J. D., Proc. Roy. Soc., (London), A197, 396, 1949.

54. Leibfried, G., Z. Physik, 127, 344, 1950.

55. Eshelby, J. D., Proc. Roy. Soc., A266, 222, 1962.

56. Mason, W. P., J. Acous. Soc. Amer. 32, 458, 1960; J. Appl. Phys. 35, 2779, 1964.

57. Mason, W. P., Appl. Phys. Letters, 6, No. 6, 111, 1965; Phys. Rev., 143, 229, 1966.

58. Weertman, J. and Salkovitz, E.I., Acta Met., 3, 1, 1955; and Reference 6.

59. Fiore, H. F. and Bauer, C. L., J. Appl. Phys., 36, 2642, 1965.

60. Friedel, J., N.P.L. Conference on the Strength of Alloys.

61. Alefeld, Georg, Phil. Mag. 11, 809, 1965; Bauer, C. L., Phil. Mag., 11, 827, 1965.

62. Blaha, F. and Langenecker, B., Acta Met., 7, 93, 1959; Langenecker, B., A.I.A.A. Journ. 1, 80, 1963.

63. Lazan, B. J., "Fatigue" Chap. 2, Amer. Soc. of Metals, 1954; Murray Lecture, p. 1-21, Soc. Exp. Stress Analysis, 1957.

64. Mason, W. P., Chap. 8, "Resonance and Relaxation in Metals", Amer. Soc. Metals, 1965

65. Wood, W. A., Torsion Cycling and Torsion Creep of Alloy Ti-6Aℓ-4V, Institute for the Study of Fatigue and Reliability, Contract Nonr 266(91), Technical Report 45 March 1967.

Table I

Data for determining the drag coefficient B and the loop length ℓ_o as a function of the temperature.

Temp°K	$Q^{-1}\omega$	f_M in MHz/sec	Q_M^{-1}	$B\times10^4$	$N\times10^{-7}$	ℓ_o
300°	4.2×10^5	50	1.8×10^{-3}	3.7	2.4	5.4×10^{-5}
200°	5.05×10^5	8	1.3×10^{-3}	3.1	2.4	$5\ \times10^{-5}$
78°	12.6×10^5	12	2.4×10^{-3}	1.24	2.4	6.2×10^{-5}
60°	14.2×10^5	17	2.15×10^{-3}	1.1	2.4	5.7×10^{-5}

$(Q^{-1}\omega)$ are limiting values for high frequencies. B in units of dyne sec./cm^2; ℓ_o in cms.

Table II

Table listing quantities necessary to calculate the phonon viscosity for lead

Temp $^{\circ}$K	$E_o/\rho C_v$ in $^{\circ}$K	K (watts/cm^2)	$\frac{E_o K}{\rho C_v \bar{v}^2} \times 10^3$
300	265	0.0067	1.95
200	166	0.01	1.82
150	116.5	0.0133	1.7
100	69.8	0.02	1.54
78	49.5	0.0256	1.39
60	34.1	0.0333	1.25

Table III

Table listing quantities necessary to calculate the phonon viscosity and phonon damping of aluminum

Temp ^{o}K	$E_o/\rho C_v$ in ^{o}K	K_L (watts/cm^2)	$\frac{E_o K}{\rho C_v \bar{V}^2} \times 10^3$	Bx10^4
300	187	0.356	5.44	31.5
200	104	0.535	4.55	26.2
150	66.5	0.715	3.88	22.2
100	34.4	1.07	3.01	17.3
77	23.2	1.39	2.63	15.2
66	18.4	1.62	2.43	14.0

$\theta = 425^{o}K$; $\bar{V} = 3.5 \times 10^5$; $B = .0706 D (E_o K/\rho C_v \bar{V}^2)$; $D = 8.15$

Table IV

Table listing quantities necessary to calculate the phonon viscosity and phonon damping of copper.

Temp ^{o}K	$E_o/\rho C_v$ in ^{o}K	K_L(watts/cm^2)	$\frac{E_o K}{\rho C_v \bar{V}^2} \times 10^3$	Bx10^4
300	200	0.125	3.7	7.85
200	114.8	0.187	3.17	6.7
150	74.5	0.25	2.74	5.8
100	39.6	0.375	2.2	4.65
77	26.2	0.486	1.88	3.98
58	17.1	0.64	1.64	3.48

$\theta = 343^{o}K$; $\bar{V} = 2.6x10^5$; $B = \frac{b^2 D}{8\pi a_o^2} \left(\frac{E_o K}{\rho C_v \bar{V}^2}\right)$; $D = 3.0$; $a_o = \frac{3}{4} b$

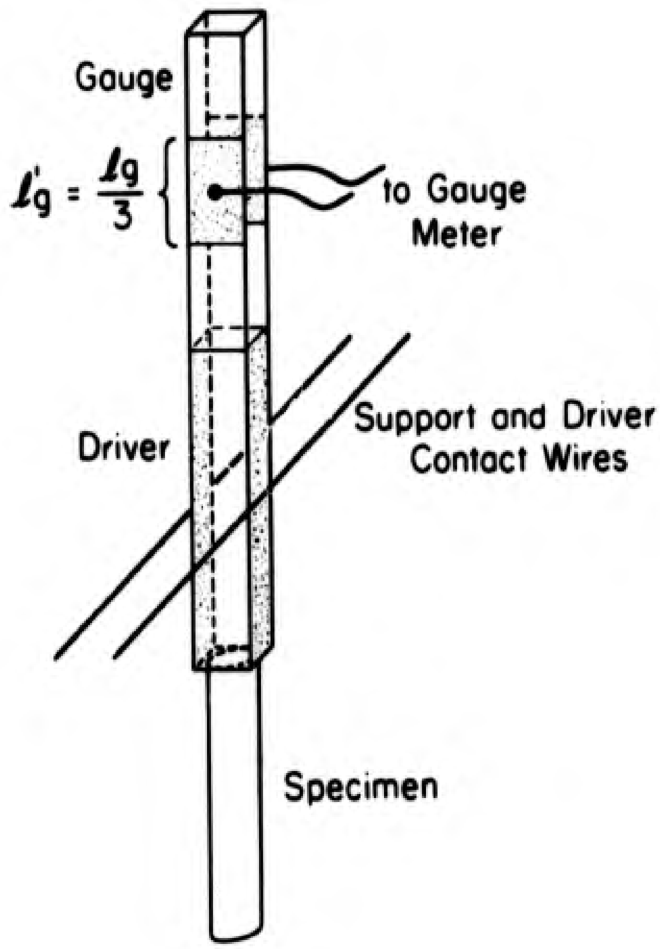

Fig. 1. Method for measuring modulus change and internal friction at low frequencies.

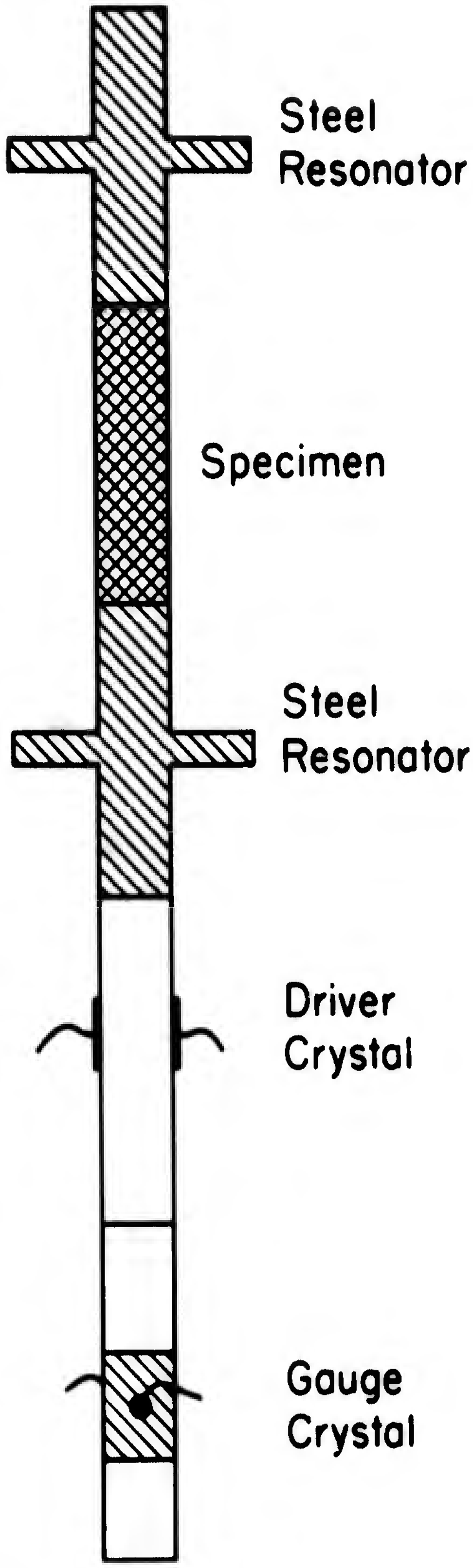

Fig. 2. Method for superposing static stresses.

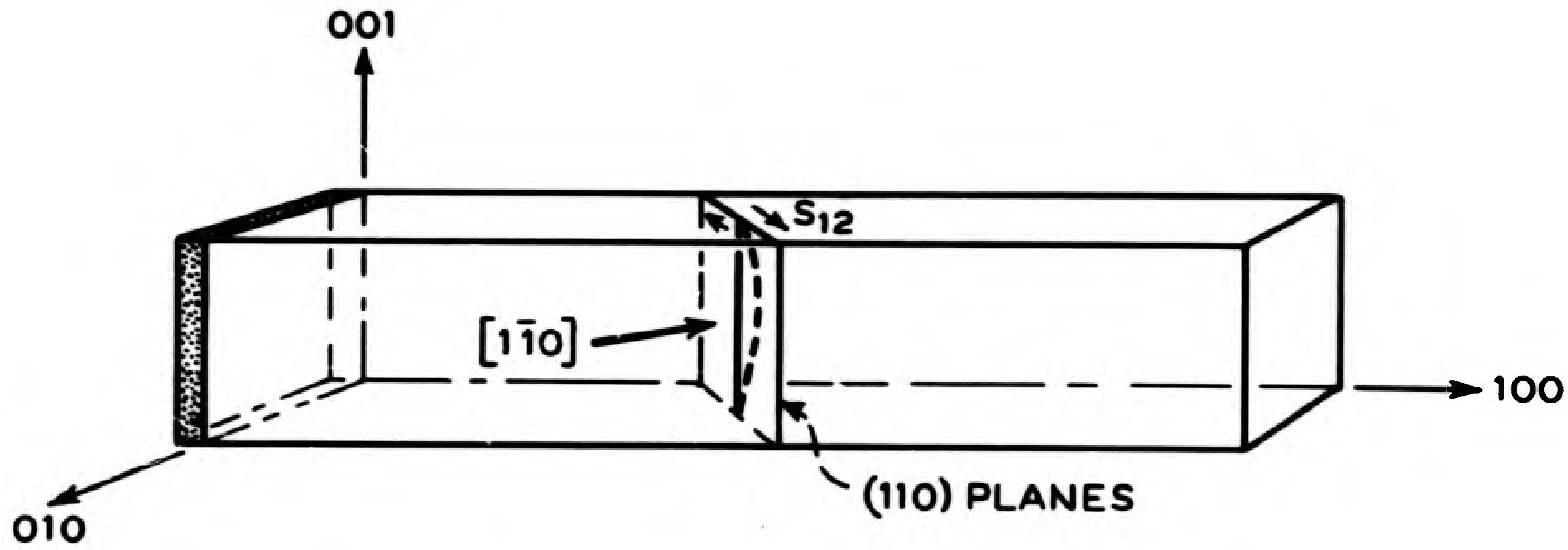

Fig. 3. Pulse method for measuring high frequency internal friction.

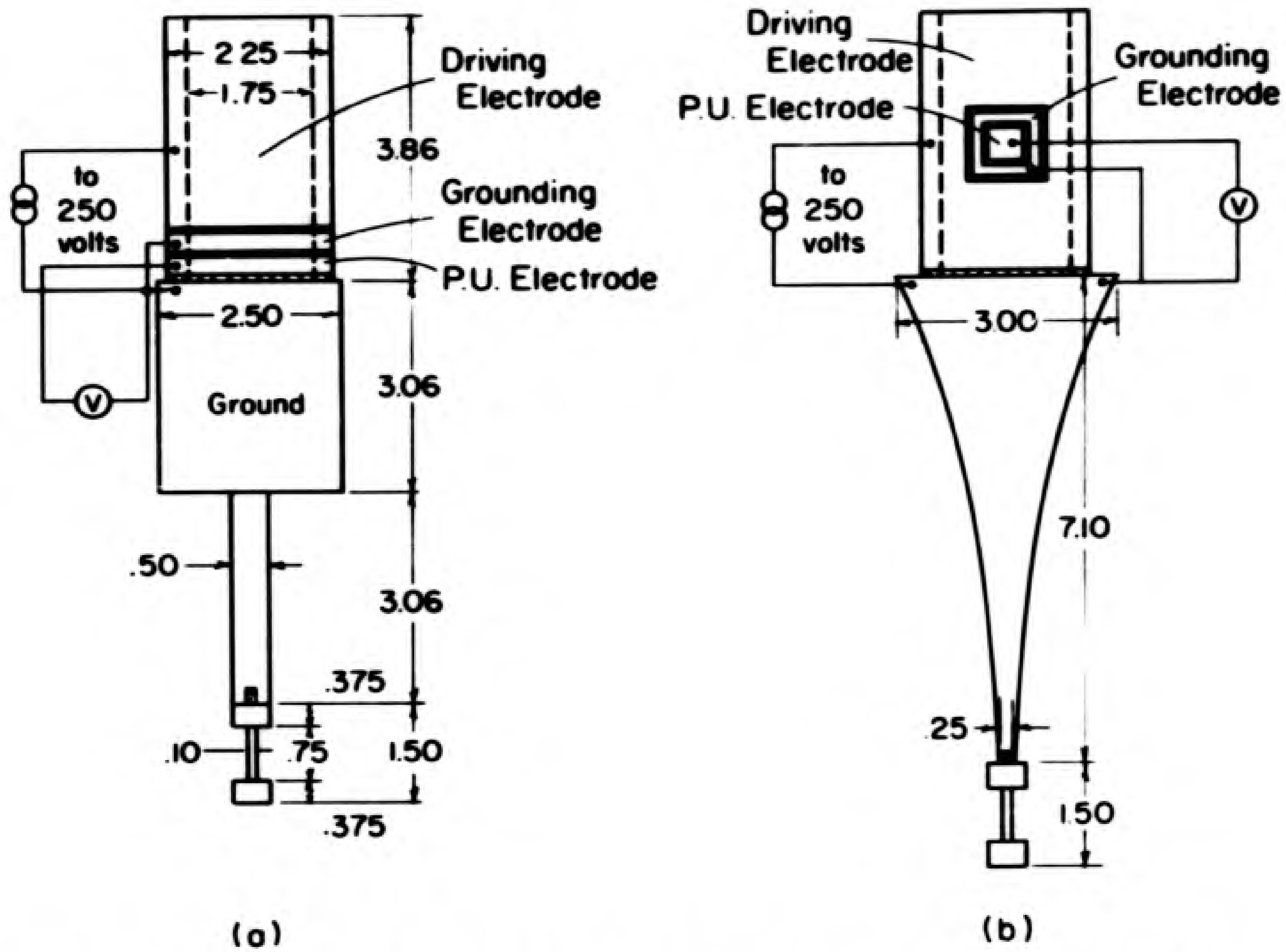

Fig. 4 a. Ceramic transducer, stub transformer and sample.

b. Ceramic transducer, exponential horn and sample.

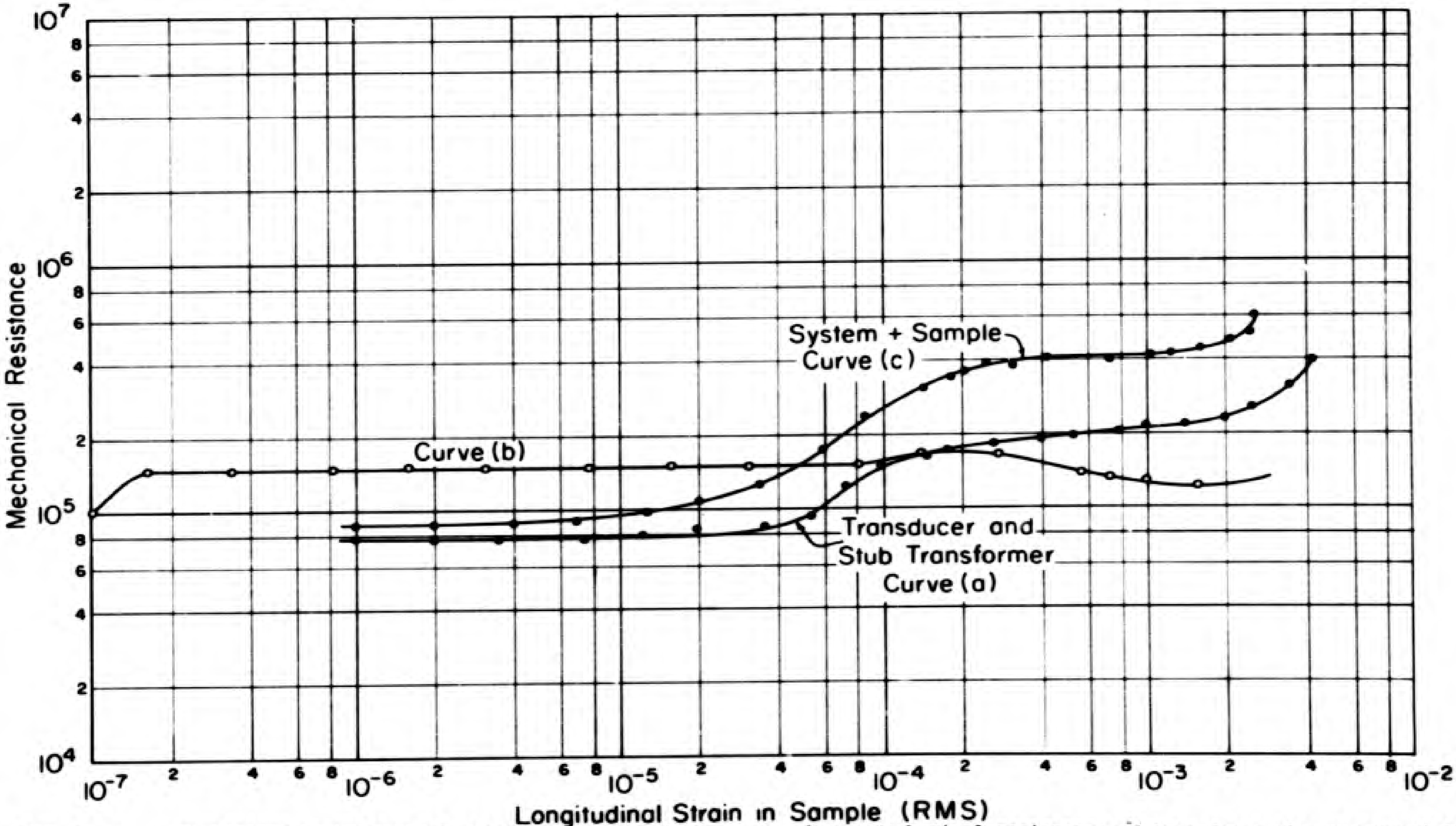

Fig. 5 a. Mechanical resistance of transducer plus stub transformer for strains present in the speciman.

b. Mechanical resistance of transducer plus exponential horn for strains present in the speciman.

c. Mechanical resistance of system plus 7075 aluminum sample.

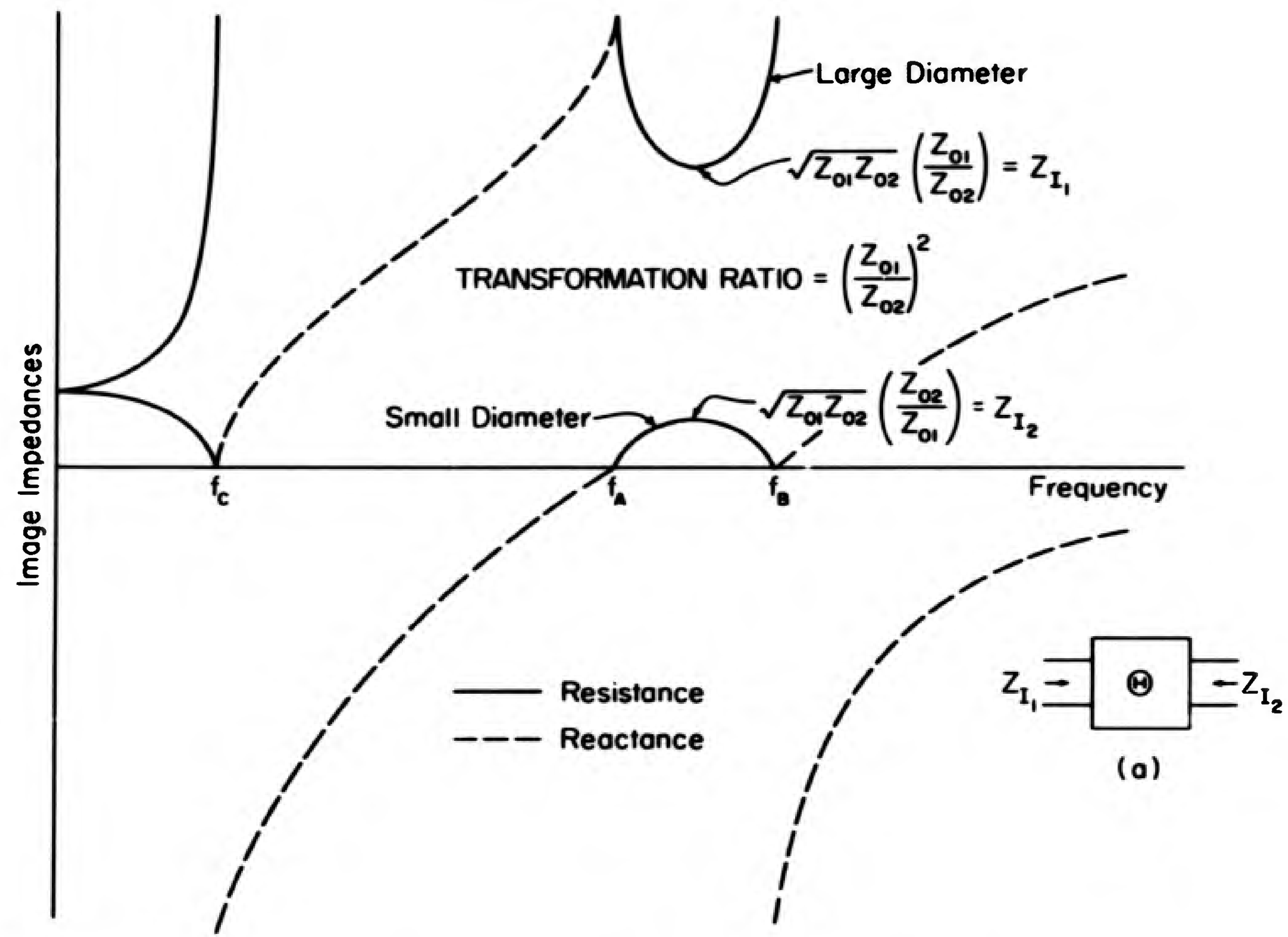

Fig. 6. Characteristic impedances of input and output of stub transformer.

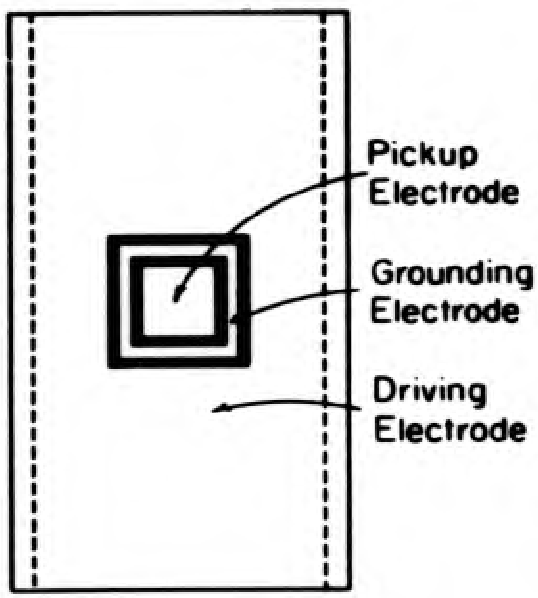

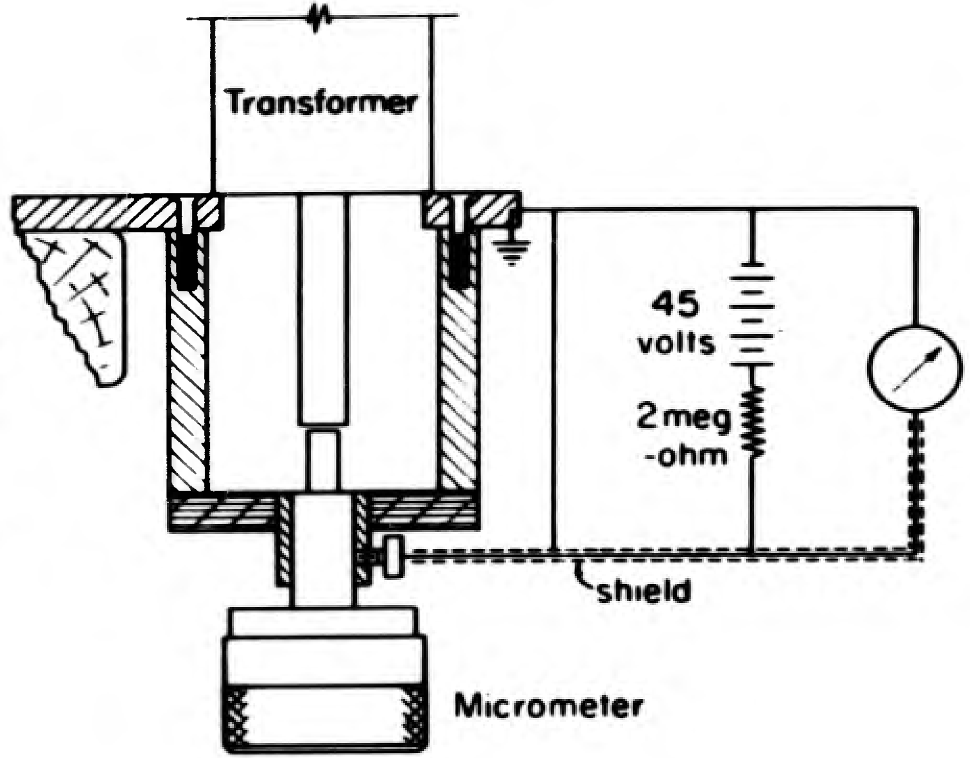

Fig. 7. Electrode arrangement for eliminating pick-up device.

Fig. 8. Electrostatic pick-up device.

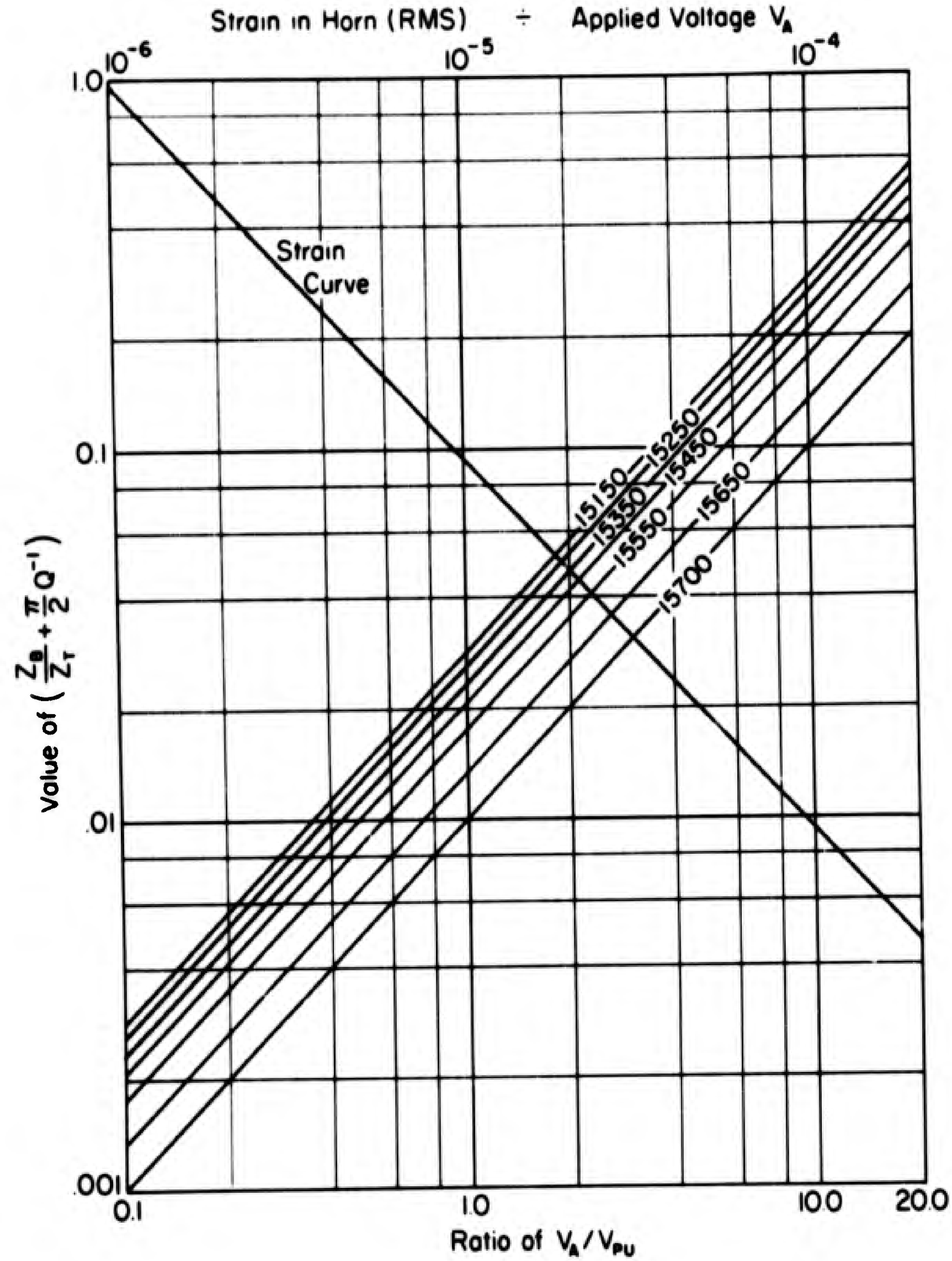

Fig. 9. Calibration curves for transducer and stub transformer.

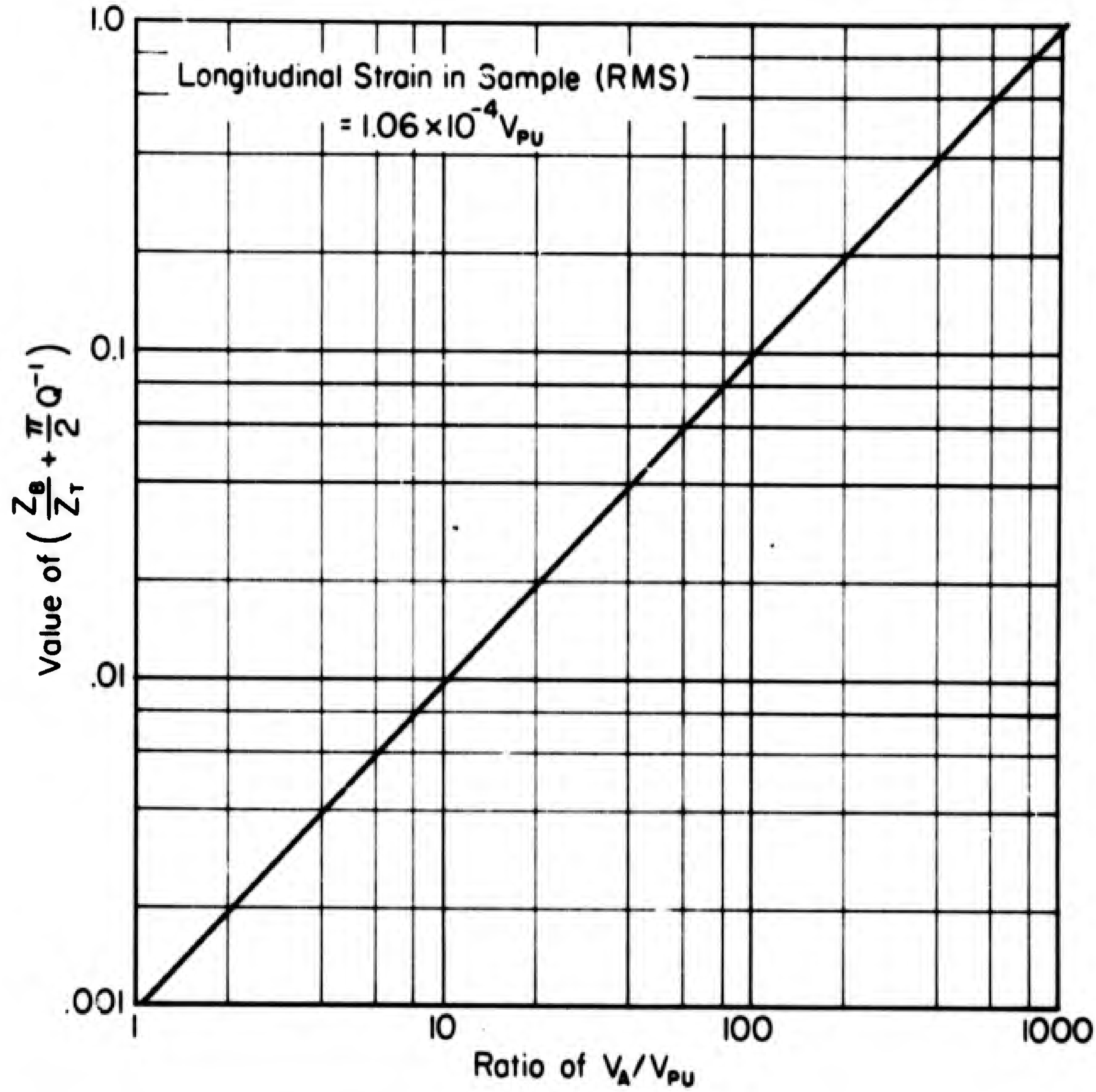

Fig. 10. **Calibration curves for exponential horn system.**

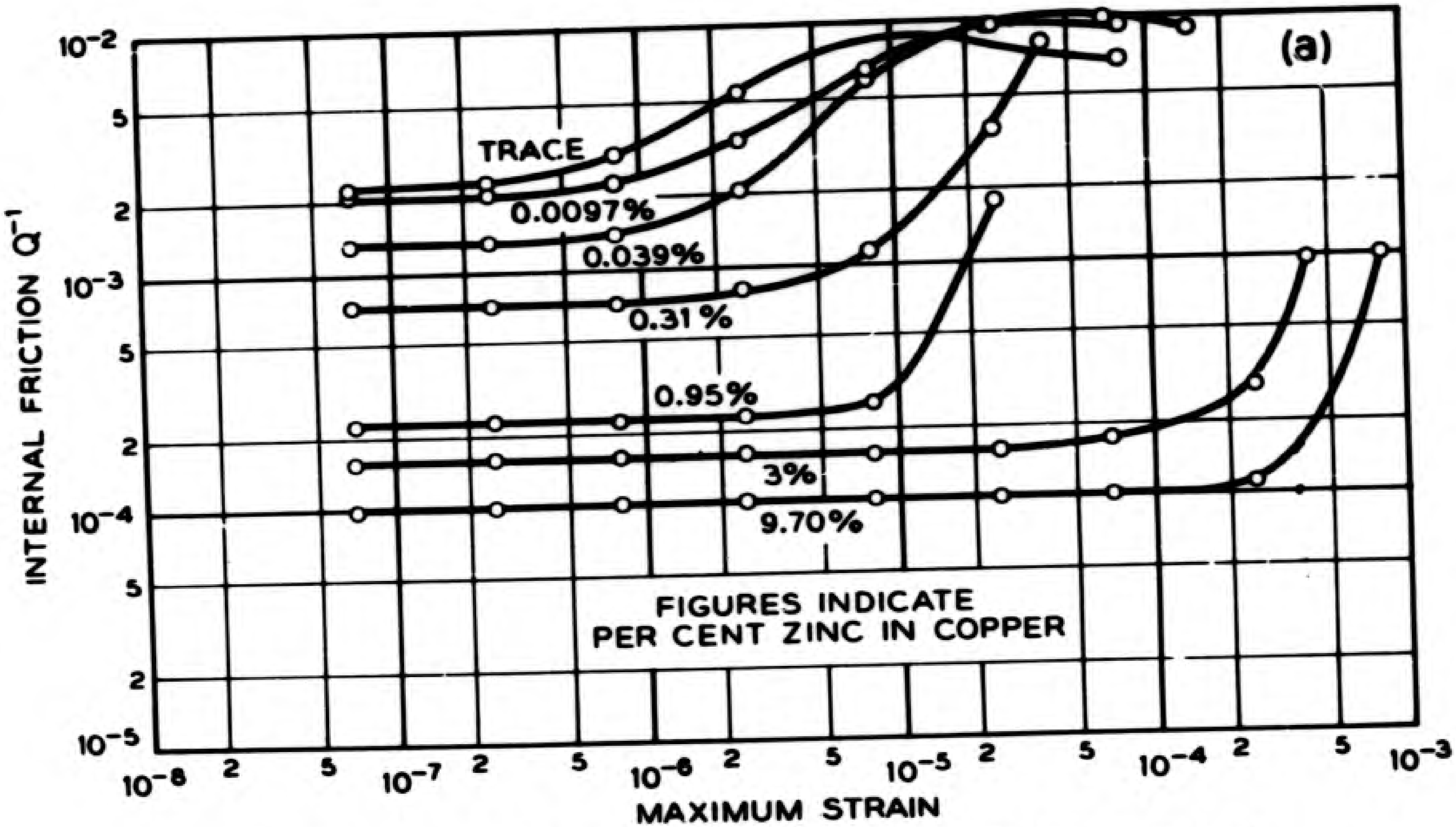

Fig. 11. Internal friction of copper, with various amounts of zinc added, as a function of the strain amplitude.

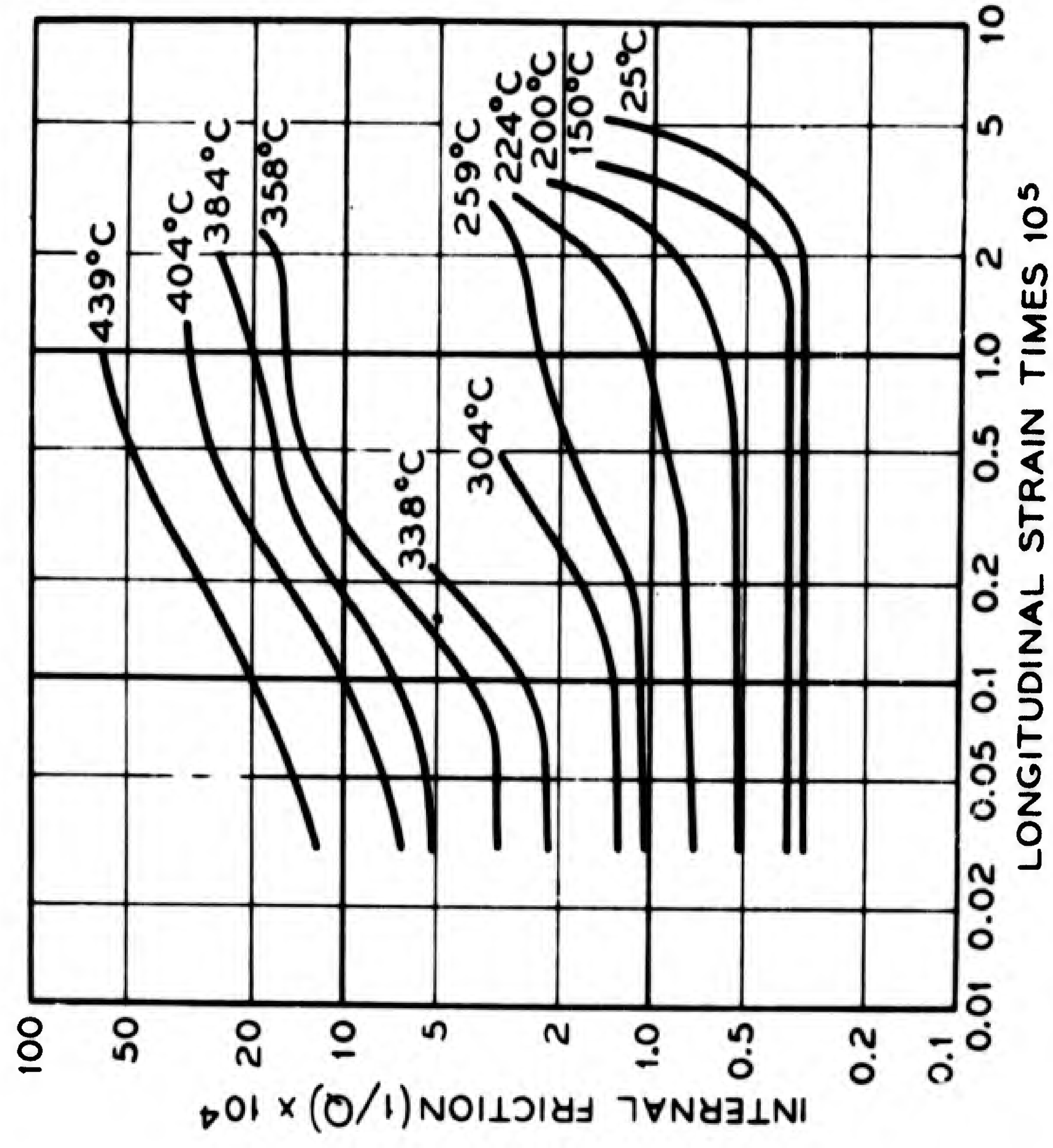

Fig. 12. Internal friction as a function of strain and temperature for a 99.995% pure aluminum single crystal.

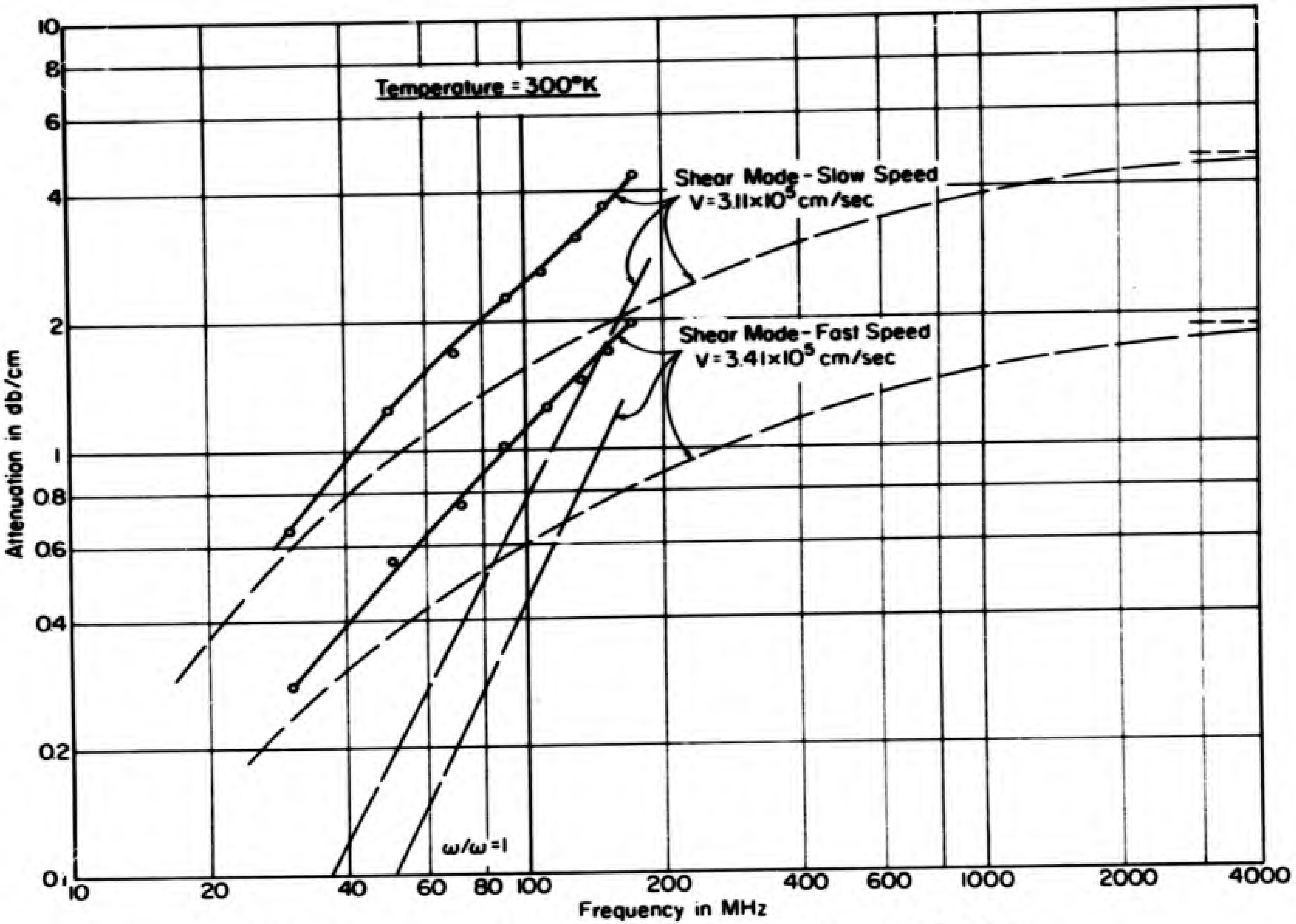

Fig. 13. Measured fast and slow shear-wave loss at 300°K as a function of the frequency. Dashed lines represent a breakdown of the loss into a square law loss and dislocation loss. Assymptotic value indicated by the dashed lines on the right.

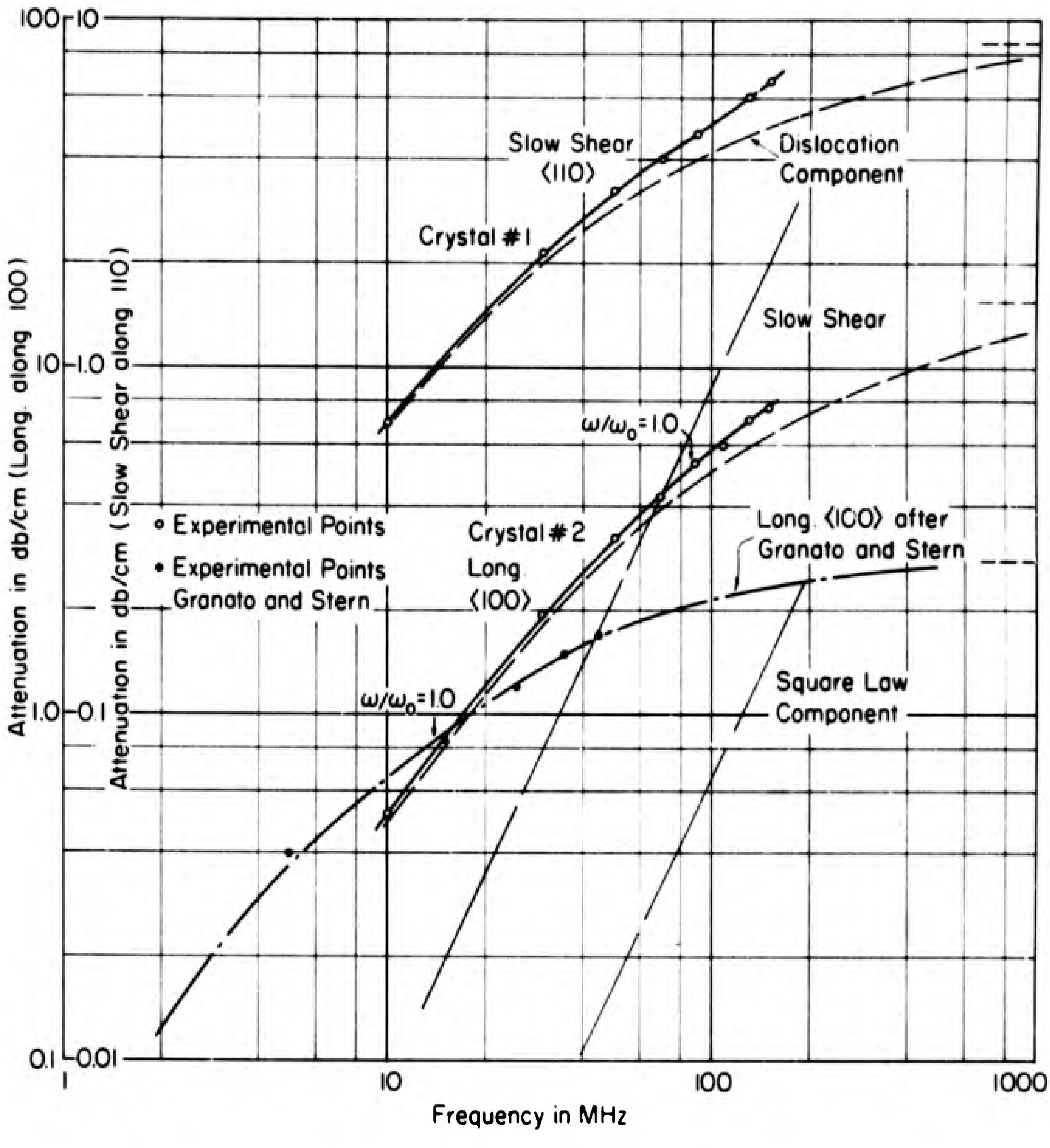

Fig. 14. Measured attenuation for longitudinal wave along <100> and slow shear wave along <110> direction. Dashed curves show breakdown into square law and dislocation loss. A comparison is given of dislocation loss along <100> measured by Granato and Stern. Assymptotic values indicated by dashed lines on the right.

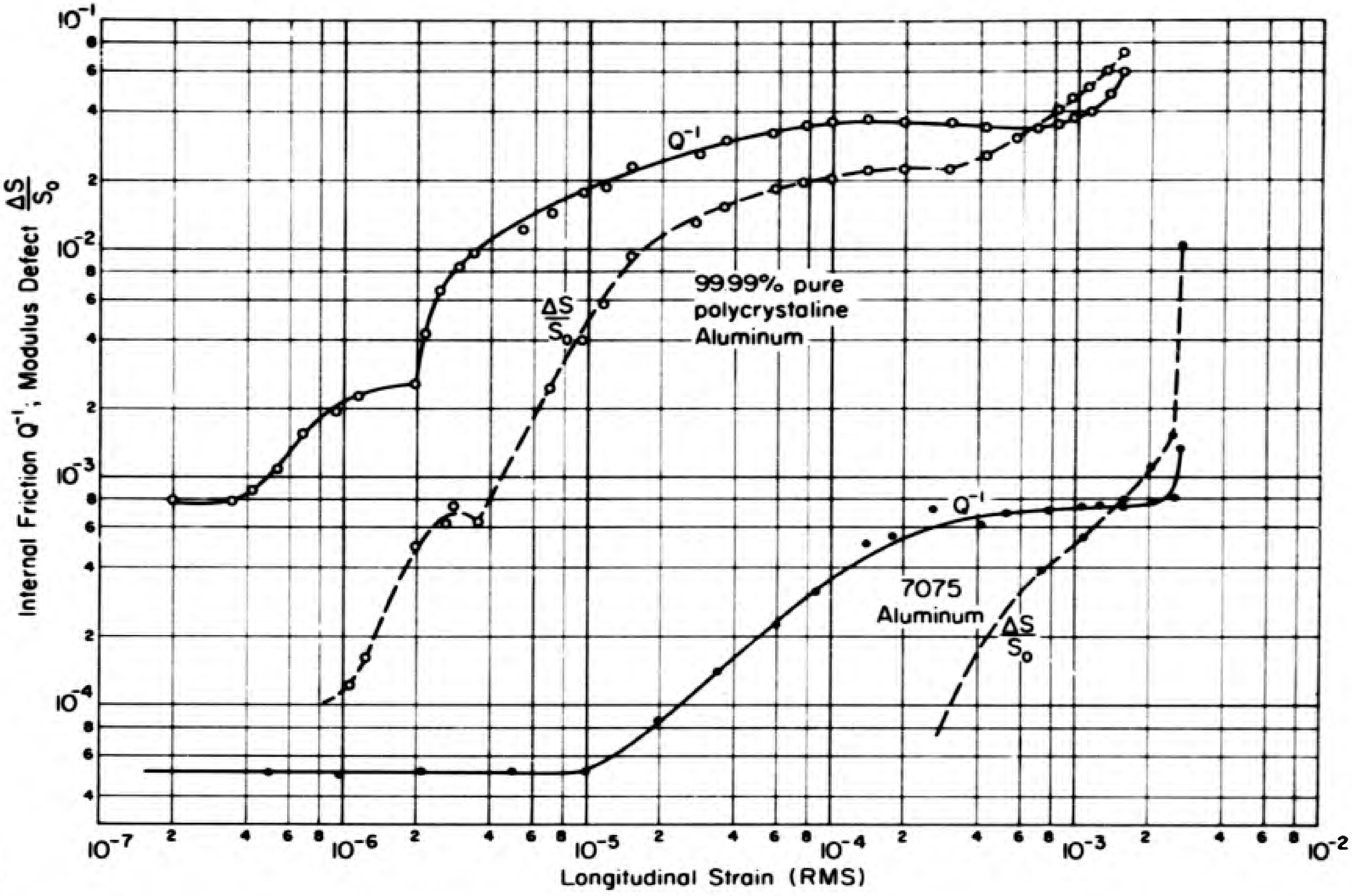

Fig. 15. High amplitude internal friction and modulus defect for 7075T6 aluminum and 99.99% pure polycrystal aluminum. Average grain size for pure aluminum is 0.1 m.m.

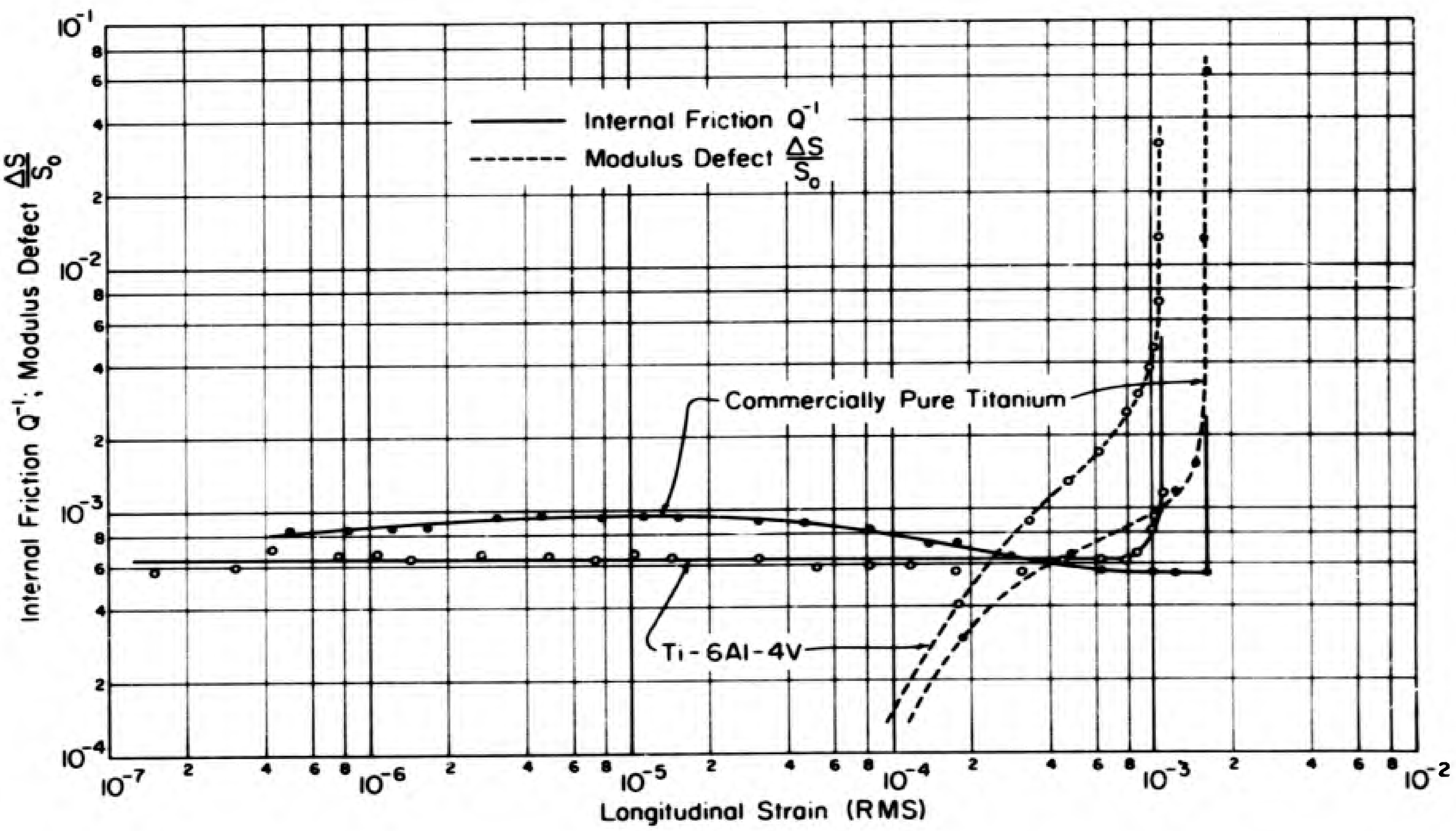

Fig. 16. High amplitude internal friction and modulus defects for commercial titanium and the alloy Ti-6% Aℓ-4%V.

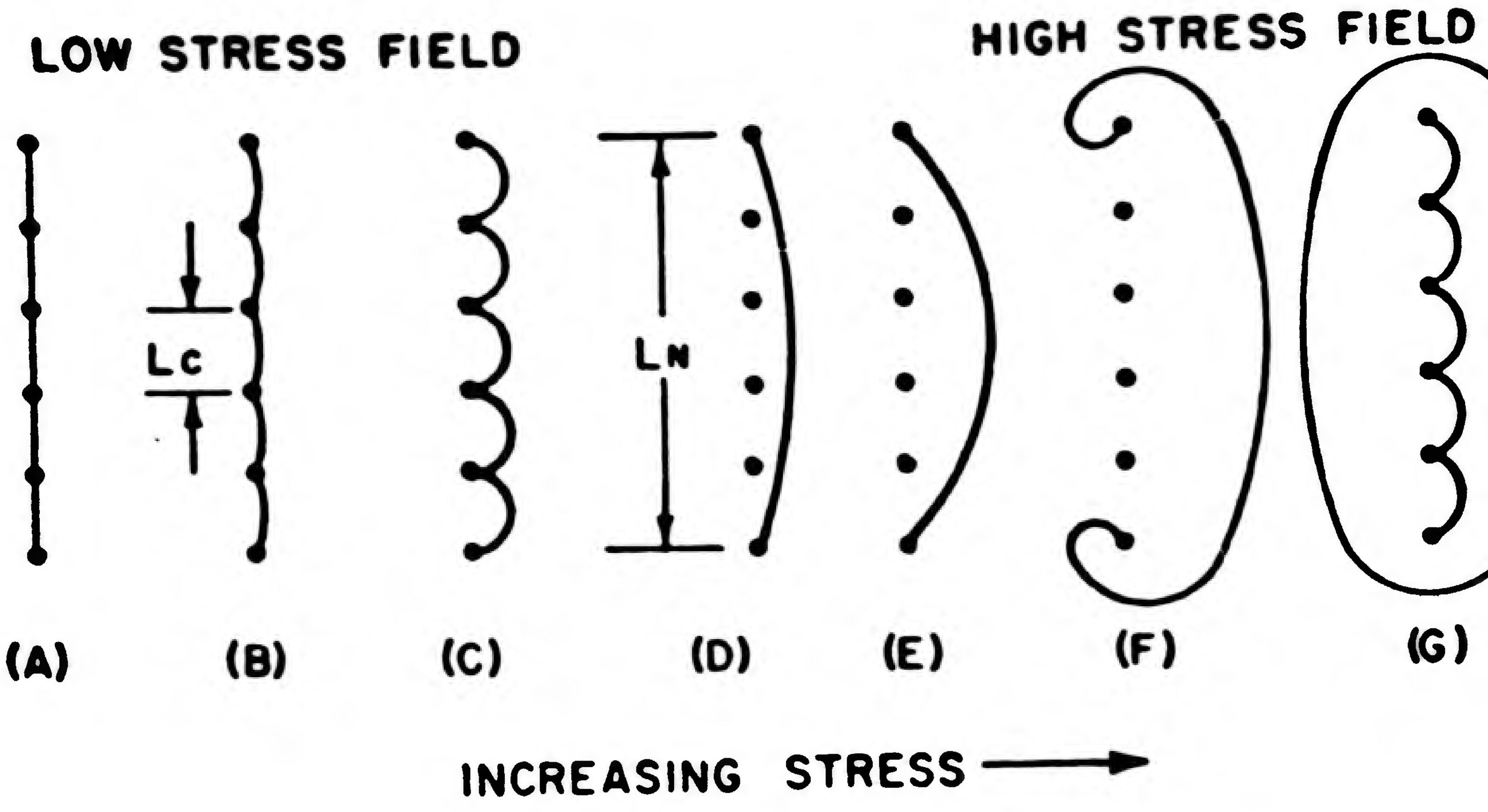

Fig. 17. Granato-Lücke mechanisms.

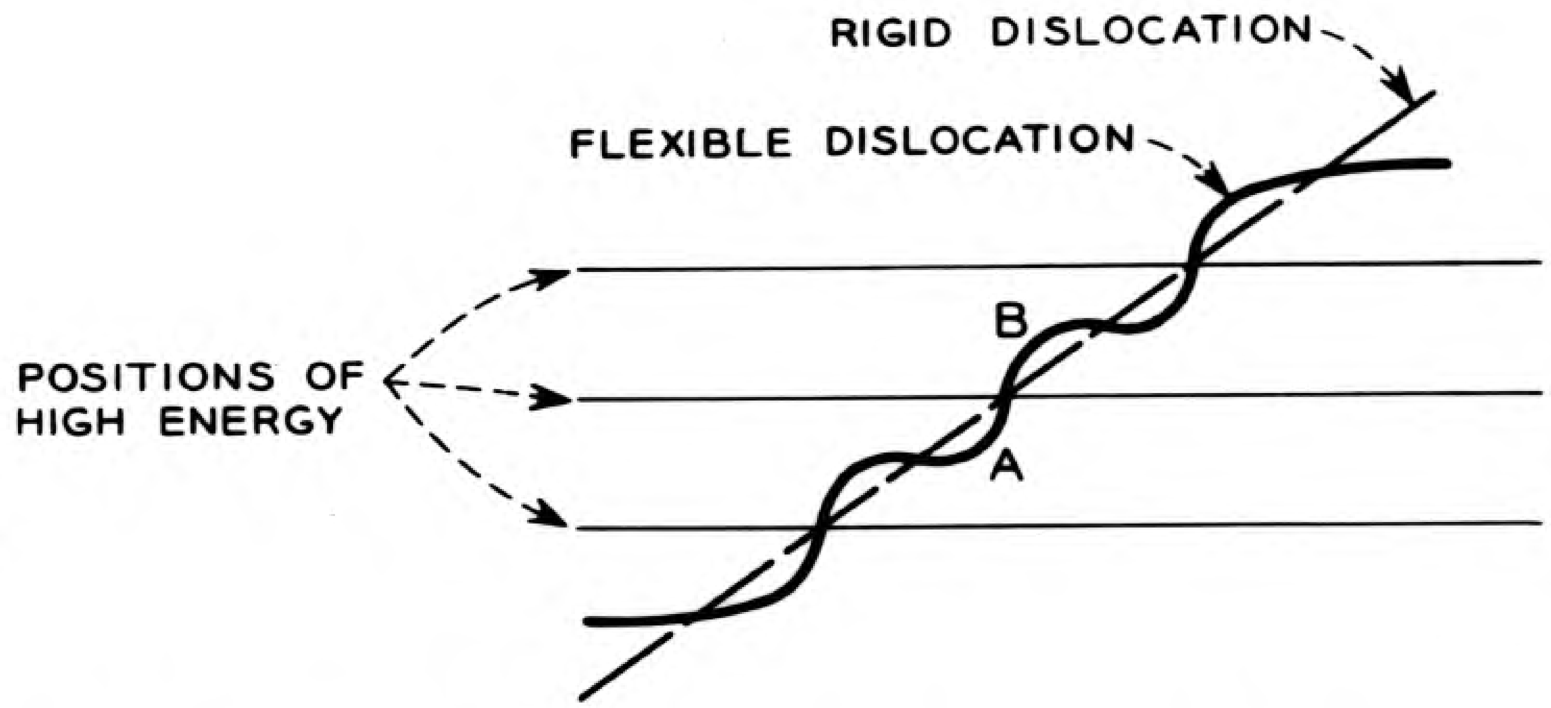

Fig. 18. **Form of zig-zag dislocation that crosses lattice rows in a slip plane (after Cottrell).**

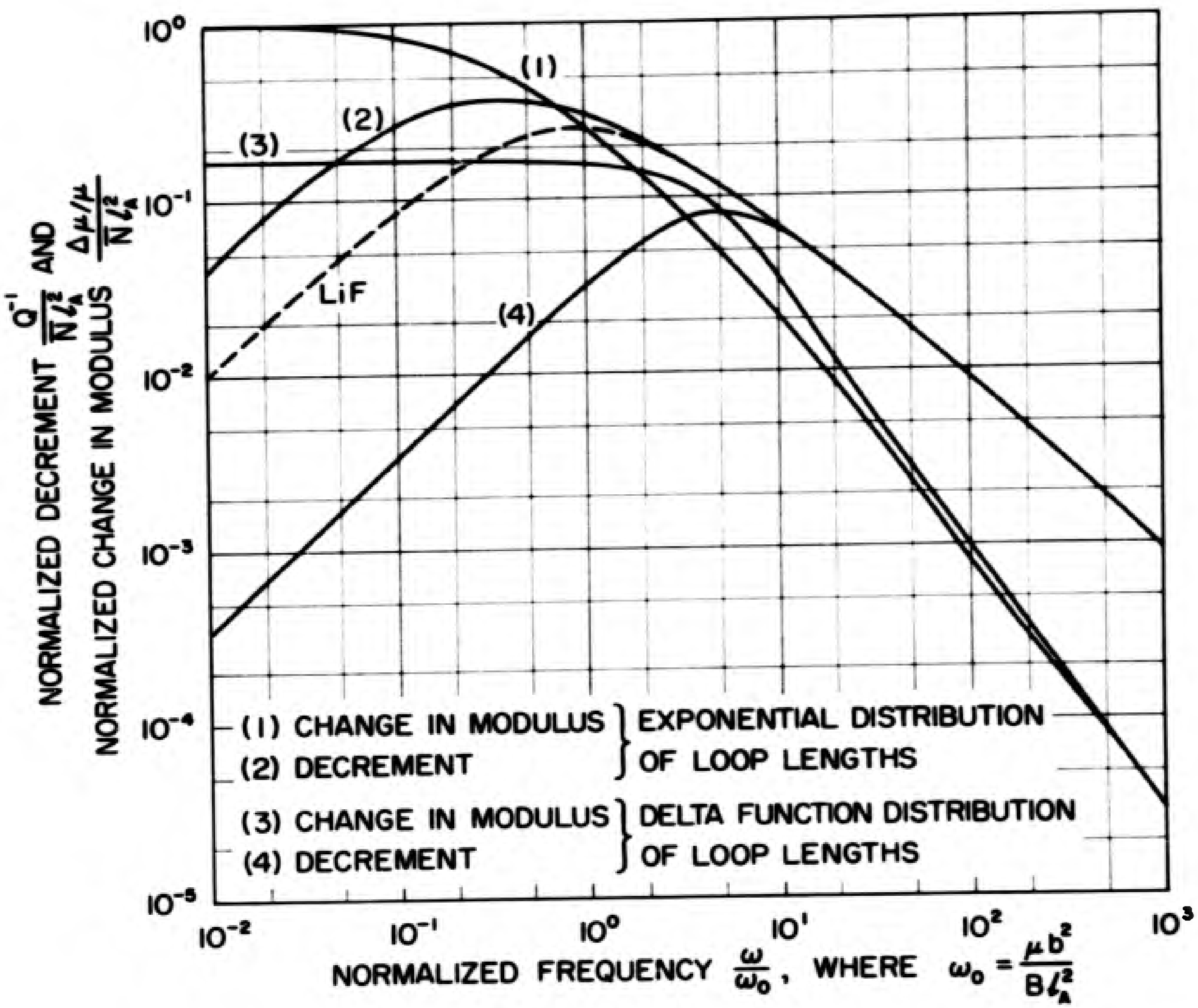

Fig. 19. Normalized internal friction and modulus defect curves for single loop distribution and exponential distribution.

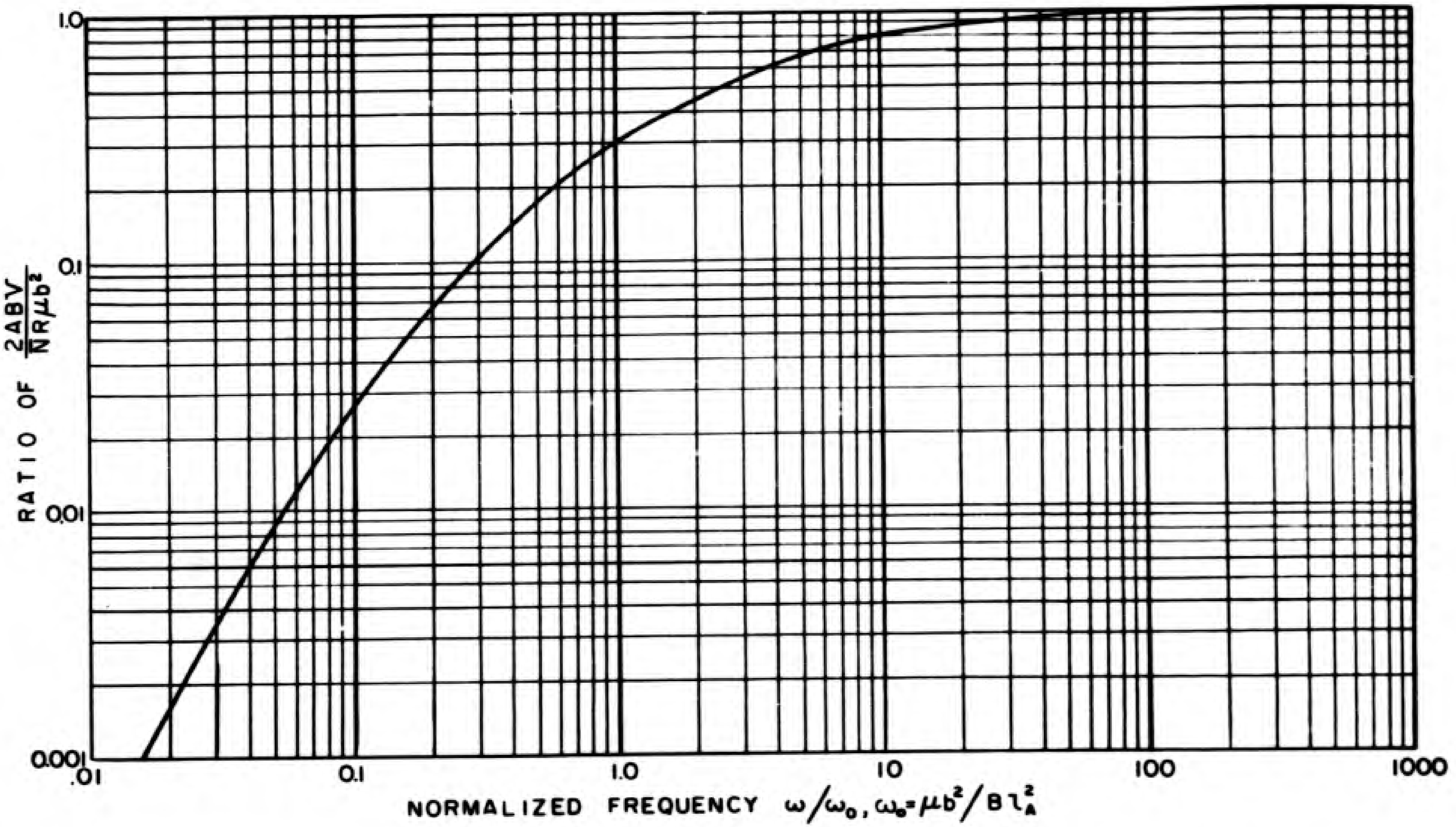

Fig. 20. Normalized attenuation curve.

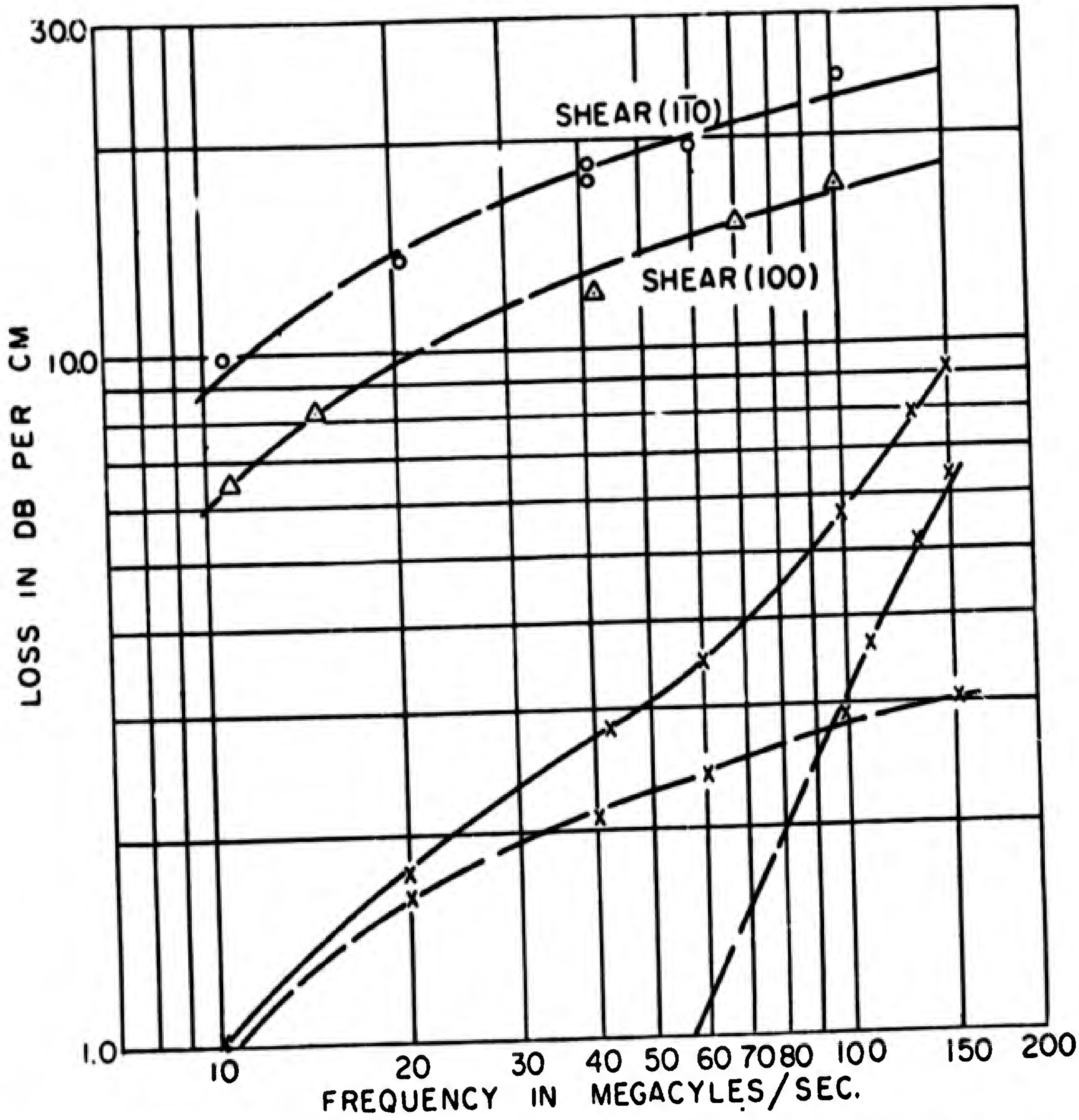

Fig. 21. Attenuation of a longitudinal and two shear waves transmitted along a <110> axis of a pure lead single crystal as a function of the frequency. Points show measured values. Dashed lines show separation into a frequency square law value and a dislocation component.

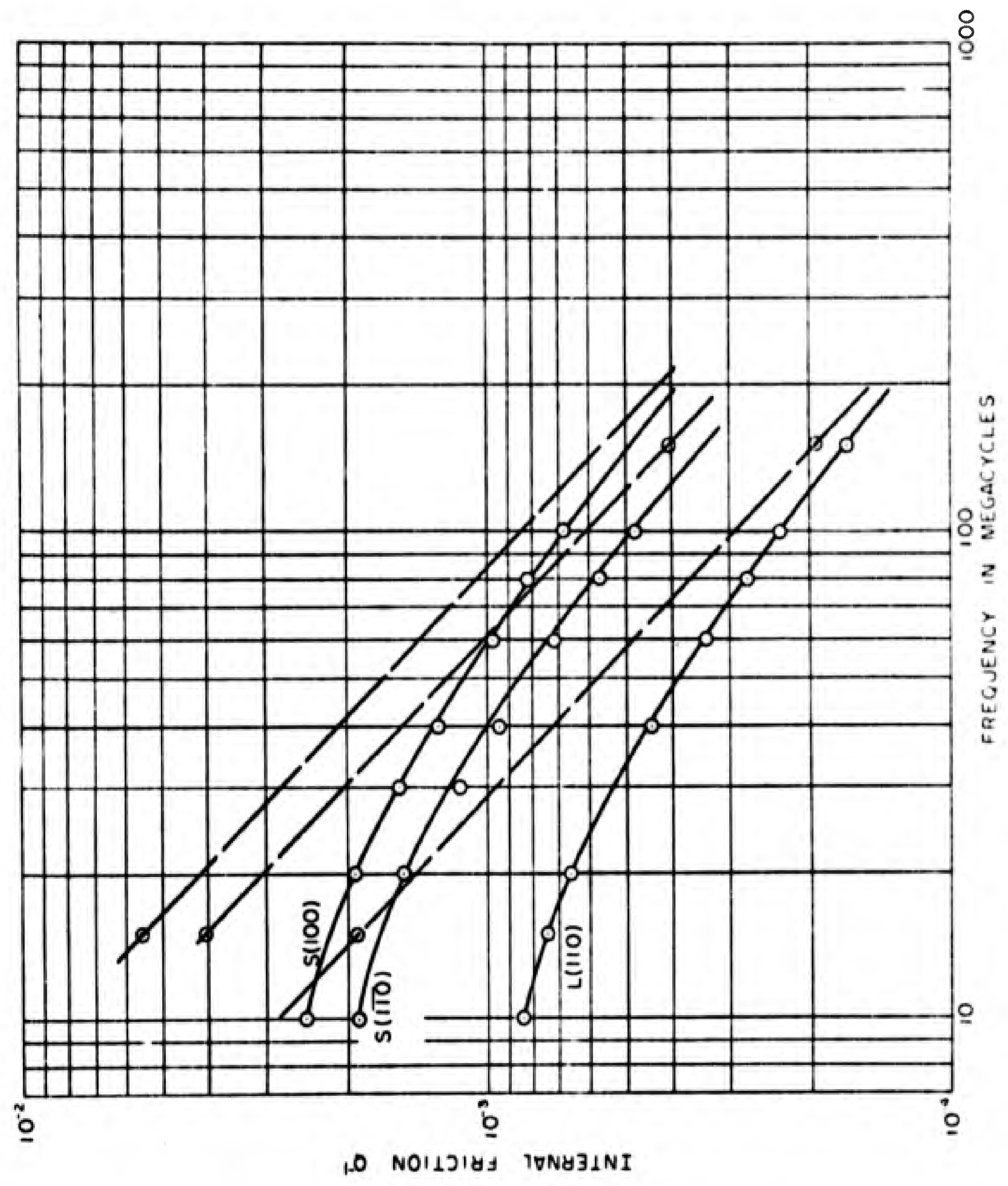

Fig. 22. Internal friction of three modes for a lead single crystal. Dashed lines show assymptotic values as determined by the standard curve of Fig. 19.

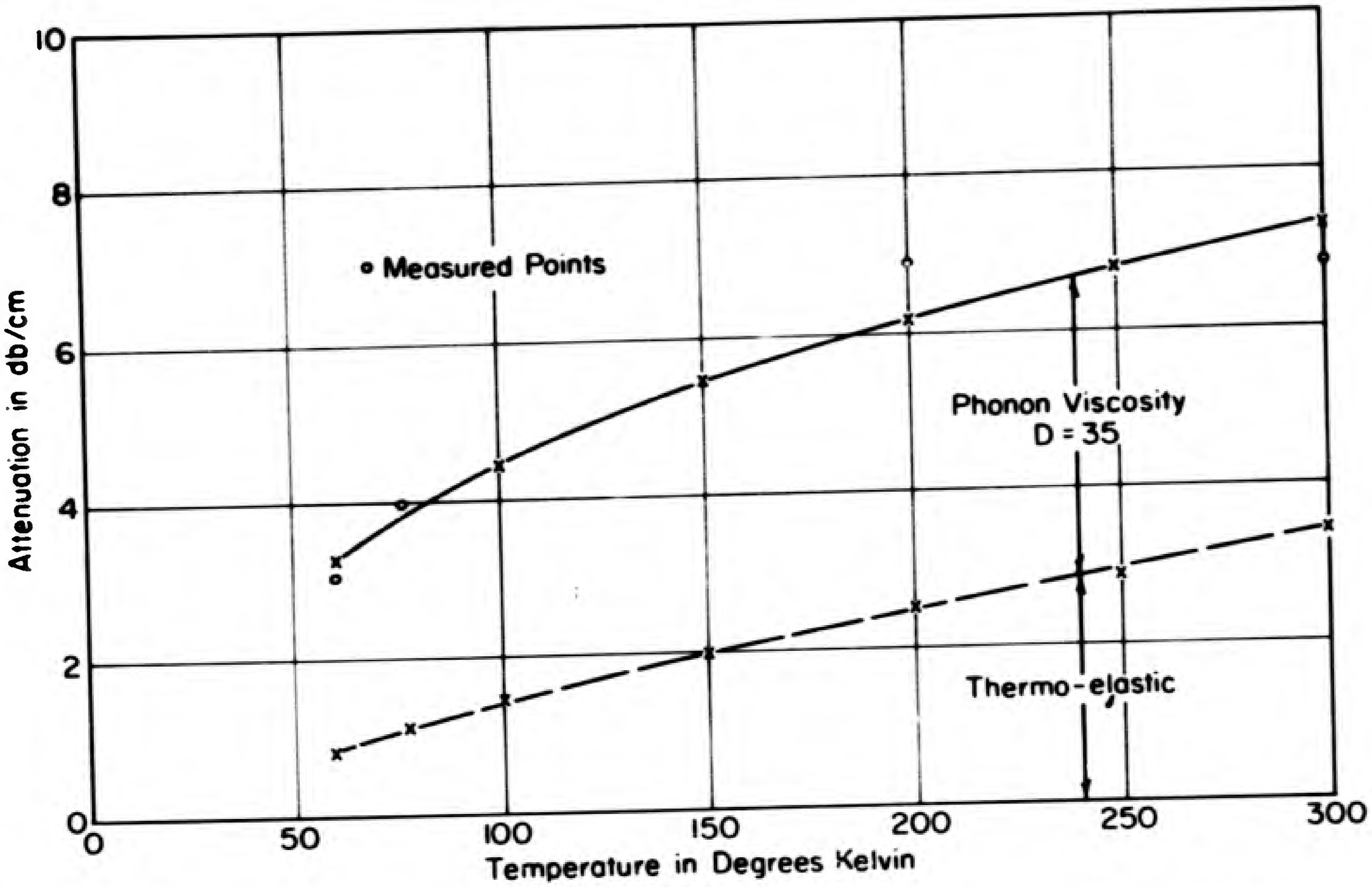

Fig. 23. Square-law attenuation for lead, measured at 150 MHz, plotted as a function of the temperature. Dashed line shows calculated thermoelastic loss while the difference between the solid and dashed lines shows phonon viscosity component with D = 35.

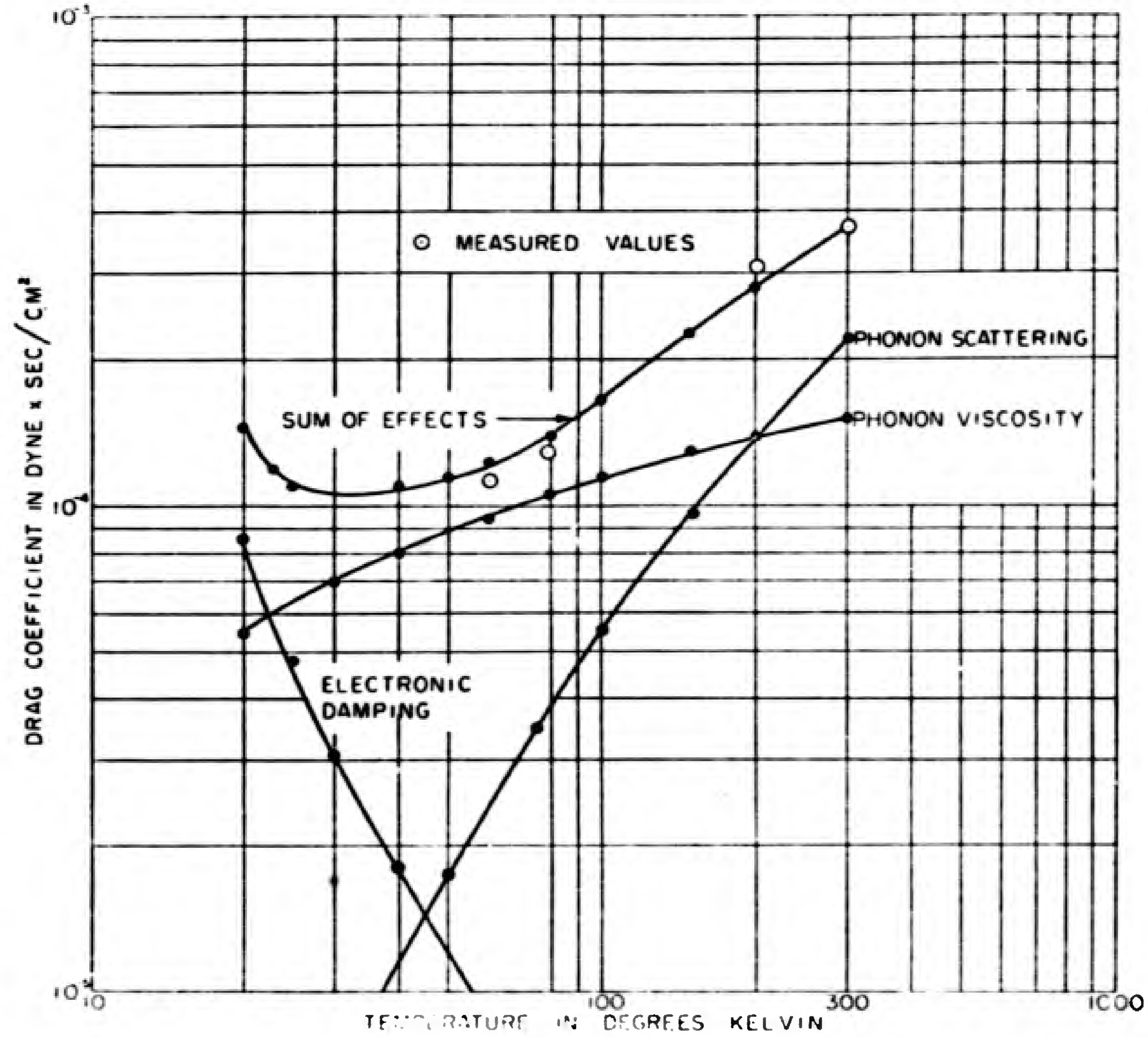

Fig. 24. Measured drag coefficients for lead (open circles) and the three components of dislocation drag.

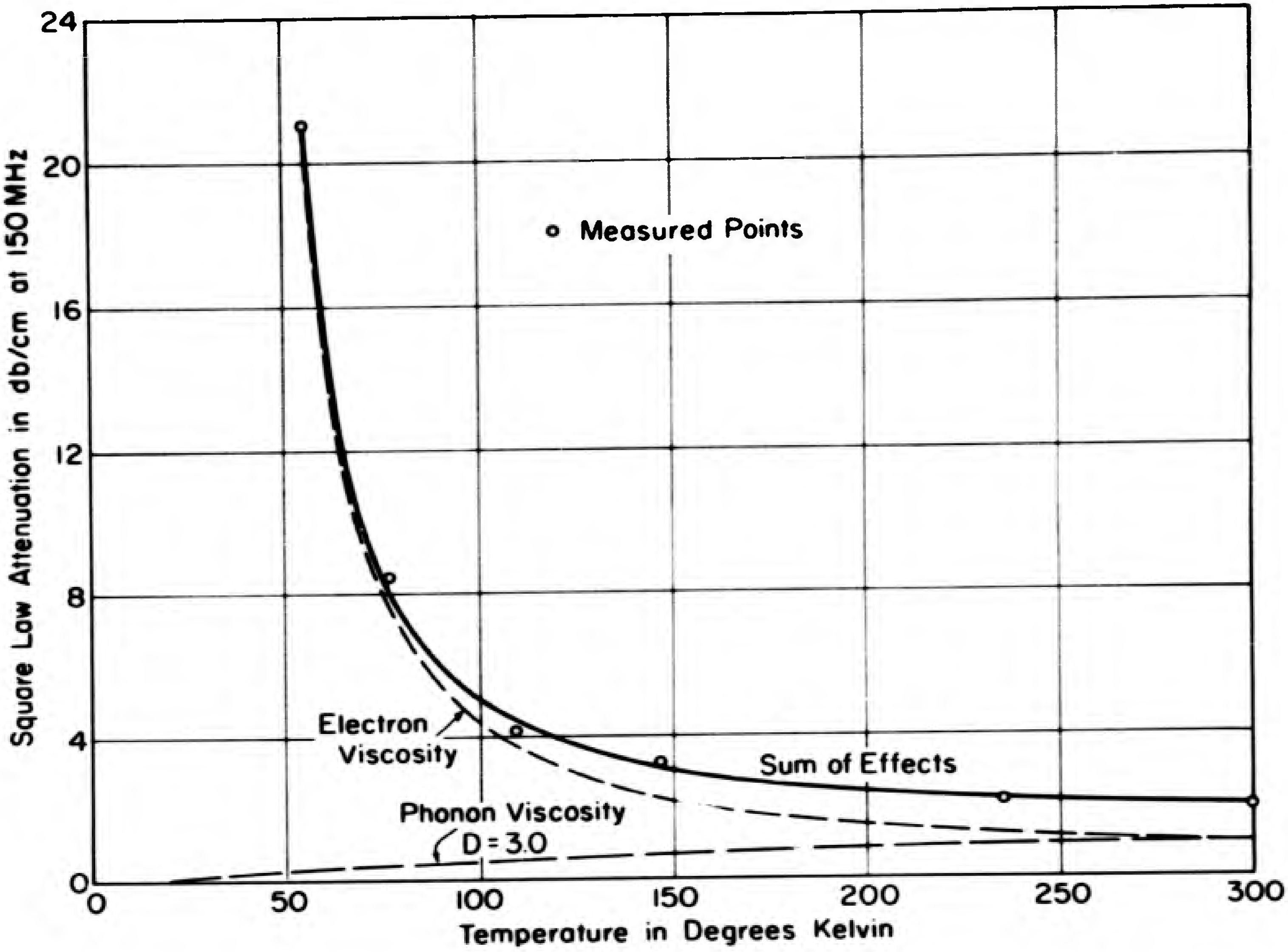

Fig. 25. Square law attenuation for copper, measured at 150 MHz, plotted as a function of the temperature. Slow shear wave along <110> (D value is 3.0).

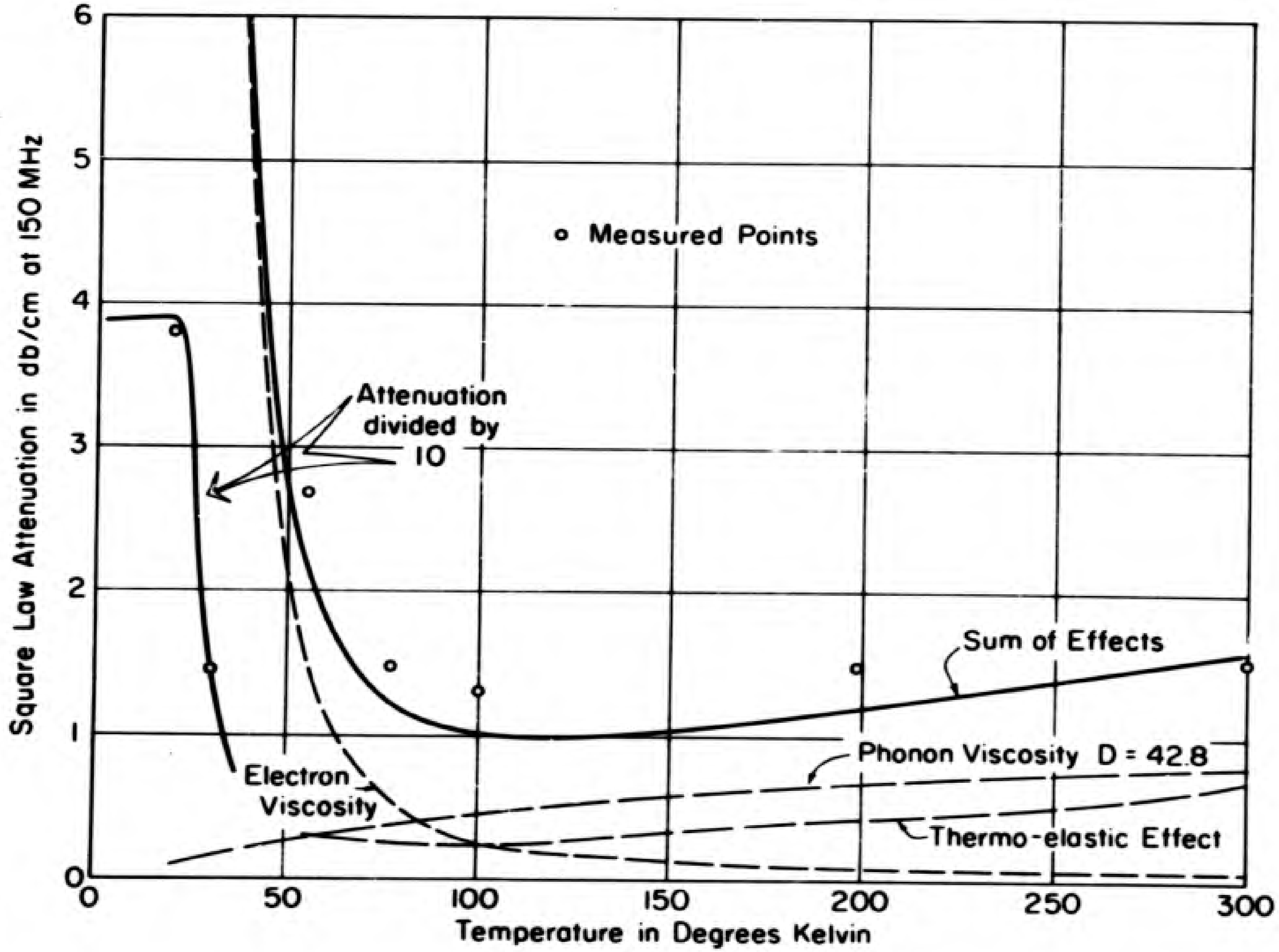

Fig. 26. Square law attenuation for copper, measured at 150 MHz, for a longitudinal wave along <100>.

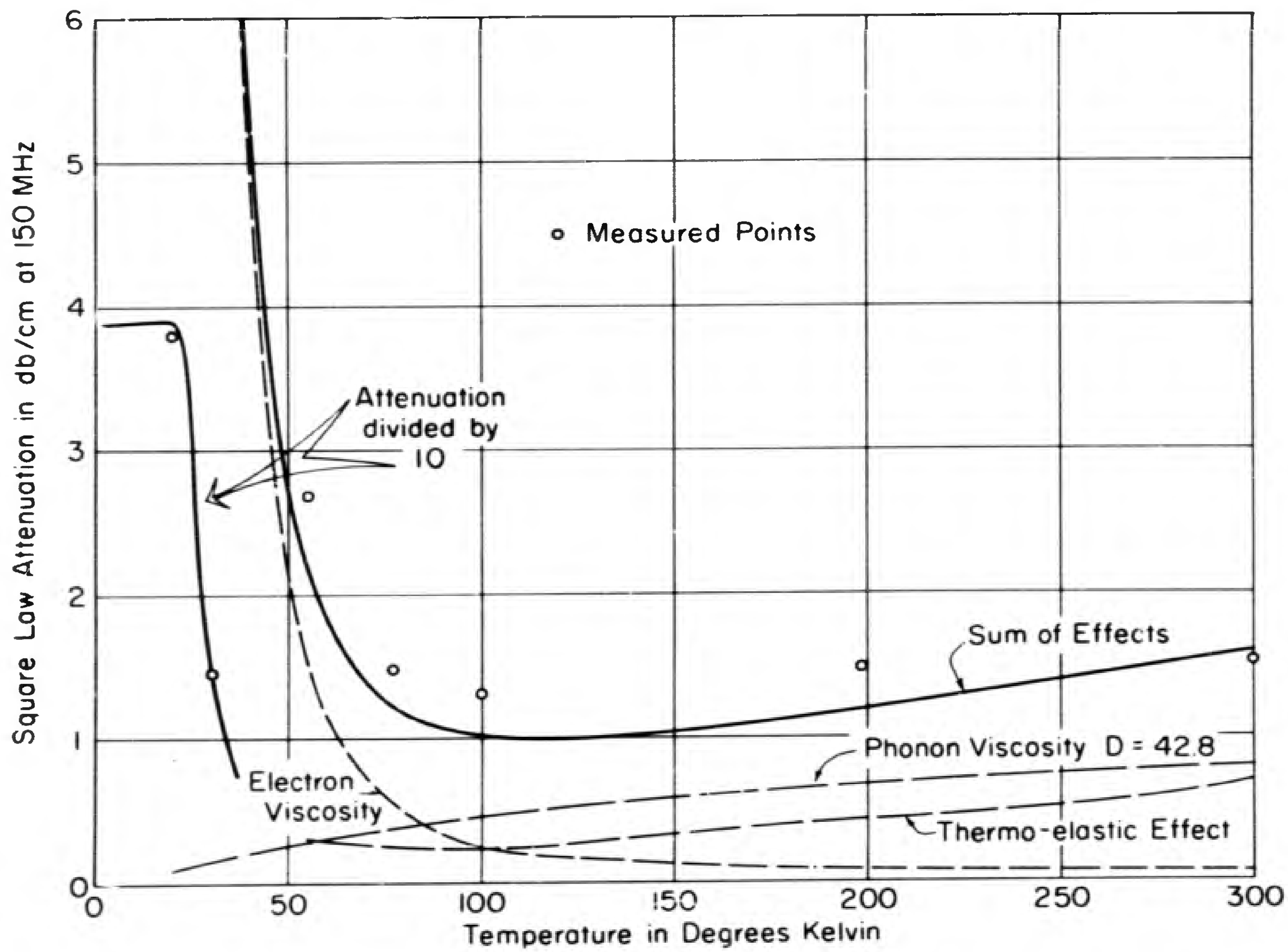

Fig. 26. Square law attenuation for copper, measured at 150 MHz, for a longitudinal wave along <100>.

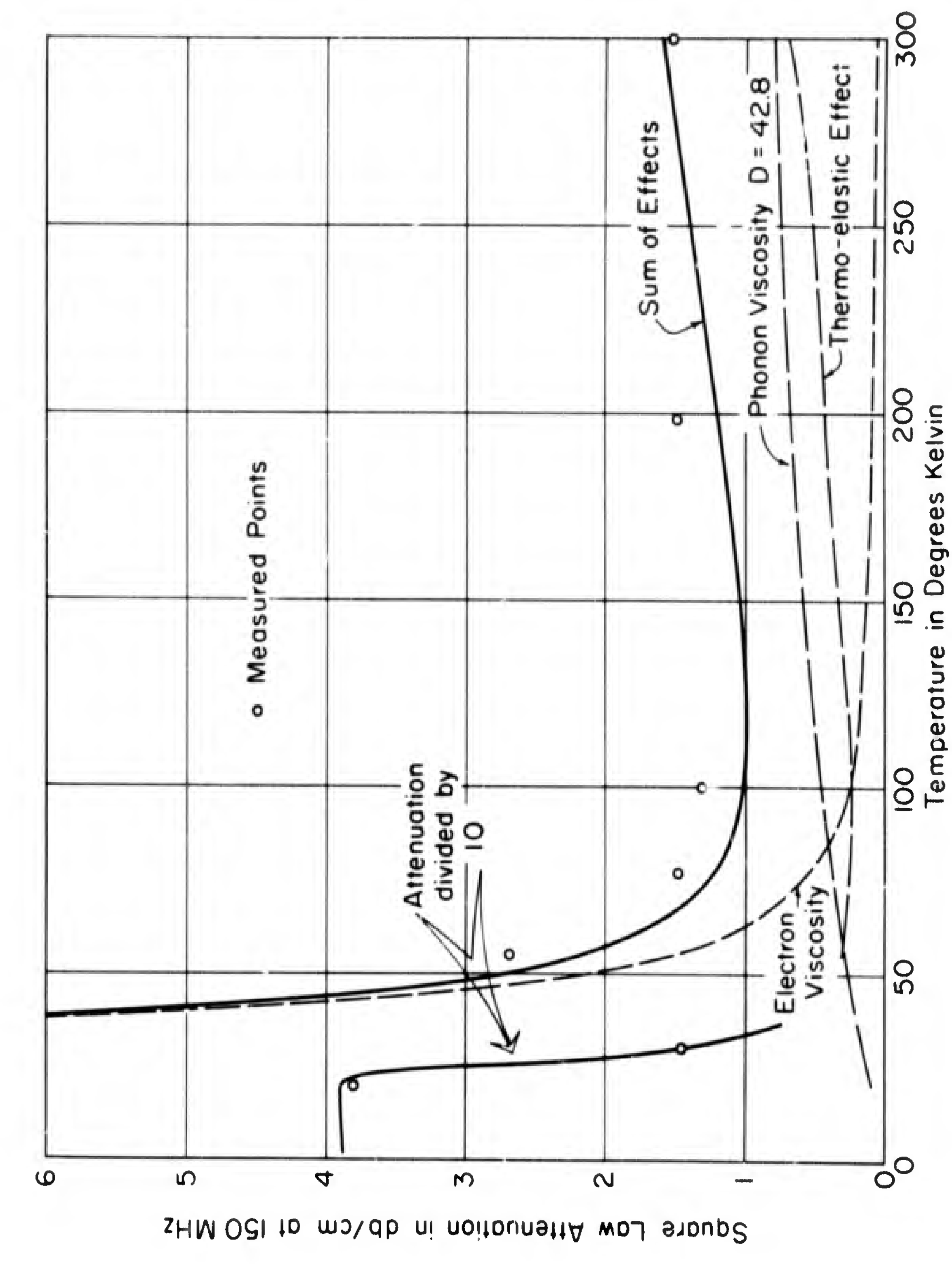

Fig. 28. Square law attenuation for slow shear wave ($v = 3.11 \times 10^5$ cms/sec) in single crystal aluminum. Dashed curves show electronic and phonon damping terms. D is evaluated as 8.6.

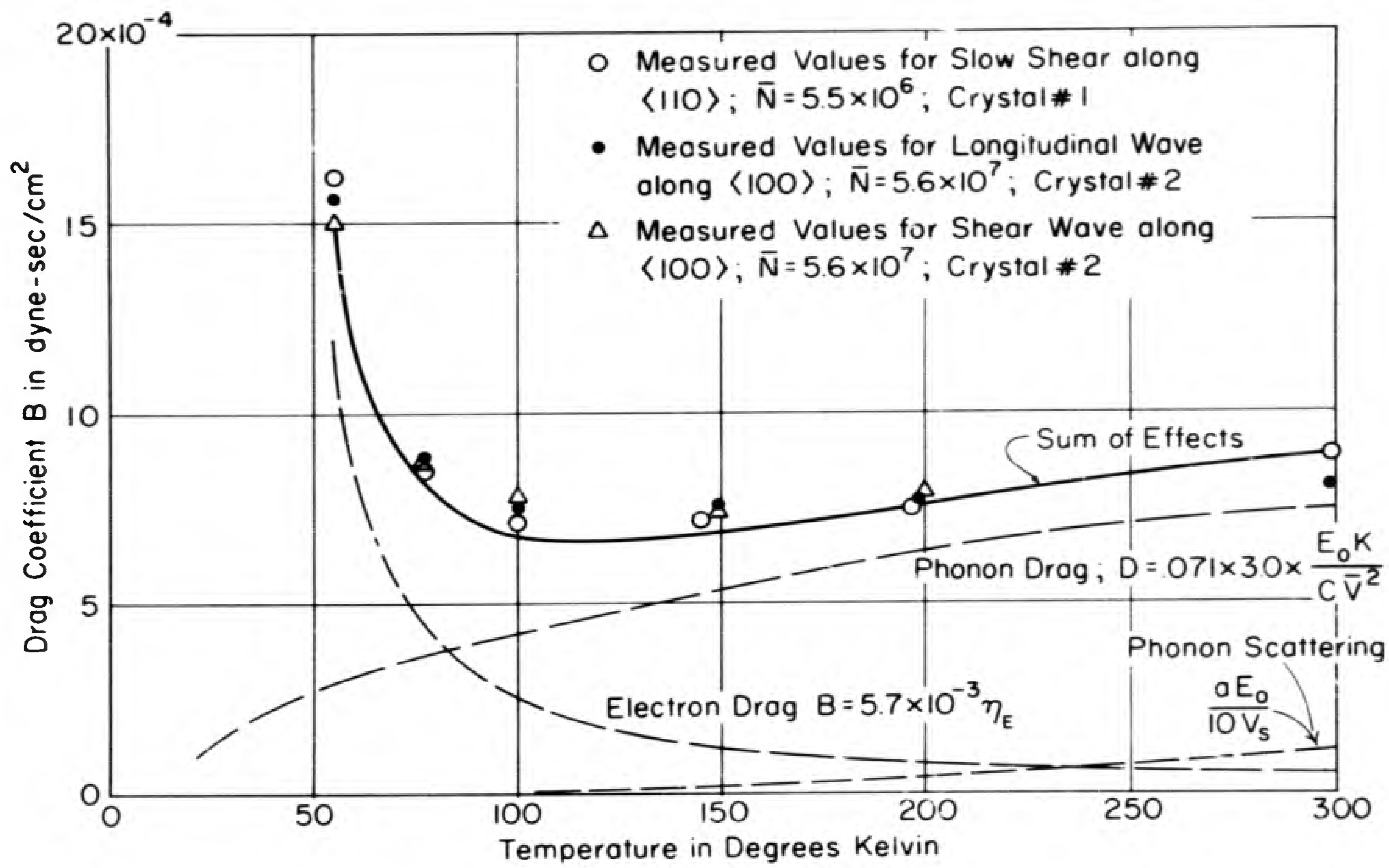

Fig. 27. Dislocation drag coefficients for copper, and the three components of dislocation drag.

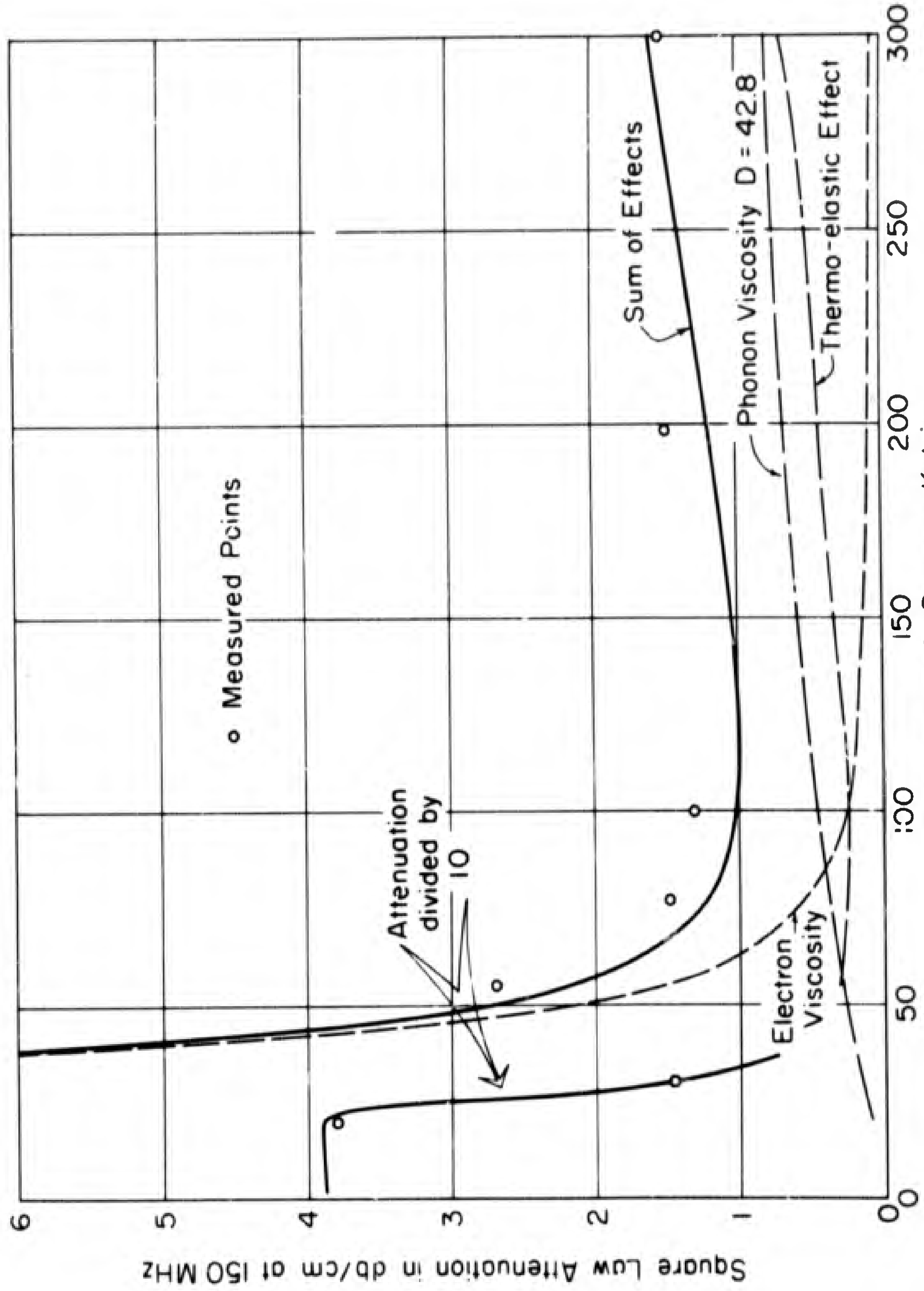

Fig. 28. Square law attenuation for slow shear wave ($v = 3.11 \times 10^5$ cms/sec) in single crystal aluminum. Dashed curves show electronic and phonon damping terms. D is evaluated as 8.6.

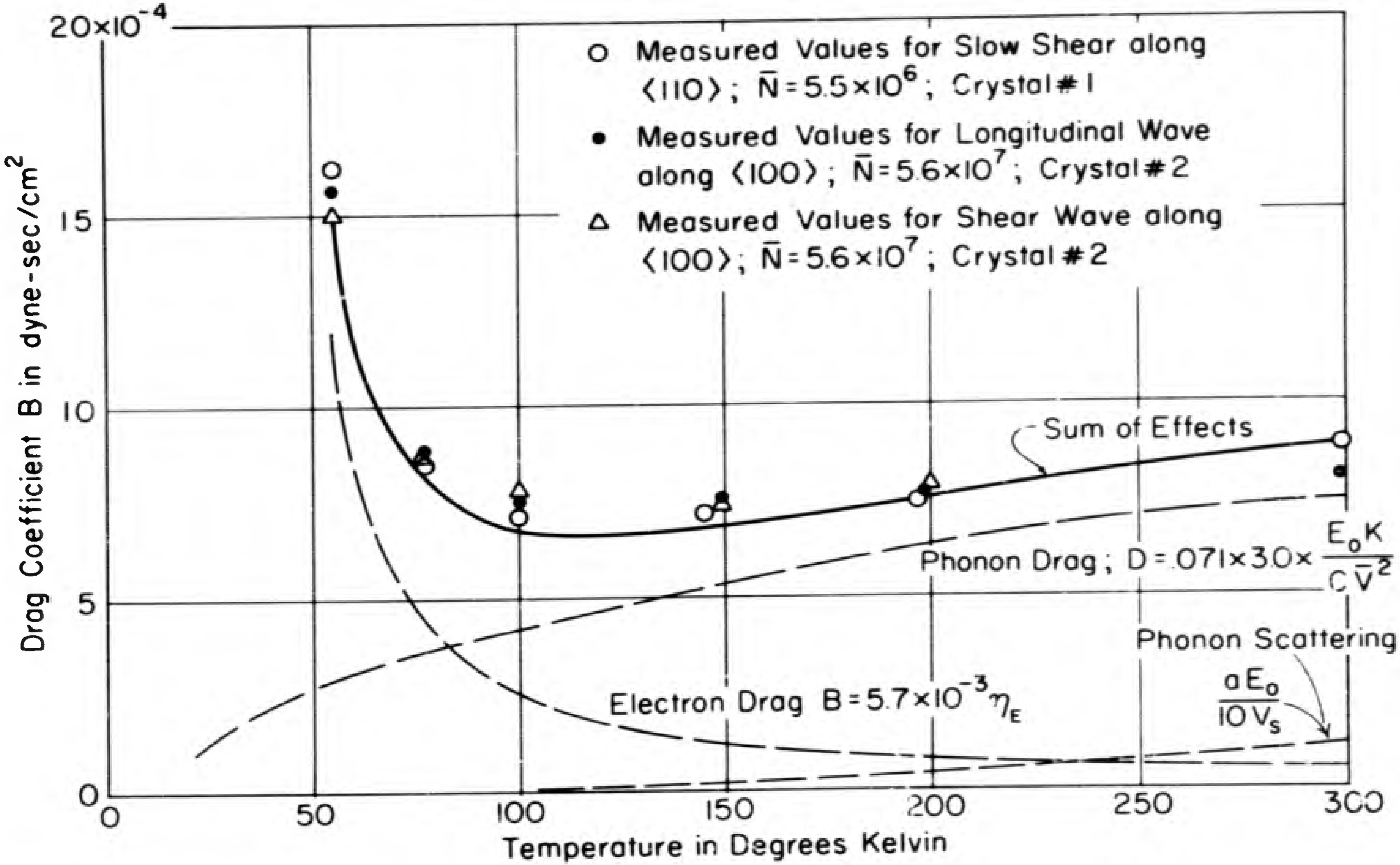

Fig. 27. Dislocation drag coefficients for copper, and the three components of dislocation drag.

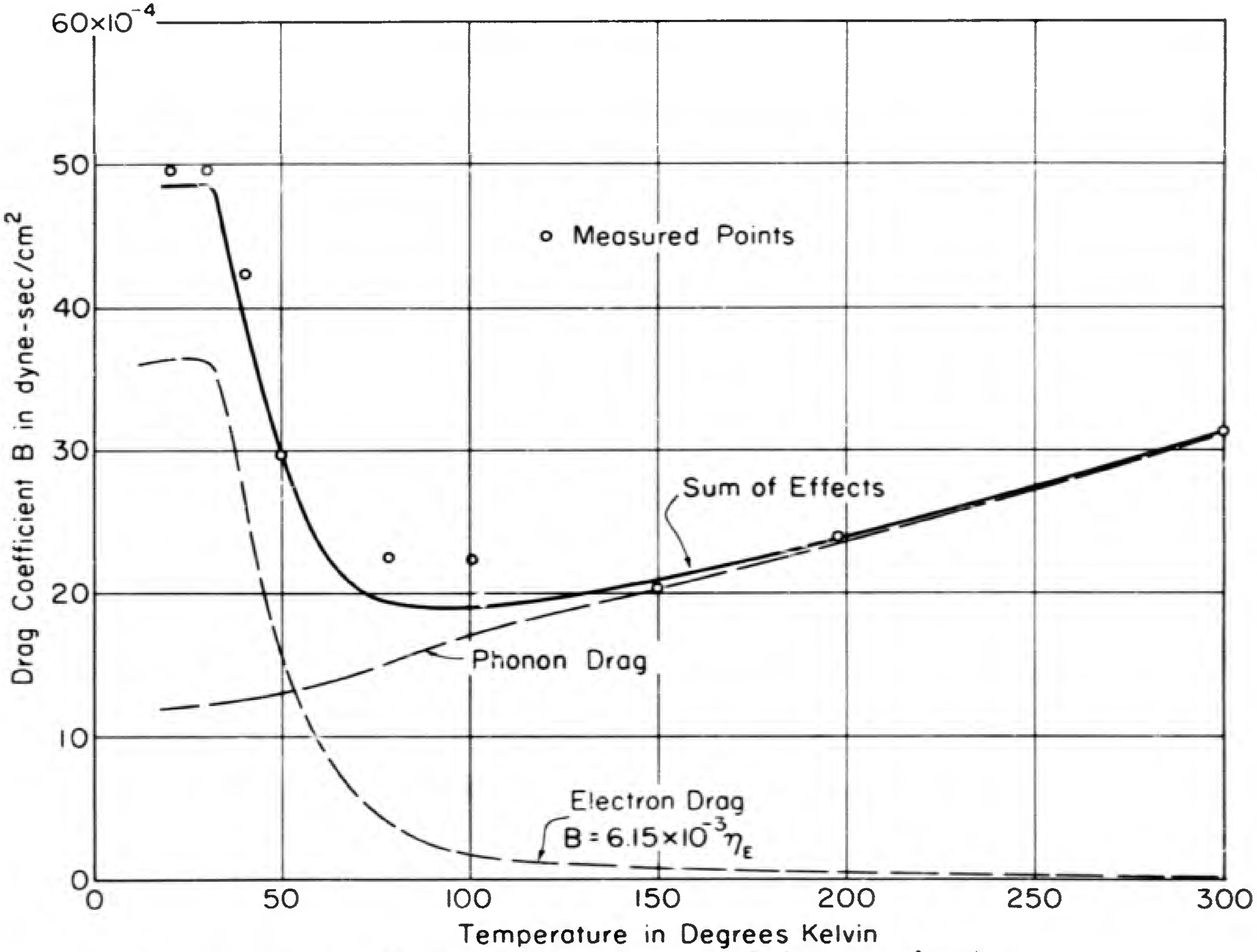

Fig. 30. D-ag coefficient for aluminum. Dashed curves show two components of damping. Phonon scattering is too small to show on scale.

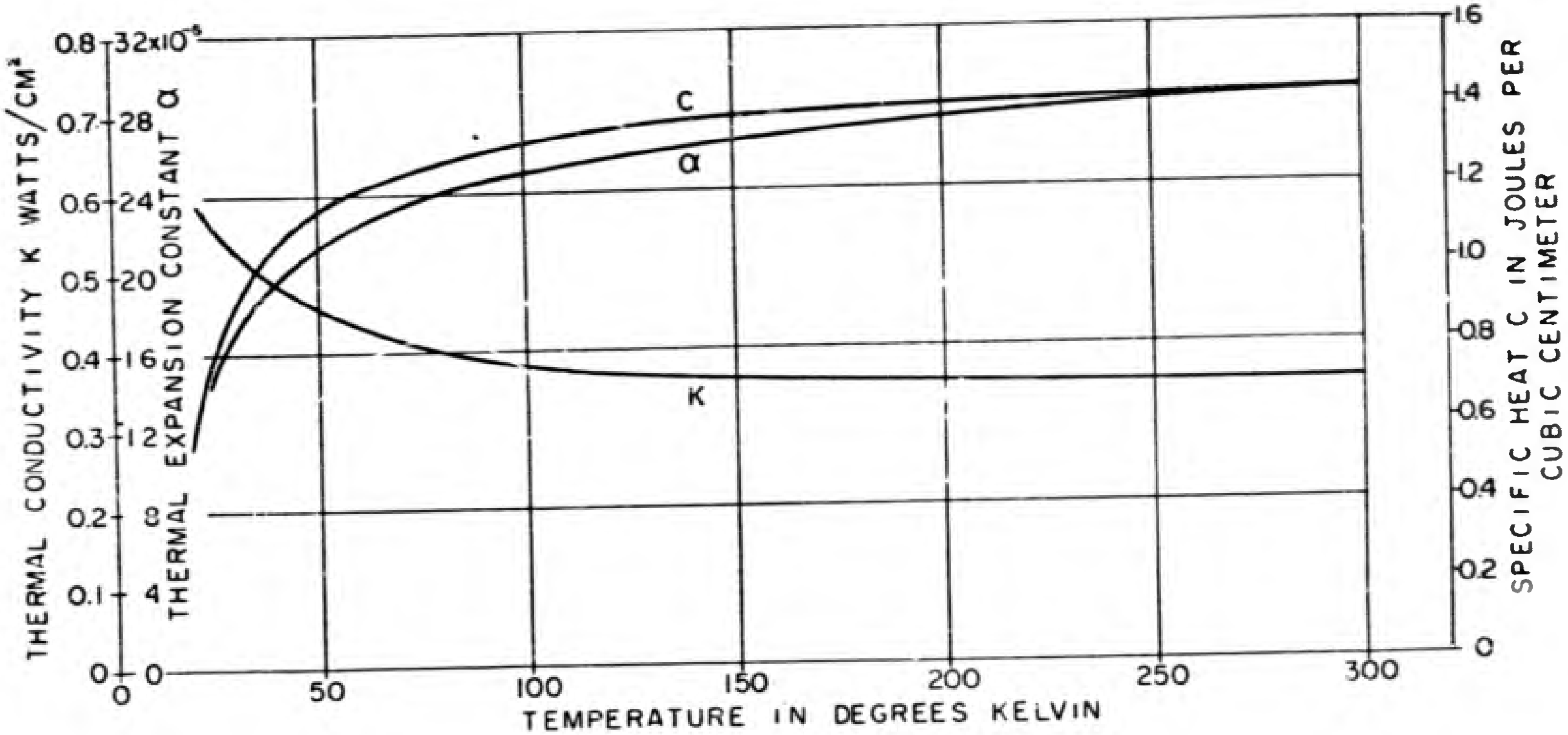

Fig. 31. Thermal properties of lead.

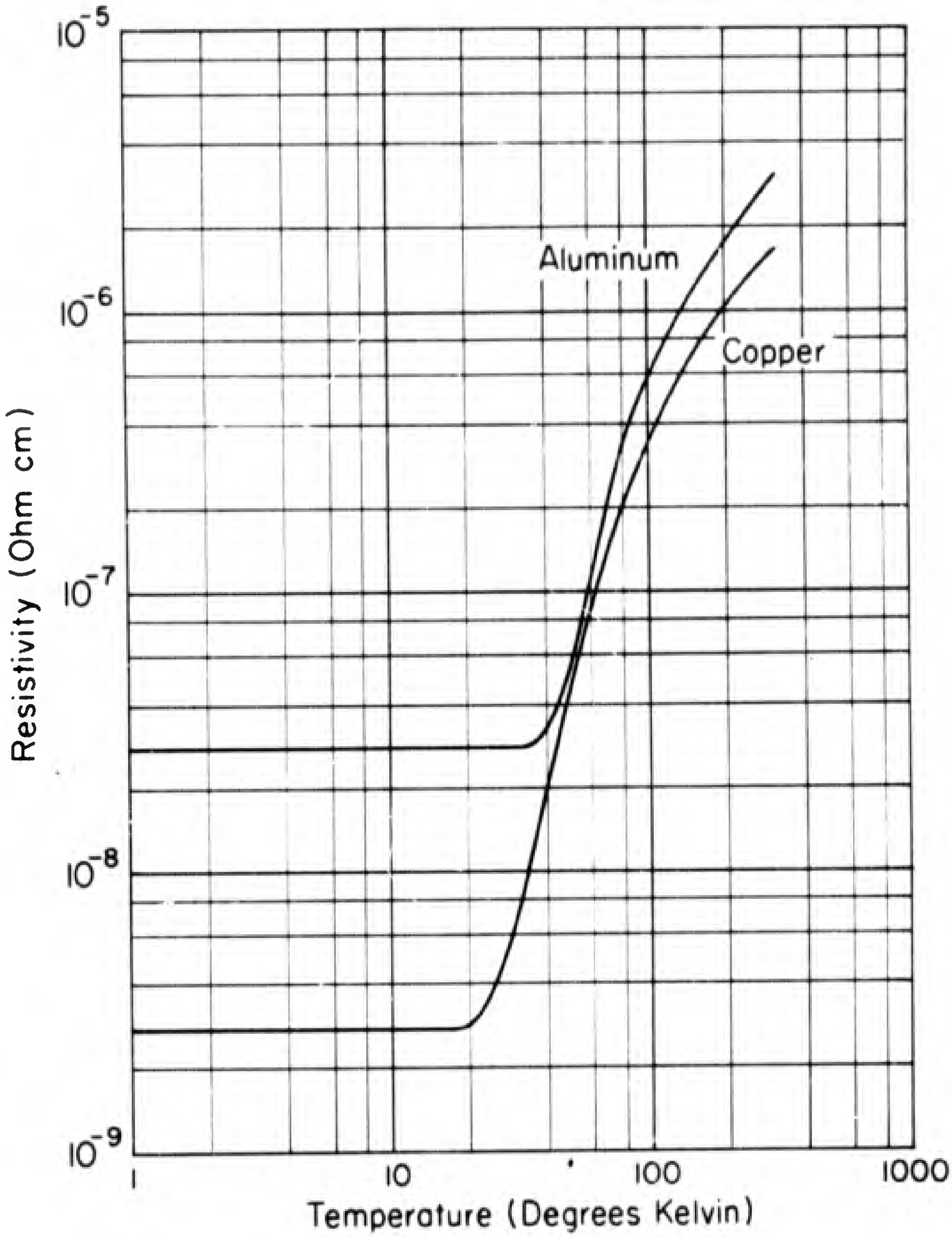

Fig. 32. Resistivity of copper and aluminum as a function of the temperature.

Unclassified

Security Classification

DOCUMENT CONTROL DATA - R&D

(Security classification of title, body of abstract and indexing annotation must be entered when the overall report is classified)

1. ORIGINATING ACTIVITY (Corporate author) Department of Civil Engineering and Engineering Mechanics, Columbia University	2a. REPORT SECURITY CLASSIFICATION Unclassified 2b. GROUP

3. REPORT TITLE

LOW AND HIGH AMPLITUDE INTERNAL FRICTION MEASUREMENTS IN SOLIDS AND THEIR RELATION TO IMPERFECTION MOTIONS

4. DESCRIPTIVE NOTES (Type of report and inclusive dates)

Technical Report

5. AUTHOR(S) (Last name, first name, initial)

Mason, W. P.

6. REPORT DATE	7a. TOTAL NO. OF PAGES	7b. NO. OF REFS
March 1967	125	65

8a. CONTRACT OR GRANT NO. Contract Nonr 266(91) b. PROJECT NO. Project No. NR 064-446 c. d.	9a. ORIGINATOR'S REPORT NUMBER(S) Contract Nonr 266(91) Project No. NR 064-446 Report No. 45 9b. OTHER REPORT NO(S) (Any other numbers that may be assigned this report)

10. AVAILABILITY/LIMITATION NOTICES

~~Qualified requesters may obtain copies of this report from DDC.~~

11. SUPPLEMENTARY NOTES	12. SPONSORING MILITARY ACTIVITY Office of Naval Research

13. ABSTRACT

The mechanical properties of single crystal and polycrystalline metals are determined largely by imperfection motions. Internal friction measurements are very sensitive methods for studying these motions. Low amplitude and high frequency measurements are conventional. A new high amplitude system capable of measuring internal friction and modulus defects is described. This can make measurements of internal friction from 10^{-4} to 0.2 with strain amplitudes up to 10^{-2}.

Typical data are shown for low amplitude, high frequency and high amplitude data. These are interpreted in terms of a modified Granato Lücke model. In the linear range dislocation drag coefficients are shown to be determined by the damping of phonons and electrons. The first non-linear range is associated with the breakaway of dislocations from pinning points. The final range involves the generation of new dislocations and is associated with instabilities and fatigue in the metal.

DD FORM 1 JAN 64 1473

Unclassified

Security Classification

Unclassified

Security Classification

14. KEY WORDS	LINK A ROLE	LINK A WT	LINK B ROLE	LINK B WT	LINK C ROLE	LINK C WT
Internal friction measurements						
High amplitude measuring system						
Electron and phonon drag coefficients						
Dislocation breakaway						
Dislocation multiplication effects						

INSTRUCTIONS

1. ORIGINATING ACTIVITY: Enter the name and address of the contractor, subcontractor, grantee, Department of Defense activity or other organization *(corporate author)* issuing the report.

2a. REPORT SECURITY CLASSIFICATION: Enter the overall security classification of the report. Indicate whether "Restricted Data" is included. Marking is to be in accordance with appropriate security regulations.

2b. GROUP: Automatic downgrading is specified in DoD Directive 5200.10 and Armed Forces Industrial Manual. Enter the group number. Also, when applicable, show that optional markings have been used for Group 3 and Group 4 as authorized.

3. REPORT TITLE: Enter the complete report title in all capital letters. Titles in all cases should be unclassified. If a meaningful title cannot be selected without classification, show title classification in all capitals in parenthesis immediately following the title.

4. DESCRIPTIVE NOTES: If appropriate, enter the type of report, e.g., interim, progress, summary, annual, or final. Give the inclusive dates when a specific reporting period is covered.

5. AUTHOR(S): Enter the name(s) of author(s) as shown on or in the report. Enter last name, first name, middle initial. If military, show rank and branch of service. The name of the principal author is an absolute minimum requirement.

6. REPORT DATE: Enter the date of the report as day, month, year, or month, year. If more than one date appears on the report, use date of publication.

7a. TOTAL NUMBER OF PAGES: The total page count should follow normal pagination procedures, i.e., enter the number of pages containing information.

7b. NUMBER OF REFERENCES: Enter the total number of references cited in the report.

8a. CONTRACT OR GRANT NUMBER: If appropriate, enter the applicable number of the contract or grant under which the report was written.

8b, 8c, & 8d. PROJECT NUMBER: Enter the appropriate military department identification, such as project number, subproject number, system numbers, task number, etc.

9a. ORIGINATOR'S REPORT NUMBER(S): Enter the official report number by which the document will be identified and controlled by the originating activity. This number must be unique to this report.

9b. OTHER REPORT NUMBER(S): If the report has been assigned any other report numbers *(either by the originator or by the sponsor)*, also enter this number(s).

10. AVAILABILITY/LIMITATION NOTICES: Enter any limitations on further dissemination of the report, other than those imposed by security classification, using standard statements such as:

(1) "Qualified requesters may obtain copies of this report from DDC."

(2) "Foreign announcement and dissemination of this report by DDC is not authorized."

(3) "U. S. Government agencies may obtain copies of this report directly from DDC. Other qualified DDC users shall request through ________________."

(4) "U. S. military agencies may obtain copies of this report directly from DDC. Other qualified users shall request through ________________."

(5) "All distribution of this report is controlled. Qualified DDC users shall request through ________________."

If the report has been furnished to the Office of Technical Services, Department of Commerce, for sale to the public, indicate this fact and enter the price, if known.

11. SUPPLEMENTARY NOTES: Use for additional explanatory notes.

12. SPONSORING MILITARY ACTIVITY: Enter the name of the departmental project office or laboratory sponsoring *(paying for)* the research and development. Include address.

13. ABSTRACT. Enter an abstract giving a brief and factual summary of the document indicative of the report, even though it may also appear elsewhere in the body of the technical report. If additional space is required, a continuation sheet shall be attached.

It is highly desirable that the abstract of classified reports be unclassified. Each paragraph of the abstract shall end with an indication of the military security classification of the information in the paragraph, represented as *(TS)*, *(S)*, *(C)*, or *(U)*.

There is no limitation on the length of the abstract. However, the suggested length is from 150 to 225 words.

14. KEY WORDS: Key words are technically meaningful terms or short phrases that characterize a report and may be used as index entries for cataloging the report. Key words must be selected so that no security classification is required. Identifiers, such as equipment model designation, trade name, military project code name, geographic location, may be used as key words but will be followed by an indication of technical context. The assignment of links, roles, and weights is optional.